Supersymmetric Dark Matter and the LHC

Alexandre Arbey

Ecole Doctorale de l'Université Claude Bernard Lyon 1

Centre de Recherche Astrophysique de Lyon

Mémoire d'Habilitation à Diriger des Recherches

par

Alexandre ARBEY

Supersymmetric Dark Matter and the LHC

Soutenance le 26 novembre 2012
à l'Université Claude Bernard Lyon 1
devant la commission d'examen composée de :

Dr. Fawzi BOUDJEMA	Rapporteur
Prof. John ELLIS	Rapporteur
Prof. Jules GASCON	Président
Dr. Gian GIUDICE	Rapporteur
Dr. Bruno GUIDERDONI	Examinateur
Prof. Pierre SALATI	Examinateur

Contents

Prelude

When I was recruited at Lyon University in 2004, my main research topics were focused on cosmological scalar fields explaining the dark matter and dark energy problems. I introduced the concept of "dark fluid", a unique complex scalar field bringing a unified explanation for the dark matter and dark energy problems encountered at cosmological scales. The dark fluid model is an inhomogeneous model, in which a scalar field can condense to form galactic halos, behaving like dark matter, or have a negative pressure in empty space. These features are the results of an adequate choice of the scalar field potential. I have shown that this model – although effective – succeeds to provide a solution simultaneously to both the dark matter and dark energy problems.

At the same time, I was becoming interested in Supersymmetry (SUSY), since this theory could bring a fundamental explanation to the dark matter problem, and the LHC would be able to probe this theory in the next few years. In particular, I remarked in many papers and seminars that the dark matter relic density constraint was always referred as a very powerful constraint to probe supersymmetry.

We decided with Nazila Mahmoudi to try to evaluate the influence of cosmological scenarios on the relic density calculation. To do so, we extended the public code authored by Nazila, SuperIso, aimed to compute flavour physics observables in the Minimal Supersymmetric extension of the Standard Model (MSSM), to include the relic density calculation in altered cosmological models, which is a feature not available in other relic density codes. This implementation required a substantial amount of work and constituted the basis for my future work.

We showed that the relic density calculation can be strongly altered by the cosmological assumptions on the early Universe (reheating, dark energy, ...). Since the Big Bang nucleosynthesis (BBN) imposes strong constraints on the cosmological models, and since no recent public code for the calculation of the the abundance of the elements was available, I decided to write my own program, AlterBBN, to compute the abundances in alternative cosmological models. We used it to better evaluate the influence of the cosmological model on the relic density calculation.

With the start of the Large Hadron Collider (LHC), I became more

interested in the phenomenology of the MSSM, and I started collaborating with Aldo Deandrea and our PhD student Ahmad Tarhini on this subject. I also worked at CERN in collaboration with Marco Battaglia and Nazila Mahmoudi. In particular, we focused our attention on the phenomenological MSSM (pMSSM), with 19 parameters. Because of the large number of parameters, it is necessary to use as many constraints as possible to restrict the large parameter space. Based on SuperIso Relic, we made numerous interfaces with other programs and build a complex machinery to study the MSSM using constraints from flavour physics, dark matter searches, LEP and Tevatron result, and the recent LHC data.

I have had the chance to be at CERN for the announcement of the boson "evidence" (in December 2011) and "discovery" (in July 2012). What an excitement and exciting time! Since then I work on the consequences of a Higgs-like particle discovery on the Higgs sector of the MSSM, in addition to other constraints from dark matter and flavour physics.

In the following, I will not describe the work on cosmological scalar field nor detail my work on the MSSM Higgs, but I will focus on my research on the MSSM and the supersymmetric dark matter, at the interface between cosmology and particle physics.

Introduction

The dark matter problem remains one of the most puzzling questions in cosmology, which appear at many different scales: galaxies, clusters, larger cosmological scales. Cosmological analyses, and in particular studies of the Cosmic Microwave Background, reveal that dark matter may be composed of non-baryonic particles, but their nature is still to be discovered.

Many new physics models provide a natural solution to the dark matter problem. Supersymmetry (SUSY), which adds to the Standard Model (SM) of particle physics a symmetry between fermions and bosons, is the most studied scenario to explain the fundamental nature of dark matter. One of the appealing features of Supersymmetry, which has contributed to promote it to the role of template model of new physics beyond the Standard Model, is the natural inclusion of a weakly interacting massive particle (WIMP) as cold dark matter (DM) candidate. In most of the cases, this is the lightest neutralino, $\tilde{\chi}_1^0$, which is the lightest supersymmetric particle (LSP). Scenarios with neutralino LSP realise the exact amount of dark matter relic density to match the precise determination obtained in the study of cosmic microwave background (CMB). This happens for neutralino masses of $\mathcal{O}(100$ GeV) due to the suggestive fact that a particle with $\sim$100 GeV mass and typical weak interaction couplings gives the correct neutralino relic density, $\Omega_{\rm CDM}h^2$ $\sim$0.1, in standard cosmology models which often referred to as the "WIMP miracle".

The search for SUSY is the main focus of the studies of physics beyond the SM at the LHC. Having acquired the status of possibly the best motivated theory of new physics over the past decades, Supersymmetry in its minimal incarnation (MSSM) with R-parity conservation leads to distinctive experimental signatures with hadrons, leptons and missing transverse energy, MET.

In this report, I will describe my work in the context of Supersymmetric Dark Matter, in light of the cosmological observations and LHC results.

In Chapter 1, I will first present the calculation of the relic density constraint in SUSY and show how the cosmological assumptions can modify the obtained results. In Chapter 2, I will present my work on the constraints of the pMSSM with neutralino dark matter, using in particular the constraints from dark matter direct detection, flavour physics and LEP, Tevatron and

LHC searches. In Chapter 3, I will focus on the results from dark matter direct detection experiments claiming for the possible discovery of a dark matter particle with a mass of about 10 GeV, and show that the pMSSM can provide a light neutralino candidate compatible with the data from all the different sectors. I will then present my future projects with respect to cosmology and particle physics. In Appendix 1, I will present SuperIso Relic, a public code that I have co-written with Nazila Mahmoudi, whose purpose is to compute flavour and dark matter constraints in the MSSM and NMSSM with standard and alternative cosmological assumptions. In Appendix 2, I will describe the AlterBBN public program, that I have written to compute the abundance of the elements generated during Big-Bang nucleosynthesis with again standard and alternative cosmological assumptions.

Chapter 1

Dark matter relic density

New physics models, and in particular supersymmetry (SUSY), provide stable particle candidates for dark matter, and one can compute their present energy density, the relic density [1]. This relic density is often compared to the dark matter density deduced from cosmological observations in order to constrain new physics parameters. The usual assumption in doing that is that the Universe is ruled by the standard model of cosmology, which assumes that radiation energy density and radiation entropy density dominate the Universe properties in the very early Universe. However, before Big-Bang nucleosynthesis (BBN) many phenomena could have modified the physical properties of the Universe, such as the expansion rate, or the entropy evolution, or even the non-thermal production of relic particles. The calculation of the relic density is altered in these cases, and for example the influence of a quintessence-like scalar field [2], or reheating and non thermal production of relic particles due to the decay of an inflaton-like scalar field [3] have already been discussed in the literature. Scenarios involving dark fluids or extra-dimensions modifying the expansion rate of the Universe have been also considered in [4]. On the other hand, with the start-up of the LHC, we can hope for new information on the physics beyond the standard model, providing more hints for the determination of the nature of dark matter.

In this chapter, we consider the calculation of the relic density beyond the cosmological standard model and consider the effects of the modification of the expansion rate and entropy content as studied in [4,5]. We will derive the necessary equations to compute the relic density in a more generic way. We also discuss the importance of the LHC data in the context of cosmology and claim that future discoveries of the LHC can lead to a better understanding of the Universe properties before BBN.

To illustrate the consequences of modifications of the cosmological model on the calculation of the relic density we consider the MSSM with R-parity conservation and show the implications on the SUSY parameter interpretation and constraints.

1.1 Relic density calculation

The density number of supersymmetric particles is determined by the Boltzmann equation, which in presence of non-thermal production of relic particles takes the form:

$$\frac{dn}{dt} = -3Hn - \langle\sigma v\rangle(n^2 - n_{eq}^2) + N_D \ , \tag{1.1}$$

where n is the number density of supersymmetric particles, $\langle\sigma v\rangle$ is the thermally averaged annihilation cross-section, H is the Hubble expansion rate and n_{eq} is the supersymmetric particle equilibrium number density. The term N_D provides a parametrization of the non-thermal production of SUSY particles which is in general temperature-dependent. The expansion rate H is determined by the Friedmann equation:

$$H^2 = \frac{8\pi G}{3}(\rho_{rad} + \rho_D) \ . \tag{1.2}$$

ρ_{rad} is the radiation energy density, which is considered to be dominant before BBN in the standard cosmological model. Following [4], we introduced in Eq. (1.2) ρ_D to parametrize the expansion rate modification. ρ_D can be interpreted either as an additional energy density term modifying the expansion (*e.g.* quintessence), or as an effective energy density which can account for other phenomena affecting the expansion rate (*e.g.* extra-dimensions).

The entropy evolution can also be altered beyond the standard cosmological model, and in presence of entropy fluctuations we give the entropy evolution equation:

$$\frac{ds}{dt} = -3Hs + \Sigma_D \ , \tag{1.3}$$

where s is the total entropy density. Σ_D in the above equation parametrizes effective entropy fluctuations due to unknown properties of the early Universe, and is temperature-dependent.

In the following, for the sake of generality, the three new parameters N_D, ρ_D and Σ_D are regarded as independent. Entropy and energy alterations are considered here as effective effects, which can be generated by curvature, phase transitions, extra-dimensions, or other phenomena in the early Universe. In a specific physical scenario, these parameters may be related, as for example in reheating models [3]. However, the large number of unanswered questions in the pre-BBN epoch and the complexity of particle physics models, which involves many different fields, can doubt the simplicity of reheating models. In particular many open questions remain in inflation, leptogenesis and baryogenesis scenarios. Therefore, a complete and realistic description of the early Universe would rely on several different fields with complementary roles, far beyond the decaying scalar field description of inflation and reheating models, and the direct dependence between

energy and entropy would in such cases be very difficult to determine at the time of the relic freeze-out. For this reason, we prefer to adopt a more conservative and effective approach in which the effective energy and entropy densities are considered as independent.

The radiation energy and entropy densities can be written as usual:

$$\rho_{rad} = g_{eff}(T)\frac{\pi^2}{30}T^4 \ , \qquad s_{rad} = h_{eff}(T)\frac{2\pi^2}{45}T^3 \ . \tag{1.4}$$

We split the total entropy density into two parts: radiation entropy density and effective dark entropy density, $s \equiv s_{rad}+s_D$. Using Eq. (1.3) the relation between s_D and Σ_D can then be derived:

$$\Sigma_D = \sqrt{\frac{4\pi^3 G}{5}}\sqrt{1+\tilde{\rho}_D}T^2\left[\sqrt{g_{eff}}s_D - \frac{1}{3}\frac{h_{eff}}{g_*^{1/2}}T\frac{ds_D}{dT}\right] \ , \tag{1.5}$$

with

$$g_*^{1/2} = \frac{h_{eff}}{\sqrt{g_{eff}}}\left(1+\frac{T}{3h_{eff}}\frac{dh_{eff}}{dT}\right) \ . \tag{1.6}$$

Following the standard relic density calculation method [1], $Y \equiv n/s$ is introduced, and Eq. (1.1) yields

$$\frac{dY}{dx} = -\frac{m_{lsp}}{x^2}\sqrt{\frac{\pi}{45G}}g_*^{1/2}\left(\frac{1+\tilde{s}_D}{\sqrt{1+\tilde{\rho}_D}}\right)\left[\langle\sigma v\rangle(Y^2-Y_{eq}^2) + \frac{Y\Sigma_D - N_D}{\left(h_{eff}(T)\frac{2\pi^2}{45}T^3\right)^2(1+\tilde{s}_D)^2}\right] \ , \tag{1.7}$$

where $x = m_{lsp}/T$, m_{lsp} is the mass of the lightest supersymmetric relic particle, and

$$\tilde{s}_D \equiv \frac{s_D}{h_{eff}(T)\frac{2\pi^2}{45}T^3} \ , \qquad \tilde{\rho}_D \equiv \frac{\rho_D}{g_{eff}\frac{\pi^2}{30}T^4} \ , \tag{1.8}$$

and

$$Y_{eq} = \frac{45}{4\pi^4 T^2 h_{eff}}\frac{1}{(1+\tilde{s}_D)}\sum_i g_i m_i^2 K_2\left(\frac{m_i}{T}\right) \ , \tag{1.9}$$

with i running over all supersymmetric particles of mass m_i and with g_i degrees of freedom. Integrating Eq. (1.7), the relic density can then be calculated using:

$$\Omega h^2 = \frac{m_{lsp}s_0 Y_0 h^2}{\rho_c^0} = 2.755\times 10^8 Y_0 m_{lsp}/\mathrm{GeV} \ , \tag{1.10}$$

where the subscript 0 refers to the present values of the parameters. In the limit where $\rho_D = s_D = \Sigma_D = N_D = 0$, standard relations are retrieved. We should note here that s_D and Σ_D are not independent variables. Using Eqs. (1.1-1.10) the relic density in presence of a modified expansion rate, of

entropy fluctuations and of non-thermal production of relic particles, can be computed provided ρ_D, N_D and s_D or Σ_D are specified. For ρ_D we follow the parametrization introduced in Ref. [4]:

$$\rho_D = \kappa_\rho \rho_{rad}(T_{BBN})\big(T/T_{BBN}\big)^{n_\rho} , \tag{1.11}$$

where T_{BBN} is the BBN temperature. Different values of n_ρ leads to different behaviors of the effective density. For example, $n_\rho = 4$ corresponds to a radiation behavior, $n_\rho = 6$ to a quintessence behavior, and $n_\rho > 6$ to the behavior of a decaying scalar field. κ_ρ is the ratio of the effective energy density to the radiation energy density at BBN time and can be negative. The role of ρ_D will be to increase the expansion rate for $\rho_D > 0$, leading to an early decoupling and a higher relic density, or to decrease it for $\rho_D < 0$, leading to a late decoupling and to a smaller relic density. Requiring that the radiation density dominates during BBN implies $|\kappa_\rho| \ll 1$. Moreover, $H^2 > 0$ imposes $|\rho_D| < \rho_{rad}$ for $\rho_D < 0$, strongly limiting the interest of negative κ_ρ as mentioned in [4].

To model the entropy perturbations, we follow the parametrization introduced in Ref. [5]:

$$s_D = \kappa_s s_{rad}(T_{BBN})\big(T/T_{BBN}\big)^{n_s} . \tag{1.12}$$

This parametrization finds its roots in the first law of thermodynamics, where energy and entropy are directly related and therefore the entropy parametrization can be similar to the energy parametrization. As for the energy density, different values of n_s lead to different behaviors of the entropy density: $n_s = 3$ corresponds to a radiation behavior, $n_s = 4$ appears in dark energy models, $n_s \sim 1$ in reheating models, and other values can be generated by curvature, scalar fields or extra-dimension effects. κ_s is the ratio of the effective entropy density to the radiation entropy density at BBN time and can be negative. The role of s_D will be to increase the temperature at which the radiation dominates for $s_D > 0$, leading to a decreased relic density, or to decrease this temperature for $s_D < 0$, leading to an increased relic density. For naturalness reason, we impose that the radiation entropy density dominates at BBN time, *i.e.* $|\kappa_s| \ll 1$. Constraints on the cosmological entropy in reheating models have already been derived in [6]; we extend here the analyses to the general parametrization (1.12) using BBN data.

A general parametrization is difficult for N_D: in many reheating models a scalar field decays into supersymmetric particles, and the non-thermal production is therefore related to the scalar field density. To avoid imposing *ad hoc* general conditions, we choose $N_D = 0$. We can however note that the main effect of the non-thermal production is an enhancement of the final number of relic particles, so that it is always possible to enhance the final relic density by assuming non-thermal production of relic particles.

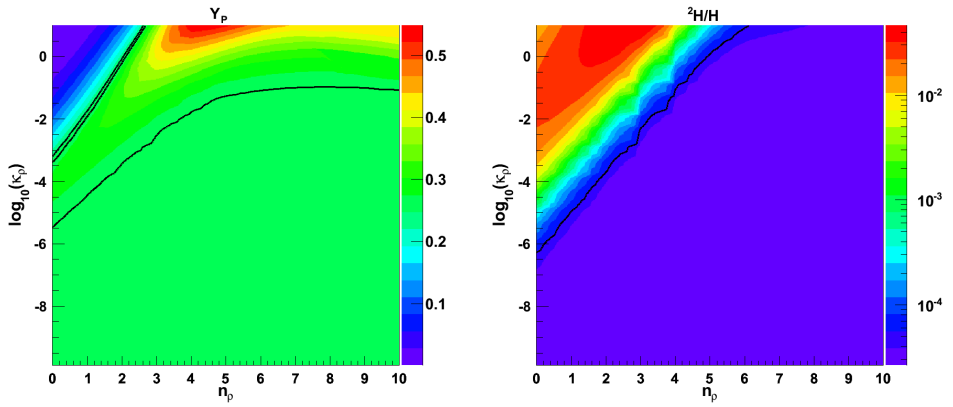

Figure 1.1: Constraints from Y_p (left) and $^2H/H$ (right) on the effective dark energy. The parameter regions excluded by BBN are located above the black lines. The colors correspond to different values of Y_p and $^2H/H$.

1.2 BBN constraints

In order to make a realistic analysis of the allowed cosmological scenarios, we apply the BBN constraints. To compute the relevant abundances of the elements, we use the public code AlterBBN, that is described in Appendix B and which includes the parametrization of the expansion rate of Eqs. (1.2), (1.11) and (1.12). We consider the rather conservative bounds of [8]:

$$\begin{aligned} &0.240 < Y_p < 0.258\ , \qquad 1.2\times10^{-5} < {}^2H/H < 5.3\times10^{-5}\ , \\ &0.57 < {}^3H/{}^2H < 1.52\ , \qquad {}^7Li/H > 0.85\times10^{-10}\ , \qquad {}^6Li/{}^7Li < 0.66\ , \end{aligned} \tag{1.13}$$

for the helium abundance Y_p and the primordial $^2H/H$, $^3H/\,^2H$, $^7Li/H$ and $^6Li/\,^7Li$ ratios. The most constraining observables are Y_p and $^2H/H$, and the constraints obtained are shown in Fig. 1.1 for (κ_ρ, n_ρ), and in Fig. 1.2 for (κ_s, n_s.) The BBN constraints can be therefore summarized as:

$$\kappa_\rho \lesssim 10^{-1.5}\ , \qquad \kappa_\rho \lesssim 10^{1.2n_\rho-6.0}\ , \tag{1.14}$$

$$\kappa_s \lesssim 10^{n_s-5.2}\ , \qquad \kappa_s \lesssim 10^{-0.8n_s+0.5}\ . \tag{1.15}$$

Also, for consistency with the CMB observations, we impose either $n_\rho \geq 4$ and $n_s \geq 3$, or $\rho_D = s_D = 0$ for $T < T_{BBN}$, so that ρ_D and s_D do not dominate after BBN.

1.3 SUSY constraints

We now consider the influence of the modified cosmological model on the supersymmetric constraints. The following computations are performed with

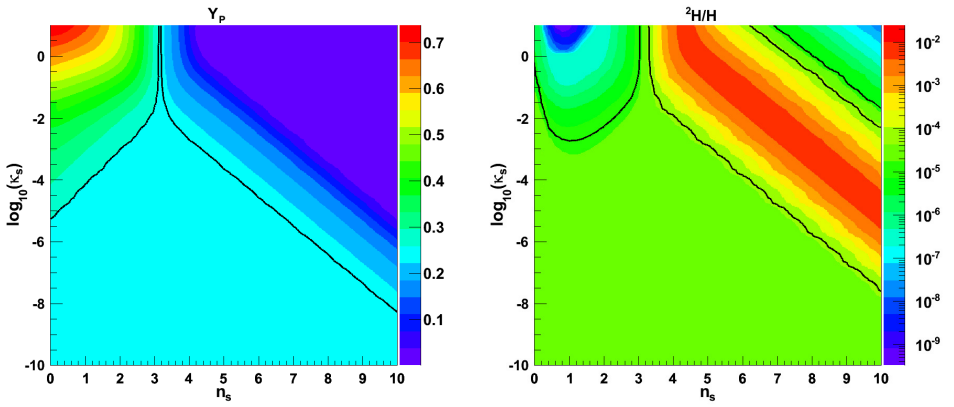

Figure 1.2: Constraints from Y_p (left) and ${}^2H/H$ (right) on the effective dark entropy. The parameter regions excluded by BBN are located above the black lines. The colors correspond to different values of Y_p and ${}^2H/H$.

`SuperIso Relic` [9, 10], that is described in Appendix A. Considering the latest WMAP data [11] with an additional 10% theoretical uncertainty on the relic density calculation, we derive the following favoured interval at 99% C.L.:

$$0.068 < \Omega_\chi h^2 < 0.155 \; . \tag{1.16}$$

For illustration purpose, the older dark matter density interval is also considered:

$$0.1 < \Omega_\chi h^2 < 0.3 \; . \tag{1.17}$$

In the following, we restrict ourselves to $n_\rho \geq 4$, $0 \leq \kappa_\rho \leq 1$, $n_s \geq 3$, $0 \leq \kappa_s \leq 1$, and consider a constrained MSSM scenario. To allow more flexibility in the Higgs sector, we focus on the Non-Universal Higgs Mass Model (NUHM), in which the parameters consist of the universal (except for the Higgs) scalar mass at GUT scale m_0, the universal gaugino mass at GUT scale $m_{1/2}$, the trilinear soft breaking parameter at GUT scale A_0, the ratio of the two Higgs vacuum expectation values $\tan\beta$, the μ parameter and the CP-odd Higgs mass m_A.

We consider first the NUHM test-point ($m_0 = m_{1/2} = 1$ TeV, $m_A = \mu = 500$ GeV, $A_0 = 0$, $\tan\beta = 40$) which gives a relic density of $\Omega h^2 \approx 0.11$, favoured by the WMAP constraints.

Three different effects are presented in Fig. 1.3: the first plot shows the influence of the presence of an additional effective density on the computed relic density. We note that when κ_ρ and n_ρ increase, the relic density increases up to a factor of 10^5. The second plot illustrates the effect of an additional entropy density, in absence of additional energy density. Here when κ_s and n_s increase, the relic density is strongly decreased down to a factor of 10^{-14}. The third plot is a more complex example of both additional

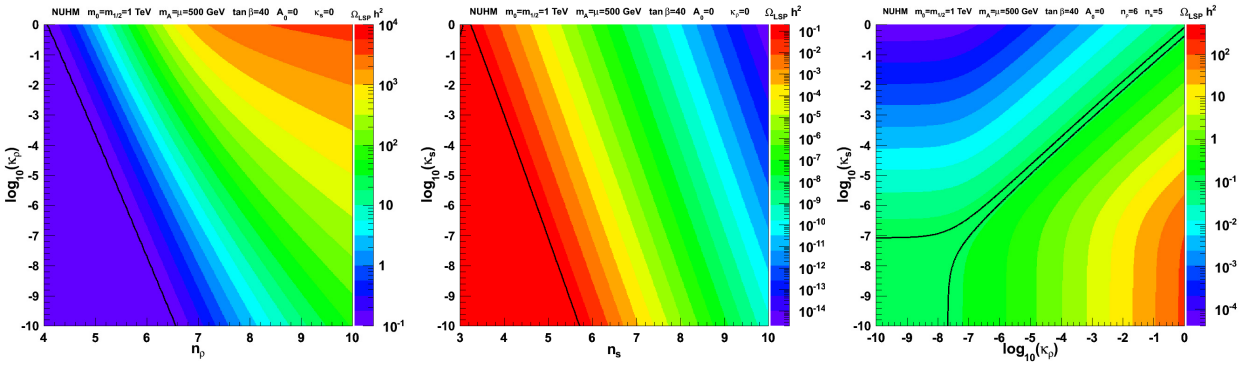

Figure 1.3: Influence of the presence of an effective energy density (left), an effective entropy (center), and both an effective energy with $n_\rho = 6$ and an entropy with $n_s = 5$ (right). The colors correspond to different values of Ωh^2. The black lines delimit the regions favoured by WMAP. The favoured zones are the lower left corners for the first two plots, and between the black lines for the last plot.

energy density with $n_\rho = 6$ and additional entropy density with $n_s = 5$. In this case, the values of the relic density varies from 10^{-4} to 10^3, and we notice a narrow strip between the WMAP lines in which the entropy and energy effects almost cancel, leading to a degenerate zone with $\Omega h^2 \approx 0.11$.

We now study the effects of our parametrizations while scanning over the NUHM parameter space. About one million random SUSY points in the NUHM parameter plane (μ,m_A) with $m_0 = m_{1/2} = 1$ TeV, $A_0 = 0$, $\tan\beta = 40$ are generated using `SOFTSUSY` [12], and for each point we compute flavour physics observables, direct limits and the relic density with `SuperIso Relic`.

In Fig. 1.4, the effects of the cosmological models on the relic density constraints are demonstrated. The first plot is given as a reference for the standard cosmological model, showing the tiny strips corresponding to the regions favoured by the relic density constraint. In the second plot, generated assuming a tiny additional energy density with $\kappa_\rho = 10^{-4}$ and $n_\rho = 6$, the relic density favoured strips are reduced, because the calculated relic densities are decreased in comparison to the relic densities computed in the standard scenario. The next plots demonstrate the influence of an additional entropy density compatible with BBN constraints. The favoured strips are this time enlarged and moved towards the outside of the plot. This effect is due to a decrease in the relic density. Note that the different scenarios shown in these plots are equivalently valid from the cosmological observations. However, the SUSY favoured parameters can be drastically different depending on the cosmological assumptions employed.

In Fig. 1.5, we consider two cosmological scenarios in which energy as well as entropy densities are present. The energy and entropy densities have

opposite effects and can compensate, and the similarity of the plots reveals the degeneracy between the two cosmological scenarios from the point of view of particle physics. However, using the BBN constraints, the scenario of the right plot can be ruled out.

An important consequence of this example is that if we discover that the particle physics scenario best in agreement with the LHC data (or future colliders) leads to a relic density in disagreement with the cosmological data constraints, important consequences on the cosmological scenario may be deduced: first, it would imply that the cosmological standard model does not describe satisfyingly the pre-BBN Universe. Second, combining all cosmological data, and in particular those from BBN, it would be possible to determine physical properties of the early Universe and constrain early Universe scenarios. As such, valuable constraints on cosmological models can be obtained from particle colliders.

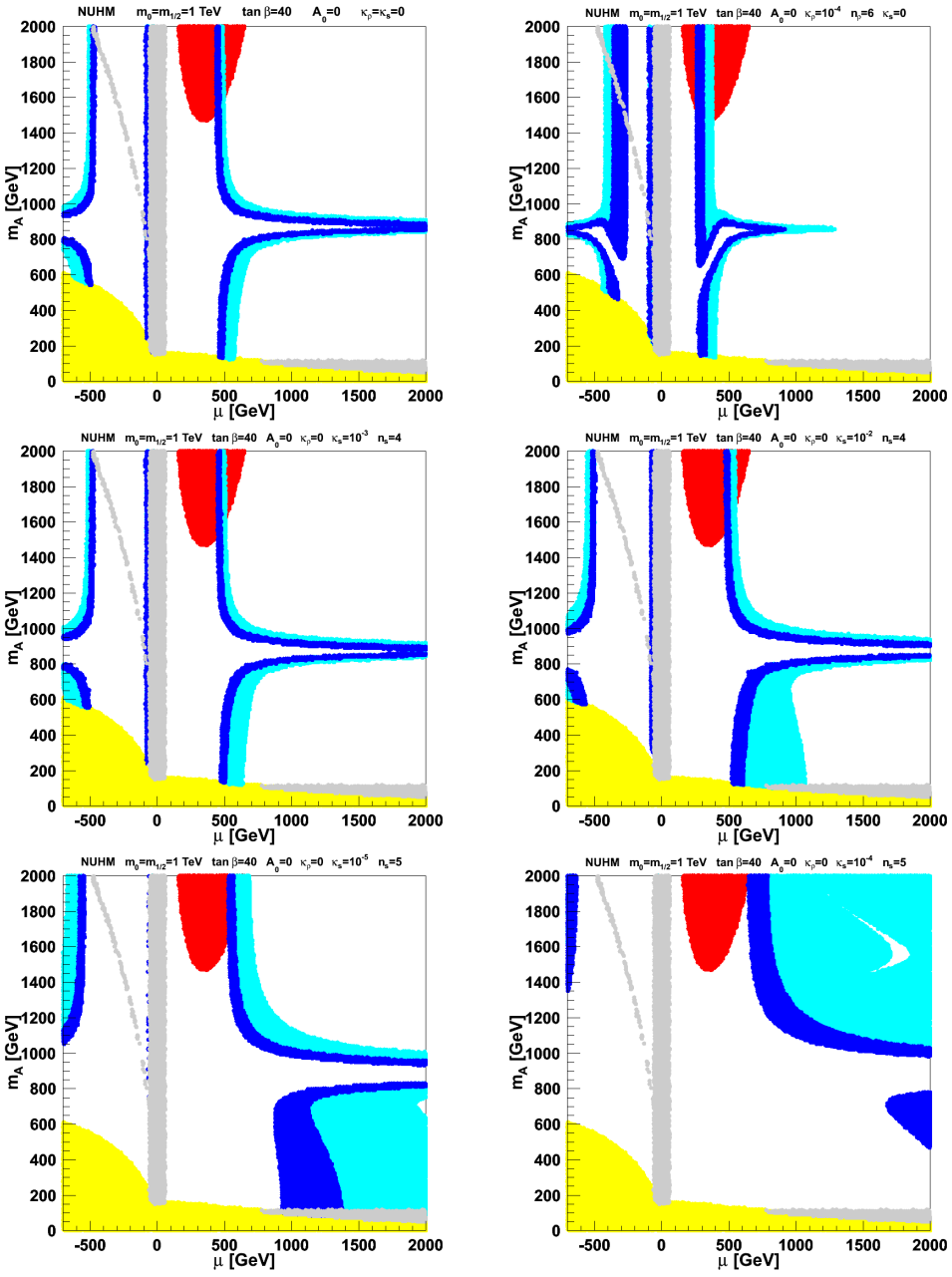

Figure 1.4: Constraints on the NUHM parameter plane (μ,m_A), from left to right and top to bottom, in the standard cosmological model, in presence of a tiny energy overdensity with $\kappa_\rho = 10^{-4}$ and $n_\rho = 6$, in presence of a tiny entropy overdensity with $\kappa_s = 10^{-3}$ and $n_s = 4$, with $\kappa_s = 10^{-2}$ and $n_s = 4$, with $\kappa_s = 10^{-5}$ and $n_s = 5$, and with $\kappa_s = 10^{-4}$ and $n_s = 5$. The red points are excluded by the isospin asymmetry of $B \to K^*\gamma$, the gray area is excluded by direct collider limits, the yellow zone involves tachyonic particles, and the dark and light blue strips are favoured by the WMAP constraints and by the older interval (1.17) respectively.

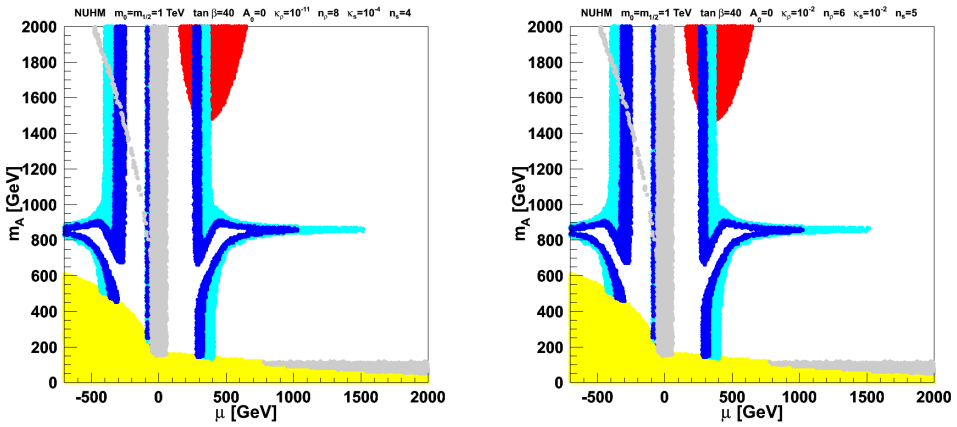

Figure 1.5: Constraints on the NUHM parameter plane (μ,m_A), in presence of a tiny energy overdensity with $\kappa_\rho = 10^{-11}$ and $n_\rho = 8$ associated to a tiny entropy overdensity with $\kappa_s = 10^{-4}$ and $n_s = 4$ on the left, and an energy overdensity with $\kappa_\rho = 10^{-2}$ and $n_\rho = 6$ associated to an entropy overdensity with $\kappa_s = 10^{-2}$ and $n_s = 5$ on the right. The colors are as in Fig. 1.4.

Bibliography

[1] H. Goldberg, Phys. Rev. Lett. **50**, 1419 (1983); L.M. Krauss, Nucl. Phys. B**227**, 556 (1983); M. Srednicki, R. Watkins and K.A. Olive, Nucl. Phys. B**310**, 693 (1988); P. Gondolo and G. Gelmini, Nucl. Phys. B**360**, 145 (1991); J. Edsjö and P. Gondolo, Phys. Rev. D**56**, 1879 (1997).

[2] M. Kamionkowski and M.S. Turner, Phys. Rev. D**42**, 3310 (1990); F. Rosati, Phys. Lett. B**570**, 5 (2003); D. Comelli, M. Pietroni and A. Riotto, Phys. Lett. B**571**, 115 (2003); P. Salati, Phys. Lett. B**571**, 121 (2003); S. Profumo and P. Ullio, JCAP **0311**, 006 (2003); R. Catena *et al.*, Phys. Rev. D**70**, 063519 (2004); C. Pallis, JCAP **0510**, 015 (2005); C. Pallis, Nucl. Phys. B**751**, 129 (2006); D.J.H. Chung *et al.*, JHEP **0710**, 016 (2007).

[3] R.J. Scherrer and M.S. Turner, Phys. Rev. D**31**, 681 (1985); T. Moroi and L. Randall, Nucl. Phys. B**570**, 455 (2000); G.F. Giudice, E.W. Kolb and A. Riotto, Phys. Rev. D**64**, 023508 (2001); N. Fornengo, A. Riotto, and S. Scopel, Phys. Rev. D**67**, 023514 (2003); C. Pallis, Astrop. Phys. **21**, 689 (2004); G. Gelmini and P. Gondolo, Phys. Rev.D**74**, 023510 (2006); G. Gelmini, P. Gondolo, A. Soldatenko and C.E. Yaguna, Phys. Rev. D**74**, 083514 (2006); M. Drees, H. Iminniyaz and M. Kakizaki, Phys. Rev. D**76**, 103524 (2007).

[4] A. Arbey and F. Mahmoudi, Phys. Lett. B**669**, 46 (2008).

[5] A. Arbey and F. Mahmoudi, JHEP **1005**, 051 (2010).

[6] M. Kawasaki, K. Kohri and N. Sugiyama, Phys. Rev. Lett. **82**, 4168 (1999); M. Kawasaki, K. Kohri and N. Sugiyama, Phys. Rev. D**62**, 023506 (2000); S. Hannestad, Phys. Rev. D**70**, 043506 (2004); K. Ichikawa, M. Kawasaki and F. Takahashi, Phys. Rev. D**72**, 043522 (2005).

[7] A. Arbey, Comput. Phys. Commun. **183**, 1822 (2012), `http://superiso.in2p3.fr/relic/alterbbn`.

[8] K. Jedamzik, Phys. Rev. D**74**, 103509 (2006).

[9] F. Mahmoudi, Comput. Phys. Commun. **178**, 745 (2008); F. Mahmoudi, Comput. Phys. Commun. **180**, 1579 (2009), `http://superiso.in2p3.fr`.

[10] A. Arbey and F. Mahmoudi, Comput. Phys. Commun. **181**, 1277 (2010), `http://superiso.in2p3.fr/relic`.

[11] E. Komatsu, et al. (WMAP Collaboration), Astrophys. J. Suppl. **192**, 18 (2011).

[12] B.C. Allanach, Comput. Phys. Commun. **143** (2002), 305.

[13] B.C. Allanach, G. Belanger, F. Boudjema and A. Pukhov, JHEP **0412**, 020 (2004); E.A. Baltz, M. Battaglia, M.E. Peskin and T. Wizansky, Phys. Rev. D**74**, 103521 (2006); L. Roszkowski, R. Ruiz de Austri and R. Trotta, Phys. Rev. D**82**, 055003 (2010).

Chapter 2

Neutralino dark matter in the pMSSM

The analysis of constraints from low energy data, dark matter density and the results of the LHC searches in generic SUSY scenarios shows that light neutralinos are still well compatible with current data. While searches for signals of strongly interacting SUSY particles in pp collisions using missing transverse energy (MET) signatures are ongoing at the LHC, ground-based direct detection DM experiments, such as XENON [1] and CDMS [2], have reached a sensitivity in spin-independent WIMP-nucleon cross section at WIMP masses of $\mathcal{O}(100$ GeV), which covers a significant fraction of the SUSY parameter space explored at the LHC.

In this chapter I discuss the complementarity of these constraints and their implications on the 19-parameter phenomenological MSSM (pMSSM) [3], where it is assumed that the lightest neutralino, χ_1^0 is the lightest supersymmetric particle (LSP).

2.1 Simulation and Tools

This study of the pMSSM parameter space with LSP neutralinos is based on the combination of several programs from spectrum generation to the computation of dark matter scattering cross sections and relic density, flavour and electroweak observables, as well as the simulation and analysis of events in 7 TeV pp collisions. This study is part of a broad program on the implications of LHC results for the MSSM through scans of the pMSSM. A detailed description of the software tools employed is given in [4]. We mention here only the software tools most relevant to this study. SUSY spectra are generated with `SOFTSUSY` [5]. The widths and decay branching fractions of SUSY particles are computed using `SDECAY` [6]. The dark matter relic density is calculated with `SuperIso Relic` [7], which provides us also with the flavour observables, and is described in Appendix A. `MicrOMEGAs` [8] is

used to compute neutralino-nucleon scattering cross-sections. Corrections to the Z^0 electroweak observables are calculated analytically. We perform flat scans of the 19 pMSSM parameters within the ranges summarised in Table 2.1. For this study, over 50 million pMSSM points have been generated in total.

Parameter	Range
$\tan\beta$	[1, 60]
M_A	[50, 2000]
M_1	[-2500, 2500]
M_2	[-2500, 2500]
M_3	[50, 2500]
$A_d = A_s = A_b$	[-10000, 10000]
$A_u = A_c = A_t$	[-10000, 10000]
$A_e = A_\mu = A_\tau$	[-10000, 10000]
μ	[-3000, 3000]
$M_{\tilde{e}_L} = M_{\tilde{\mu}_L}$	[50, 2500]
$M_{\tilde{e}_R} = M_{\tilde{\mu}_R}$	[50, 2500]
$M_{\tilde{\tau}_L}$	[50, 2500]
$M_{\tilde{\tau}_R}$	[50, 2500]
$M_{\tilde{q}_{1L}} = M_{\tilde{q}_{2L}}$	[50, 2500]
$M_{\tilde{q}_{3L}}$	[50, 2500]
$M_{\tilde{u}_R} = M_{\tilde{c}_R}$	[50, 2500]
$M_{\tilde{t}_R}$	[50, 2500]
$M_{\tilde{d}_R} = M_{\tilde{s}_R}$	[50, 2500]
$M_{\tilde{b}_R}$	[50, 2500]

Table 2.1: pMSSM parameter ranges adopted in the scans (in GeV when applicable).

Event generation of inclusive SUSY samples in *pp* collisions is performed with `PYTHIA` [9]. Cross sections for *pp* collisions are rescaled to their NLO values by the k-factors obtained with `Prospino` [10]. LHC generated events are passed through fast detector simulation using `Delphes` [11] tuned for the CMS detector. The event reconstruction follows the procedure of the CMS SUSY analyses as discussed in [4].

2.2 Constraints

To constrain the pMSSM parameter space, we apply different limits, from cosmological data, flavour physics, electroweak data, and collider searches.

2.2.1 Dark Matter

Dark matter constraints arise from the relic density determination, $\Omega_{\rm CDM}h^2$, mostly from the analysis of the WMAP data [12], and from direct detection experiments. For the relic density, we consider two intervals: the tight WMAP bound of $0.068< \Omega_\chi h^2 < 0.155$ which includes the theoretical uncertainties. We study also the effects of a loose limit where we request that the neutralino contribution, $\Omega_\chi h^2$, is non zero and below, or equal to, the upper limit set by the WMAP result: $10^{-4} < \Omega_\chi h^2 < 0.155$. This leaves the possibility of other sources of dark matter alongside the lightest neutralino.

The results of dark matter direct detection experiments are more problematic. The claims from the experiments reporting an excess of events compatible with the signal of a light WIMP must be confronted with the limits obtained by XENON [1] and CDMS [2], which has also performed analyses relaxing the energy cut-off [13] and, more recently, searched for an annual modulation of the event rate [14]. In this study we consider only the XENON limit [1].

2.2.2 Flavour Physics

Flavour physics sets important constraints on the SUSY parameters. We impose bounds from b and c meson decays, which have been discussed in details in [4]. In particular, the decay $B_s^0 \to \mu^+\mu^-$, which can receive extremely large SUSY contributions at large $\tan\beta$ [15], deserves special attention. An excess of events in this channels was reported by the CDF-II collaboration at the Tevatron [16] and upper limits have been set by the LHCb [17] and CMS [18] collaborations at LHC. Recently the LHCb collaboration has presented their latest result for the search of this decay based on 1 fb^{-1} of data. A 95% C.L. upper limit on its branching fraction is set at 4.5×10^{-9} [17], which closely approaches the SM prediction of $(3.53 \pm 0.38) \times 10^{-9}$ for the rate of this process [19]. After accounting for theoretical uncertainties, estimated at the 10% level, the constraint $\mathrm{BR}(B_s^0 \to \mu^+\mu^-) < 5 \times 10^{-9}$ is used in this analysis.

2.2.3 SUSY searches at LEP-2 and Tevatron

The general constraints on SUSY particle masses from direct searches at lower energy colliders are summarised in Table 2.2.

2.2.4 Higgs and SUSY searches at LHC

The searches conducted by ATLAS and CMS on the 7 TeV data have already provided a number of constraints relevant to this study. First, the MET analyses [21, 22] have excluded a fraction of the MSSM phase space corresponding to gluinos below ∼600 GeV and scalar quarks of the first two

Particle	Limits	Conditions
$\tilde{\chi}_2^0$	62.4	$\tan\beta < 40$
$\tilde{\chi}_3^0$	99.9	$\tan\beta < 40$
$\tilde{\chi}_4^0$	116	$\tan\beta < 40$
$\tilde{\chi}_1^\pm$	92.4	$m_{\tilde{\chi}_1^\pm} - m_{\tilde{\chi}_1^0} < 4$ GeV
	103.5	$m_{\tilde{\chi}_1^\pm} - m_{\tilde{\chi}_1^0} > 4$ GeV
$\tilde{e}_R$	73	
$\tilde{e}_L$	107	
$\tilde{\tau}_1$	81.9	$m_{\tilde{\tau}_1} - m_{\tilde{\chi}_1^0} > 15$ GeV
$\tilde{u}_R$	100	$m_{\tilde{u}_R} - m_{\tilde{\chi}_1^0} > 10$ GeV
$\tilde{u}_L$	100	$m_{\tilde{u}_L} - m_{\tilde{\chi}_1^0} > 10$ GeV
$\tilde{t}_1$	95.7	$m_{\tilde{t}_1} - m_{\tilde{\chi}_1^0} > 10$ GeV
$\tilde{d}_R$	100	$m_{\tilde{d}_R} - m_{\tilde{\chi}_1^0} > 10$ GeV
$\tilde{d}_L$	100	$m_{\tilde{d}_L} - m_{\tilde{\chi}_1^0} > 10$ GeV
$\tilde{b}_1$	248	$m_{\tilde{\chi}_1^0} < 70$ GeV, $m_{\tilde{b}_1} - m_{\tilde{\chi}_1^0} > 30$ GeV
	220	$m_{\tilde{\chi}_1^0} < 80$ GeV, $m_{\tilde{b}_1} - m_{\tilde{\chi}_1^0} > 30$ GeV
	210	$m_{\tilde{\chi}_1^0} < 100$ GeV, $m_{\tilde{b}_1} - m_{\tilde{\chi}_1^0} > 30$ GeV
	200	$m_{\tilde{\chi}_1^0} < 105$ GeV, $m_{\tilde{b}_1} - m_{\tilde{\chi}_1^0} > 30$ GeV
	100	$m_{\tilde{b}_1} - m_{\tilde{\chi}_1^0} > 5$ GeV
$\tilde{g}$	195	

Table 2.2: Constraints on the SUSY particle masses (in GeV) from searches at LEP and the Tevatron [20].

generations below ∼400 GeV. These are included using the same analysis discussed in [4], extended to an integrated luminosity of 5 fb^{-1}. Then, the search for the $A^0 \to \tau^+\tau^-$ decay [23,24] has excluded a significant fraction of the (M_A, $\tan\beta$) plane at low values of M_A and large to intermediate values of $\tan\beta$.

In addition ATLAS and CMS reported the discovery of a boson with mass ∼125 GeV [13, 25]. It has in particular important implication on the scalar top mass [26]. Here, we require $123 < M_h < 127$ GeV.

2.3 Current and projected bounds

We consider here four sets of constraints on SUSY parameters. These are i) from direct searches for SUSY particles with MET signatures and ii) from dark matter direct detection experiments, iii) from direct searches for A^0 bosons in the channel $A^0 \to \tau^+\tau^-$ and iv) from the $B_s \to \mu^+\mu^-$ rare decay. These constraints, originating from different sectors of the theory, are all

sensitive to the SUSY parameters most relevant for setting the couplings and decay branching fractions of the light h^0 bosons. Their combination provides the boundary conditions for the parameter space where we test the possible suppression or enhancement of the yields in the LHC Higgs searches. We start from the situation outlined by the current data and project towards the status of these bounds at the time of the completion of the LHC run at the end of 2012, assuming no signal is observed beyond the Higgs signal, except for the $B_s \to \mu^+\mu^-$ decays, for which we assume a branching fraction equal to its SM expectation.

2.3.1 Direct $\tilde{g}$ and $\tilde{q}$ searches at LHC

The direct searches for MET signatures with jets and leptons probe $\tilde{g}$ and $\tilde{q}$ masses up to ∼500 GeV with 1 fb^{-1} and ∼750 GeV with 15 fb^{-1} at 7 TeV [4, 27, 28]. While these are significantly constraining its parameter space, they are hardly decisive in disproving the MSSM as a viable theory. In fact, the gluino and squark masses can be pushed beyond those kinematically accessible in the current LHC run and still the MSSM would have all those features which have made SUSY so popular as SM extension, though at the cost of an increase of the fine tuning parameter.

Figure 2.1 shows the fractions of accepted pMSSM points which are compatible with the results of the CMS analyses in the fully hadronic [21] and in the leptonic channels [29,30] on 1 fb^{-1} and its projection for 15 fb^{-1} at 7 TeV, as a function of the masses of the lightest squark of the first two generations $\tilde{q}_{1,2}$ and of the $\tilde{t}_1$. In the upper left panel of Figure 2.1 we also present the improvement of the sensitivity to scalar quarks of the first two generation for 8 TeV LHC operation. From the results of generic scalar quark searches, which are not optimised for $\tilde{t}$, and dedicated $t\bar{t}$ + MET analyses, as that of ref. [31], 15 fb^{-1} of LHC data should be sensitive to MSSM solutions with light scalar quarks of the third generation with masses ∼300-400 GeV (see also [32]). Sensitivity beyond this mass limit is limited by the small production cross sections and the large backgrounds from top events. On the other hand, after removing pMSSM points excluded by the LHC searches, the acceptance w.r.t. other variables of interest here, such as M_A and $\tan\beta$, is flat, indicating that the gluino and scalar quark searches do not influence the Higgs sector parameters.

2.3.2 Dark matter direct detection experiments

Dark matter direct detection experiments have made great progress exploring $\tilde{\chi}p$ scattering cross sections in the range predicted by the MSSM [1,2]. In particular, the 2011 XENON 100 result [33], places a 90% C.L. upper bound on the spin-independent $\tilde{\chi}p$ cross section around 10^{-8} pb for $M_{\rm WIMP} \simeq$ 100 GeV and excludes ≃20% of the accepted pMSSM points in our scan,

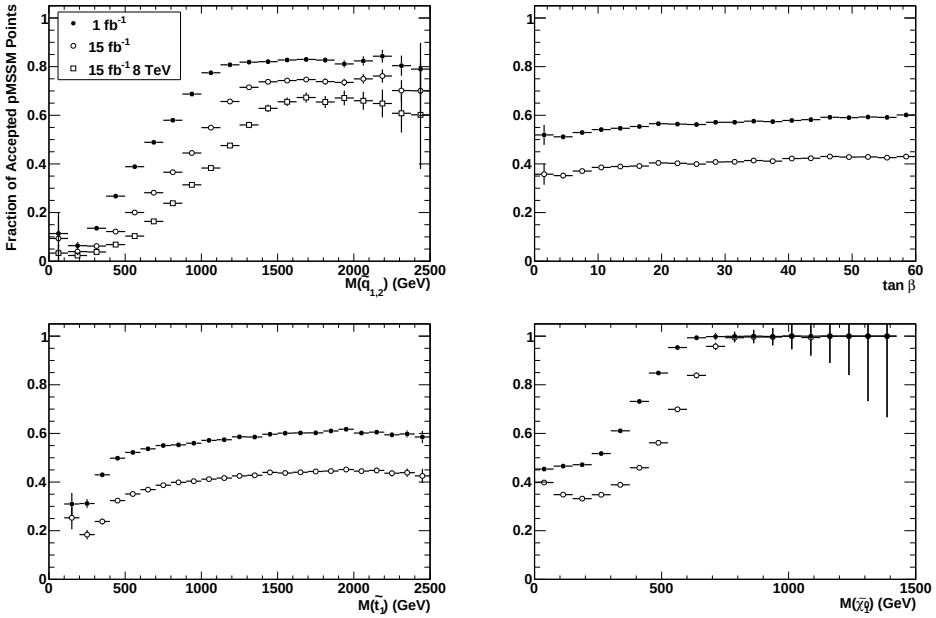

Figure 2.1: Fraction of accepted pMSSM points not excluded by the SUSY searches on 1 (filled circles) and 15 fb^{-1} of LHC data at 7 TeV (open circles) and at 8 TeV (open squares) as a function of the mass of the lightest squark of the first two generations (upper left panel), of the mass of the scalar top $\tilde{t}_1$ (lower left panel), of $\tan\beta$ (upper right panel) and of the mass of the lightest neutralino $\tilde{\chi}_1^0$ (lower right panel).

while the 2012 bound [1] excludes $\simeq$50% of the accepted pMSSM scan points within our scan range. The $\tilde{\chi}p$ spin-independent scattering process has contributions from scalar quark exchange and t-channel Higgs exchange [34]. The latter dominates over a vast region of the parameter space with the Higgs coupling to the proton depending on its coupling to gluons, through a heavy quark loop and to non-valence quarks. The scattering cross section retains a strong sensitivity on the CP-odd boson mass as highlighted in Figure 2.2 which shows the pMSSM points retained after the 2011 XENON 100 and 2012 XENON 100 data. The 2012 data excludes all solutions with $M_A \lesssim$ 200 GeV, independent on the value of $\tan\beta$.

2.3.3 Direct $A^0 \to \tau^+\tau^-$ searches at LHC

The result of the direct search for the A^0 boson at the LHC is a very constraining piece of information on the $(M_A, \tan\beta)$ plane. The CMS collaboration has presented the results of a search for neutral Higgs bosons decaying into τ pairs based on 1.1 fb^{-1} of integrated luminosity [35] and recently re-

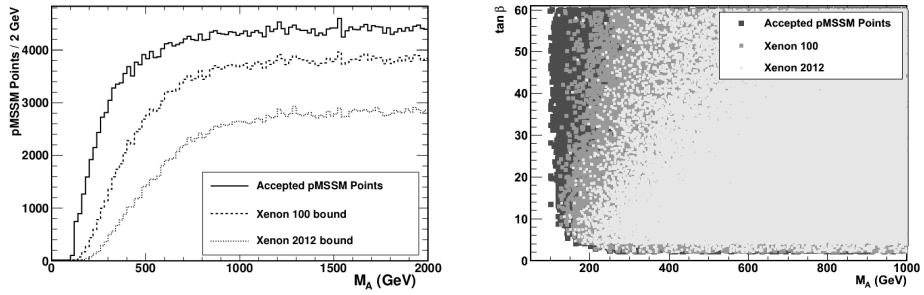

Figure 2.2: Distribution of pMSSM points after the dark matter direct detection constraint projected on the M_A (left panel) and $(M_A, \tan\beta)$ plane (right panel) for all accepted pMSSM points (medium grey), points not excluded by the 2011 XENON-100 data (dark grey) and by the 2012 XENON-100 data (light grey).

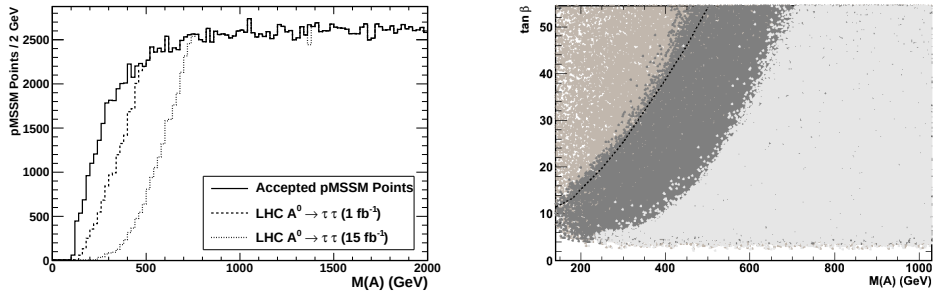

Figure 2.3: Distribution of pMSSM points after the $A^0 \to \tau^+\tau^-$ search projected on the M_A (left panel) and $(M_A, \tan\beta)$ plane (right panel) for all accepted pMSSM points (medium grey), points not excluded with 1 fb^{-1} of data (dark grey) and the projection for the points not excluded with 15 fb^{-1} of data (light grey). The dashed line on the $(M_A, \tan\beta)$ plot indicates the 95 % C.L. limit derived by CMS in the M_h-max scenario with $M_{\text{SUSY}} =$ 1 TeV for 1.1 fb^{-1}.

ported an update based on the analysis of 4.6 fb^{-1} [25, 36]. The search not revealing any significant excess of events, limits on the product of production cross section and decay branching fraction as a function of the boson mass, corresponding to the 95% C.L. expected bound are given in [37]. In order to map these bounds on the $(M_A, \tan\beta)$ plane for the pMSSM and project them to 15 fb^{-1} of data, we compute the product of production cross section and decay branching fraction into τ pairs for the A^0 for each accepted pMSSM point. First we validate our procedure by taking the contour of the points

having this product equal to that corresponding to the CMS expected limit. The right panel of Figure 2.3 shows this region for pMSSM points compared to the published CMS contour. These agree within 15%. Then, we rescale the product to reproduce the projected limit for 15 fb^{-1} and remove the points which can be excluded if no signal is observed. Figure 2.3 shows the points surviving this selection in the M_A and $(M_A, \tan\beta)$ parameter space. We note that the 2012 data should severely constrain the low M_A scenario by removing all solutions with $M_A < 220$ GeV and restricting the region with $M_A < 400$ GeV to $\tan\beta$ values below 10. However, a tiny region with $220 < M_A < 350$ GeV survives for $\tan\beta \simeq 5$.

2.3.4 $B_s^0 \to \mu^+\mu^-$ at LHC

The decay $B_s \to \mu^+\mu^-$ is very sensitive to the presence of SUSY particles. At large $\tan\beta$, the SUSY contribution to this process is dominated by the exchange of neutral Higgs bosons, and very restrictive constraints can be obtained on the supersymmetric parameters [15]. Indeed, the couplings of the neutral Higgs bosons to b quark and muons are proportional to $\tan\beta$, which can lead to enhancement of orders of magnitude compared to the SM value, which is helicity suppressed.

The $B_s \to \mu^+\mu^-$ decay has been searched for at the Tevatron and the LHC. The CDF experiment has reported an excess of events corresponding to a branching fraction of $(1.8^{+1.1}_{-0.9})\times10^{-8}$ [38]. The LHCb, ATLAS and CMS collaborations did not observe any significant excess and released recently a 95% C.L. combined limit of $\mathrm{BR}(B_s \to \mu^+\mu^-) < 4.2 \times 10^{-9}$ [39], which is about 20% above the SM, while the 2011 combined CMS and LHCb results was $\mathrm{BR}(B_s \to \mu^+\mu^-) < 1.1 \times 10^{-8}$ [40], about 4 times above the SM predictions.

We compared our accepted pMSSM points to the CMS+LHCb 2011 result, as well as to the projected constraint in the case of observation of the decay with a SM-like rate of $\mathrm{BR}(B_s \to \mu^+\mu^-) = (3.4 \pm 0.7)\times10^{-9}$, to which we have attached a 20% total relative uncertainty, by the end of the 2012 run. The results are presented in Figure 2.4 in the M_A and $(M_A,$ $\tan\beta)$ planes. The previous limit affects the low M_A values up to 700 GeV, excluding large $\tan\beta$ values, below $M_A \sim$200 GeV. The projected constraint has a stronger impact, with more than half of the spectrum being excluded for $M_A \lesssim 700$ GeV. However, the low $\tan\beta$ region at $\tan\beta \sim 5$ remains largely unaffected also by this constraint.

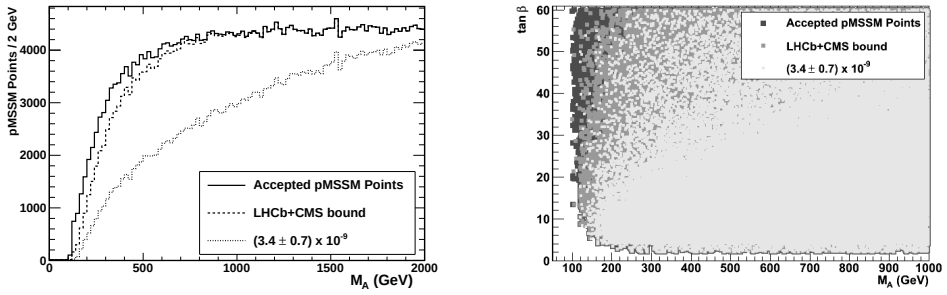

Figure 2.4: Distribution of pMSSM points after the $B_s \to \mu^+\mu^-$ constraint projected on the M_A (left panel) and $(M_A, \tan\beta)$ plane (right panel) for all accepted pMSSM points (medium grey), points not excluded by the combination of the 2011 LHCb and CMS analyses (dark grey) and the projection for the points compatible with the measurement of the SM expected branching fractions with a 20% total uncertainty (light grey).

2.4 Consequences of the discovery of the h^0 boson at LHC

The ATLAS and CMS experiments have recently announced the discovery of a SM-like Higgs boson with a mass value of ∼125 GeV [25,36]. We consider the effect of the observation of a Higgs boson with a mass in the range $123 < M_h < 127$ GeV.

The determination of the mass of the lightest Higgs boson with an accuracy of order of one GeV places some significant constraints on the SUSY parameters, in particular in the typical mixing scenario, where its central value corresponds to a mass close to the edge of the range predicted in the MSSM. In order to evaluate these constraints, we select the accepted pMSSM points from our scans, which have $123 < M_h < 127$ GeV. These are ≃20% of the points not already excluded by the LHC SUSY searches with 1 fb^{-1} in our scan, where parameters are varied in the ranges given in the central column of Table 2.1.

Figure 2.5 shows the points fulfilling these conditions, which are also allowed by the other 2011 data constraints and by the 2012 projection. The parameter space is defined by three combinations of variables: M_A – $\tan\beta$, M_A – $M_{\tilde{\chi}^0_1}$ and M_A – $M_{\tilde{q}_3}$, where $M_{\tilde{q}_3}$ is the minimum of the masses of the $\tilde{t}_1$ and $\tilde{b}_1$ squarks. We observe that imposing the value of M_h selects a broad wedge in the (M_A, $\tan\beta$) plane, at rather heavy A^0 masses and moderate to large values of $\tan\beta$ and extending beyond the projected sensitivity of the searches in the $A^0 \to \tau^+\tau^-$ but also that of direct DM detection and would be compatible with a SM-like value for the rate of the $B^0_s \to \mu^+\mu^-$

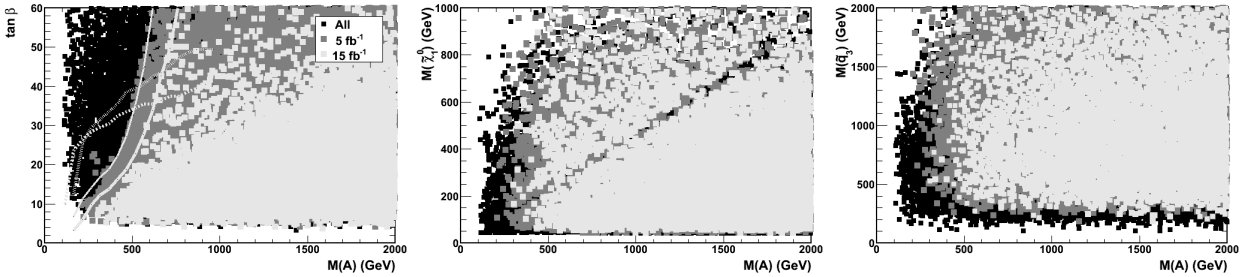

Figure 2.5: pMSSM points in the $(M_A,\ \tan\beta)$ (left panel), $(M_A,\ M_{\tilde{\chi}_1^0})$ (centre panel) and $(M_A,\ M_{\tilde{q}_3})$, where $M_{\tilde{q}_3}$ is the minimum of the masses of the $\tilde{t}_1$ and $\tilde{b}_1$ squarks, (right panel) parameter space, giving $123 < M_H < 127$ GeV. The different shades of grey show all the valid pMSSM points without cuts (black) and those fulfilling the Higgs mass cut allowed by the 2011 data (dark grey) and by the projected 2012 data (light grey), assuming no signal beyond the lightest Higgs boson is observed. The lines in the left plot show the regions which include 90% of the scan points for the $A \to \tau^+\tau^-$ and $B_s \to \mu^+\mu^-$ decays at the LHC and the dark matter direct detection at the XENON experiment. The narrow corridor along the diagonal in the $(M_A,\ M_{\tilde{\chi}_1^0})$ plane corresponds to the A^0 funnel region where the $\chi\chi \to A$ annihilation reduces $\Omega_\chi h^2$ below the accepted range.

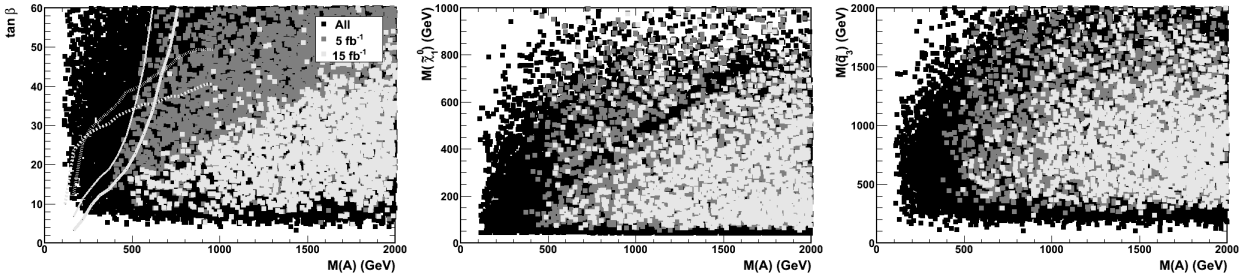

Figure 2.6: pMSSM points in the parameter planes $(M_A,\ \tan\beta)$ (left panel), $(M_A,\ M_{\tilde{\chi}_1^0})$ (centre panel) and $(M_A,\ M_{\tilde{q}_3})$ (right panel), where $M_{\tilde{q}_3}$ is the minimum of the masses of the $\tilde{t}_1$ and $\tilde{b}_1$ squarks, giving $123 < M_h < 127$ GeV, after imposing the additional requirements on the Higgs rates. The color coding is the same as for Figure 2.5.

decay. Next, we impose the condition that the yields in the $\gamma\gamma$, W^+W^- and Z^0Z^0 final states reproduce the observed rates of events reported by the ATLAS and CMS collaborations. We require that $1 \leq R_{\gamma\gamma} < 3$ and $0.3 < R_{W^+W^-/Z^0Z^0} < 2.5$. The points fulfilling these constraints are shown

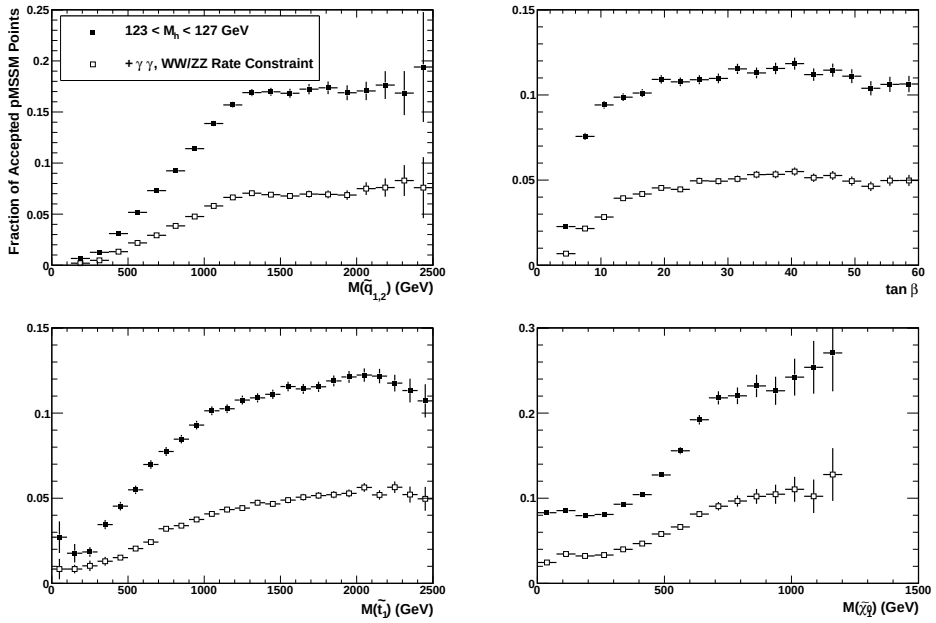

Figure 2.7: Fraction of accepted pMSSM points, with $123 < M_h < 127$ GeV (filled squares), not excluded by the SUSY searches with 15 fb^{-1} of 7 TeV data as a function of the mass of the lightest squark of the first two generations (upper left panel), of the mass of the scalar top $\tilde{t}_1$ (lower left panel), of $\tan\beta$ (upper right panel) and of the lightest neutralino $\tilde{\chi}_1^0$ (lower right panel). The open square points show the fraction of pMSSM points after imposing the additional requirements on the Higgs rates.

in Figure 2.6. Here, we observe that the wedge in the (M_A, $\tan\beta$) plane is further restricted and solutions with $M_{\chi_1^0} > M_A$ are also strongly suppressed.

The effect of the Higgs constraints on some pMSSM parameters is shown in Figure 2.7, in terms of the fraction of valid pMSSM points, fulfilling the general requirements discussed in Section 2, those from searches by the end of 2012 and giving $123 < M_h < 127$ GeV. In particular, a comparison of Figure 2.7 with Figure 2.1, which differ for the requirements on M_h, shows that values of $\tan\beta \leq 6$ become disfavoured, while the masses of scalar quarks are not significantly affected. Imposing the condition that the yields in the $\gamma\gamma$, W^+W^- and Z^0Z^0 final states are consistent with the observed rates of candidate Higgs events reduces the fraction of accepted points preferentially at large masses of $\tilde{t}_1$, $\tilde{q}_{1,2}$ and $\tilde{\chi}_1^0$.

In order to estimate the effect of the program used for computing the h^0 mass and decay branching fractions, we repeat the analysis using `FeynHiggs` and compare the results. We observe that 20.1% and 25.2% of the accepted pMSSM points in our scan have Higgs mass in the range $123 < M_h <$

127 GeV using `SoftSUSY` and `FeynHiggs`, respectively. Of these 12% have $R_{\gamma\gamma} \geq 1$ using `HDECAY` and 7.2% using `FeynHiggs`.

Finally, we compute the fine tuning parameter Δ, using the definition of ref. [41], for the points in the accepted Higgs mass range and for those having also the γ, WW and ZZ rates within the constraints used above, and find that 20.6% and 18.4% of them have $\Delta < 100$.

Bibliography

[1] E. Aprile *et al.* (XENON100 Collaboration), arXiv:1207.5988.

[2] Z. Ahmed, et al. (CDMS-II Collaboration), Science **327**, 1619 (2010).

[3] A. Djouadi, et al., hep-ph/9901246.

[4] A. Arbey, M. Battaglia, F. Mahmoudi, Eur. Phys. J. **C72**, 1847 (2012).

[5] B. C. Allanach, Comput. Phys. Commun. **143**, 305 (2002).

[6] M. Muhlleitner, A. Djouadi, Y. Mambrini, Comput. Phys. Commun. **168**, 46 (2005).

[7] F. Mahmoudi, Comput. Phys. Commun. **178**, 745 (2008); F. Mahmoudi, Comput. Phys. Commun. **180**, 1579 (2009); A. Arbey, F. Mahmoudi, Comput. Phys. Commun. **181**, 1277 (2010).

[8] G. Belanger, F. Boudjema, A. Pukhov, et al., Comput. Phys. Commun. **180**, 747 (2009).

[9] T. Sjostrand, S. Mrenna, P. Z. Skands, JHEP **05**, 026 (2006).

[10] W. Beenakker, R. Hopker, M. Spira, hep-ph/9611232.

[11] S. Ovyn, X. Rouby, V. Lemaitre, arXiv:0903.2225.

[12] E. Komatsu, et al. (WMAP Collaboration), Astrophys. J. Suppl. **192**, 18 (2011).

[13] Z. Ahmed, et al. (CDMS-II Collaboration), Phys. Rev. Lett. **106**, 131302 (2011).

[14] Z. Ahmed, et al. (CDMS Collaboration), arXiv:1203.1309.

[15] A. Akeroyd, F. Mahmoudi, D. Martinez Santos, JHEP **1112**, 088 (2011).

[16] T. Aaltonen, et al. (CDF Collaboration), Phys. Rev. Lett. **107**, 239903 (2011).

[17] R. Aaij, et al. (LHCb Collaboration), Phys. Rev. Lett. **108**, 231801 (2012).

[18] S. Chatrchyan, et al. (CMS Collaboration), JHEP **1204**, 033 (2012).

[19] F. Mahmoudi, S. Neshatpour, J. Orloff, JHEP **1208**, 092 (2012).

[20] J. Beringer *et al.* (Particle Data Group Collaboration), Phys. Rev. D **86**, 010001 (2012).

[21] S. Chatrchyan, et al. (CMS Collaboration), Phys. Rev. Lett. **107**, 221804 (2011).

[22] G. Aad, et al. (ATLAS Collaboration), Phys. Lett. B **710**, 67 (2012).

[23] G. Aad, et al. (ATLAS Collaboration), Phys. Lett. **B705**, 174 (2011).

[24] S. Chatrchyan, et al. (CMS Collaboration), Phys. Lett. B **713**, 68 (2012).

[25] G. Aad *et al.* (ATLAS Collaboration), Phys. Lett. B **716**, 1 (2012).

[26] A. Arbey, M. Battaglia, A. Djouadi, et al., Phys. Lett. **B708**, 162 (2012).

[27] J. A. Conley, J. S. Gainer, J. L. Hewett, et al., arXiv:1103.1697.

[28] S. Sekmen, S. Kraml, J. Lykken, et al., JHEP **1202** (2012) 075.

[29] CMS Collaboration, CMS-PAS-SUS-11-010.

[30] CMS Collaboration, CMS-PAS-SUS-11-011.

[31] G. Aad, et al. (ATLAS Collaboration), Phys. Rev. Lett. **108**, 041805 (2012).

[32] M. Papucci, J. T. Ruderman, A. Weiler, JHEP **1209**, 035 (2012).

[33] E. Aprile, et al. (XENON 100 Collaboration), Phys. Rev. Lett. **107**, 131302 (2011).

[34] G. Jungman, M. Kamionkowski, K. Griest, Phys. Rept. **267**, 195 (1996).

[35] S. Chatrchyan, et al. (CMS Collaboration), Phys. Rev. Lett. **106**, 231801 (2011).

[36] S. Chatrchyan *et al.* (CMS Collaboration), Phys. Lett. B **716**, 30 (2012).

[37] CMS Collaboration, CMS-PAS HIG-11-009.

[38] T. Aaltonen, B. Álvarez González, S. Amerio, et al. (CDF Collaboration), Phys. Rev. Lett. **107**, 191801. (2011)

[39] ATLAS, CMS and LHCb Collaborations, LHCb-CONF-2012-017, CMS-PAS-BPH-12-009, ATLAS-CONF-2012-061.

[40] CMS and LHCb Collaborations, LHCb-CONF-2011-047, CMS-PAS-BPH-11-019.

[41] M. Perelstein, C. Spethmann, JHEP **04**, 070 (2007).

Chapter 3

Light neutralino dark matter

The possibility that the LSP mass is much smaller than the electroweak scale, is put forward by three dark matter direct detection experiments, which have reported a possible signal of WIMP interaction corresponding to very light particles, $5 < M_{\rm CDM} < 15$ GeV close to the edge of the XENON-100 and CDMS sensitivity [1, 2]. These are the DAMA experiment [3, 4] at the Laboratory Nazionali del Gran Sasso, Italy, the CoGENT experiment [5, 6] in the Soudan mine and the CRESST experiment [7], also at Gran Sasso. While there is still substantial debate on the interpretation of these data and the compatibility of the reported results with the exclusion bounds established by the CDMS and XENON experiments [8] an agreement could only be possible in the low neutralino mass region. Therefore it is interesting to explore the feasibility of light neutralino solutions in generic SUSY models and their compatibility with the results of the LEP and LHC searches.

Here we consider SUSY scenarios with the lightest neutralino mass in the range $5 < M_{\chi_1^0} < 40$ GeV in the 19-parameter pMSSM model [9]. The use of the pMSSM enables us to access scenarios which are not available in constrained SUSY models, such as the CMSSM.

There have been already several studies of the SUSY parameter space with light neutralinos [10]. They considered either a constrained MSSM scenario or more generic analyses in effective MSSM scenarios where gaugino masses are not unified at the GUT scale. In addition, analyses within the NMSSM scenarios were also performed [11]. Compared to those studies we consider here a broader phase space of parameters and study for the first time the light neutralinos in the pMSSM in its full glory with 19 free parameters. In particular, we do not assume degenerate masses for the right and left handed squarks, contrary to the previous work. By this choice, different squark mixings are allowed and scenarios with light squarks and reduced couplings to the Z^0 boson can be realised in our scans of the parameter space. This study reveals therefore scenarios not yet identified in the earlier work. We employ a large statistics of more than 500 M pMSSM points

Parameter	Range
$\tan\beta$	[1, 60]
M_A	[50, 2000]
M_1	[-300, 300]
M_2	[-650, 650]
M_3	[0, 2500]
$A_d = A_s = A_b$	[-10000, 10000]
$A_u = A_c = A_t$	[-10000, 10000]
$A_e = A_\mu = A_\tau$	[-10000, 10000]
μ	[-3000, 3000]
$M_{\tilde{e}_L} = M_{\tilde{\mu}_L}$	[0, 2500]
$M_{\tilde{e}_R} = M_{\tilde{\mu}_R}$	[0, 2500]
$M_{\tilde{\tau}_L}$	[0, 2500]
$M_{\tilde{\tau}_R}$	[0, 2500]
$M_{\tilde{q}_{1L}} = M_{\tilde{q}_{2L}}$	[0, 2500]
$M_{\tilde{q}_{3L}}$	[0, 2500]
$M_{\tilde{u}_R} = M_{\tilde{c}_R}$	[0, 2500]
$M_{\tilde{t}_R}$	[0, 2500]
$M_{\tilde{d}_R} = M_{\tilde{s}_R}$	[0, 2500]
$M_{\tilde{b}_R}$	[0, 2500]

Table 3.1: pMSSM parameter ranges adopted in the scans (in GeV when applicable).

for a generic scan and more than 500 M extra points for specific scans, and impose the latest constraints from the LHC data, including those from Higgs and monojet searches. In particular, in view of the discovery of a scalar boson compatible with the SM-Higgs [12, 13], we study the effect of a Higgs boson in the range $122.5 < M_h < 127.5$ GeV. We use a realistic simulation, validated on the results of full simulation and reconstruction to study the phenomenology of these scenarios and the response of the standard SUSY searches on 5 fb^{-1} of data at 7 TeV [14].

3.1 The pMSSM Phase Space with light neutralino LSP

The technics employed here to study the pMSSM parameter space with light neutralinos is very similar to the one described in Chapter 2. We perform flat scans of the 19 pMSSM parameters within the ranges summarised in Table 3.1. For this analysis, over one billion pMSSM points have been generated in total.

In addition to the programs described in Section 2.1, event generation of inclusive SUSY samples in e^+e^- and pp collisions is performed with `PYTHIA` [15]. Samples of e^+e^- events are reconstructed at generator level to assess their observability at LEP-2. Hadronic jets are clustered using the `PYCLUS` algorithm with $d_{join} = 2.5$ GeV.

3.1.1 Constraints

To constrain the pMSSM parameter space, we apply the same limits as in Section 2.2, as well as some specific constraints described below.

Dark Matter

In addition to the relic density constraint described in Section 2.2.1, here we take into consideration the claims from the DAMA [3,4], CoGENT [5,6] and CRESST [7] experiments reporting an excess of events compatible with the signal of a light WIMP and we accept pMSSM points with $5 \leq M_{\chi_1^0} < 40$ GeV and $10^{-7} < \sigma_{\chi p}^{\rm SI} < 10^{-3}$ pb, in order to be in the region where data could be reconciled with the XENON and CDMS limits [1,2].

Other cosmological bounds can come from indirect detection signatures, but they are subject to large cosmological and astrophysical uncertainties. We do not impose them as a constraints in the analysis but we comment on the consequences of the Fermi-LAT results [17] in Section 3.1.2.

Electroweak data

The precision Z^0 line-shape and other electroweak observables place serious constraints on light SUSY particles. In particular, the accurate measurements of the Z^0 total width and its partial decay widths obtained at LEP provide a tight bound to the contribution from new particles with mass below $M_{Z^0}/2$. The scenarios considered here with light χ_1^0 are constrained from the neutralino contribution to the Z^0 invisible width. We compute the SM Z^0 total width and that into neutrinos using `ZFitter` [18] for the input parameter ranges $115 < M_H < 145$ GeV, $M_{\rm top} = (172.9 \pm 1.1)$ GeV and $\alpha_s(M_Z^2) = 0.1184 \pm 0.0007$. We obtain a SM Z^0 total width $\Gamma_{\rm tot} = (2494.83 \pm 0.54)$ MeV and invisible width $\Gamma_{\rm inv} = (501.62 \pm 0.10)$ MeV, where the uncertainty reflects the range of values used for the input parameters. These have to be compared to the average of LEP measurements giving (2495.2 ± 2.3) and (499.0 ± 1.5) MeV, respectively. We exclude light neutralinos with a contribution to the Z^0 invisible width larger than 3 MeV. This restricts the acceptable points to those where the $\tilde{\chi}_1^0$ is bino-like and its contribution to the Z^0 width, Γ_χ, is negligible so that it can evade the LEP electroweak bounds and corresponds to relatively large values of the higgsino mass parameter $|\mu|$.

The Z^0 total width constrains the masses of the lightest chargino, $\tilde{\chi}_1^{\pm}$, and of the squarks of the first two generations, $\tilde{q}$, to be above 45 GeV. Squarks of the third generation can evade these constraints for specific values of their $\theta_{\tilde{q}}$ angle in the mass mixing matrix, corresponding to a vanishing Z^0 coupling, $I_3^q \cos^2\theta_{\tilde{q}} - Q_{\tilde{q}} \sin^2\theta_W$. We also compute the $\tilde{b_1}\bar{\tilde{b}}_1$ contribution to the Z^0 width for each generated pMSSM points and require it to be smaller than 5 MeV, to satisfy the hadronic Z^0 width limits.

SUSY searches at LEP-2 and Tevatron

We appy the general constraints on SUSY particle masses from direct searches at lower energy colliders given in the Section 2.2.3. However, we note that constraints from SUSY searches at LEP-2 and Tevatron can be evaded in case of small mass splittings with the lightest neutralino, corresponding to low energy, or transverse energy, released in the detector or to vanishing couplings. Since these are crucial for assessing the viability of several of the small mass splitting solutions highlighted in this study, we explicitly study the detectability of the points fulfilling our selection criteria. For each point we generate an inclusive SUSY sample of 10k events in e^+e^- collisions at $\sqrt{s} = 208$ GeV and apply the LEP-2 reconstruction and selection criteria of the analyses of [19]. First, we consider the $\chi_1^+\chi_1^-$ and $\chi_2^0\chi_1^0$ channels and adopt the SM backgrounds estimated in the original analyses for these channels. We compute the cross sections and the number of signal events passing the selection criteria. We compare these cross sections to the minimum excluded value as a function of $M_{\chi_1^{\pm}}$ and $\Delta M = M_{\chi_1^{\pm}} - M_{\chi_1^0}$ from the final combination of the LEP-2 results. We reject points which give a cross section in excess to that excluded by the combined LEP-2 data for the same ΔM and a number of selected signal events larger than the SM background. A first estimate indicates that chargino masses smaller than 40 GeV are excluded by LEP data, independently from ΔM. Therefore, we impose the constraint $M_{\chi_1^{\pm}} > 40$ GeV in the following, and we will analyse a posteriori the exclusion of the points passing all the other constraints.

Then, we consider the $\tilde{b}_1\bar{\tilde{b}}_1$ channel for small $\Delta M = M_{\tilde{b}_1} - M_{\chi_1^0}$ values. We simulate $e^+e^- \to \tilde{b}_1\bar{\tilde{b}}_1$ at $\sqrt{s} = 208$ GeV for each point fulfilling our cuts. Again, we compare the production cross section to the minimum value excluded by the combination of the results of the LEP-2 experiments as a function of ΔM and reject points with cross sections in excess to this value.

Monojet and monophoton searches at LHC

The results of the searches for monojets and isolated photons [20] can be used to set constraints on the quark-neutralino couplings and thus on the χp scattering cross-sections [21, 22]. In particular, the constraints derived for the spin-dependent cross-sections are more severe than those from direct

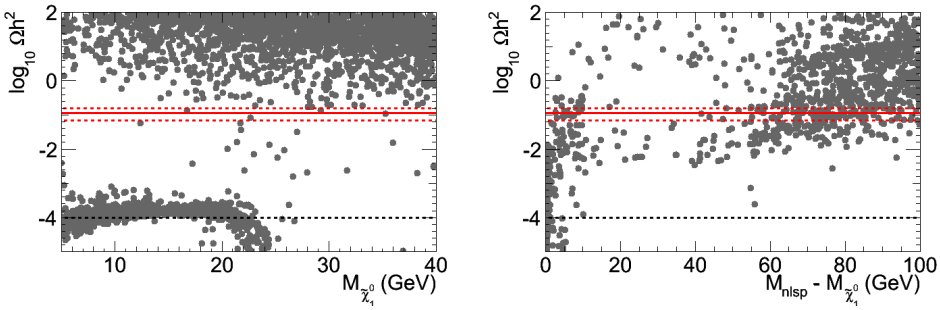

Figure 3.1: Relic density in function of the $\tilde{\chi}_1^0$ mass (left panel) and NLSP mass (right panel). All the points in these plots pass the constraints described in section 3.1.1. The continuous red line corresponds to the WMAP dark matter central values, and the dashed red lines to the upper and lower limits that we impose. The dashed black line corresponds to the lower limit that we use when relaxing the lower WMAP constraint.

detection experiments. Contrary to dark matter direct searches, the collider limits do not depend on astrophysical assumptions, such as the inferred local density of dark matter, which suffers from large uncertainties.

Here we apply the constraints on both spin-dependent and spin-independent $\sigma_{\chi p}$ from the LHC searches to our pMSSM points.

3.1.2 Allowed Regions

We select the valid pMSSM points fulfilling the requirements discussed above; in particular the light neutralino mass in the range $5 < M_{\tilde{\chi}_1^0} < 40$ GeV, relic dark matter density as given in section 3.1.1 and spin-independent scattering cross-section $10^{-7} < \sigma_{\chi p}^{\mathrm{SI}} < 10^{-3}$ pb.

In general, for such a light LSP the relic density is larger than the upper relic density constraint, as shown in Fig. 3.1. However, if the mass difference between the next lightest supersymmetric particle (NLSP) and the LSP, ΔM, is small enough, the relic density is strongly decreased by the coannihilations of the two particles in the early universe and $\Omega_\chi h^2$ can even fall below the lower limit applied for this study. pMSSM points compatible with the relic density constraint have values of the ΔM mass splitting of just a few GeV. The situation for the scattering cross-section is reversed: most of the selected pMSSM points have small scattering cross-sections, as shown in Fig. 3.2. In order to increase it up to the values highlighted by the direct search experiments claiming a light WIMP signal, $\sigma_{\chi p}^{\mathrm{SI}} \sim 10^{-6}$ pb, we have to require ΔM values below 1 GeV, which corresponds to a requirement opposite to that found for the relic density. Therefore, we can respect all the constraints imposed on the pMSSM points with light neutralinos only

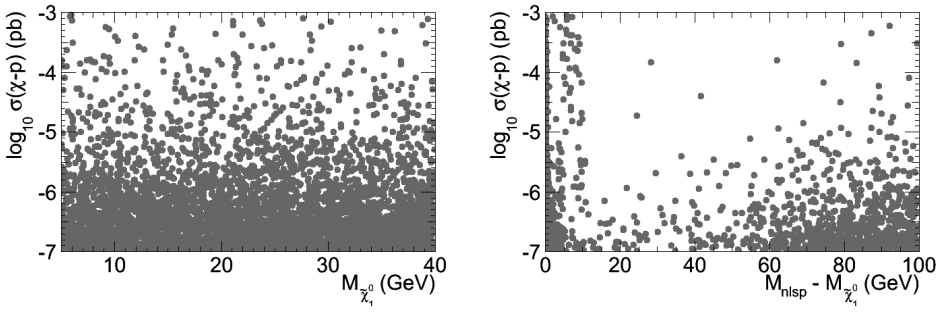

Figure 3.2: Spin independent χ-p scattering cross-section as a function of the $\tilde{\chi}_1^0$ mass (left panel) and NLSP mass (right panel). All the points in these plots pass the constraints described in section 3.1.1.

for few, very specific scenarios.

The effect of the collider data, SUSY and monojet searches, flavour and electroweak constraints, on the pMSSM points generated with our scan is shown in Fig. 3.3. The collider constraints decrease the number of points without significantly modifying their distribution in the $M_{\tilde{\chi}_1^0} - \sigma_{\chi p}^{SI}$ space. However, the electroweak constraints have a significant impact in removing points at large scattering cross-sections, especially for larger values of the neutralino mass. The constraints from Higgs searches alone is shown in Fig. 3.4. Again, the Higgs mass constraint reduces the number of points, but does not modify their overall distribution. Using the points from the generic pMSSM scan, we find 20 and 5 points passing all the selections in the region of interest, for the loose and tight WMAP constraints, respectively. The effect of the various selection criteria on the number of scan points retained is summarised in Table 3.2. The relic density constraint in this region of the parameter space is rejecting a particularly large fraction of pMSSM points. This underscores the difficulty to harmonise the large scattering cross-section corresponding to the possible light WIMP signals and the WMAP results discussed above. In order to improve the statistics for specific scenarios, we perform specific scans within restricted parameter sets starting from the points passing the relic density constraints. We identify three distinct classes of pMSSM solutions: i) the NLSP is a slepton slightly above the LEP limit, with a neutralino of about 30 GeV ii) the lightest chargino is degenerate with the $\tilde{\chi}_1^0$, often with a compressed gaugino spectrum and light Higgs bosons and iii) a scalar quark is degenerate with the $\tilde{\chi}_1^0$ while other scalar quarks and leptons are relatively heavy. Given the Higgs mass constraints, the possible light squarks for class iii) are those of the first and second generations or the lightest scalar bottom quark, $\tilde{b}_1$.

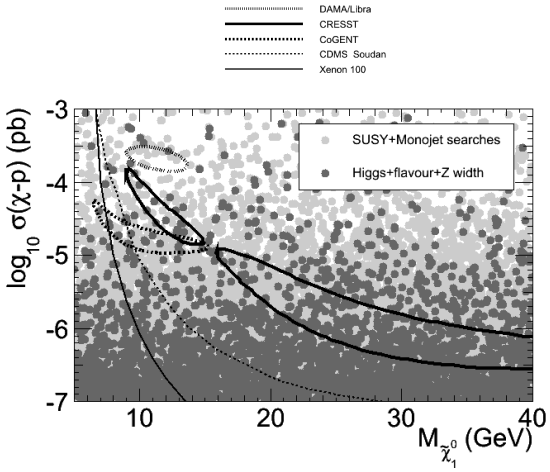

Figure 3.3: Spin independent χ-p scattering cross-section as a function of the $\tilde{\chi}_1^0$ mass. The light gray points are consistent with the direct and monojet search limits (Higgs searches excluded). The dark gray points pass the constraints from flavour physics, the Z decay constraints, and the Higgs mass limit $122.5 < M_h < 127.5$ GeV. The thick contour lines correspond to the zones favoured by DAMA, CRESST and CoGENT, and the thin lines to the exclusion limits by CDMS and XENON.

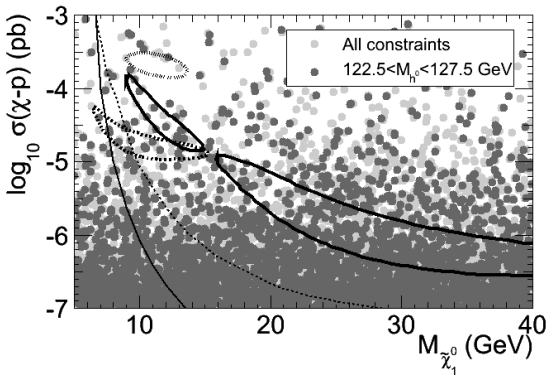

Figure 3.4: Spin independent χ-p scattering cross-section as a function of the $\tilde{\chi}_1^0$ mass. The light gray colour corresponds to the points passing all the constraints presented in Fig. 3.3, except the Higgs mass limit $122.5 < M_h < 127.5$ GeV. The dark gray points also pass the Higgs mass limits. The contour lines are the same as in Fig. 3.3.

$\tilde{\ell}$ NLSP

We consider here the case of points with slepton NSLP. An example of a viable mass spectrum is given in Fig. 3.5. Since the mass limits from LEP-2

Selection	pMSSM points	Selection Efficiency	Cumulative Efficiency
Valid points with light χ_1^0, large $\sigma(\chi p)$	1 M	–	–
Monojet searches	280 k	0.28	0.28
SUSY searches	90 k	0.33	0.09
LEP searches	50 k	0.60	0.05
Flavour physics	20 k	0.37	0.02
Higgs searches	10 k	0.47	0.01
Loose WMAP limit	20	2×10^{-3}	2×10^{-5}
Tight WMAP limit	5	0.25	5×10^{-6}

Table 3.2: Scan statistics for the generic scan.

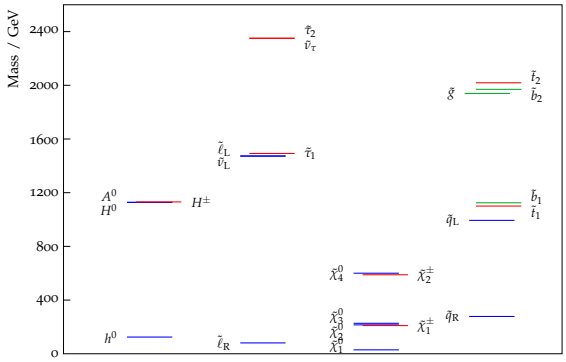

Figure 3.5: Typical mass spectrum corresponding to the slepton NLSP scenario (class i) with $M_{\tilde{\chi}_1^0} = 29.2$ GeV and $M_{\tilde{e}_R,\ \tilde{\mu}_R} = 80.1$ GeV

are higher for left-handed sleptons, right-handed sleptons are favoured by the relic density constraint, which requires a small splitting. Beyond the small mass of the NLSP sleptons, this scenario remains relatively standard. However, a neutralino mass of about at least 20 GeV is needed to accommodate the upper relic density bound, as can be seen from Fig. 3.1, since the ΔM splitting remains relatively large. Therefore, this scenario has only a limited interest corresponding to a region which is inside the exclusion contours by the CDMS and XENON experiments.

We also check the cosmological constraints by considering the indirect detection constraints by Fermi-LAT [17]. The points passing all the constraints have neutralino annihilation cross-sections times relative velocity to $q\bar{q}$ smaller than 2×10^{-30} cm^3/s, which is several orders of magnitude below the current Fermi-LAT limits and makes them compatible also with dark

matter indirect detection limits.

$\tilde{\chi}_1^{\pm}$ NLSP

Next we consider points where the NSLP is the lightest chargino, $\chi_1^{\pm}$ and the ΔM mass splitting is small. This scenario corresponds generally to a compressed gaugino spectrum, with a small splitting between the chargino and neutralino masses. To accommodate the upper bound of the relic density constraint, a mass splitting of a few GeV between the lightest chargino and the lightest neutralino is generally required. As a consequence, the spin independent χ-p scattering cross-section is predicted to be relatively small, of order $10^{-6} - 10^{-7}$ pb. Since this scenario has a small spin independent χ-p scattering cross-section, it is marginal in accommodating the claims for WIMP direct detection and corresponds to a region well inside the CDMS and XENON exclusion curves. Furthermore, the production cross-section of $\chi_1^+\chi_1^-$ and $\chi_2^0\chi_1^0$ in this scenario at LEP-2 is large, 2.5 to 16 pb, and the detection efficiency of the LEP-2 analyses is $\sim$ 0.015 - 0.035, corresponding to about 20 to 250 detected signal events. The cross-section upper limit from the combination of the data of the LEP-2 experiments [23] in this mass region is $\leq$1 pb excluding all the points selected for this scenario.

Light $\tilde{q}_{L,R}$ NLSP

We move over to the case of a scalar quark NLSP with small mass splitting with the lightest neutralino. The upper bound on the relic density constraint imposes a ΔM value of a few GeV. The degenerate squark can be any of the squarks with the exception of the scalar top, since this is required to be heavier to accommodate the h^0 mass range highlighted by the LHC data. This scenario is the most interesting as it can provide us with a large spin independent χ-p scattering cross-section associated to a small neutralino mass (see Fig. 3.9). However, the couplings of the light squark to the Z and h^0 bosons are in general large. In particular, the Z decay width into squarks excludes this scenario, unless the squark decouples from the Z. This happens for specific values of the squark mixing angle. Since the first and second generation squarks do not mix, they are excluded leaving only a degenerate scalar bottom $\tilde{b}_1$ as a viable scenario.

The third generation left-handed squarks have a common mass in the pMSSM and a very light $\tilde{b}_1$ is only possible if the right-handed bottom squark is very light. In this case, the mixing angle θ_b is large, close to $\pi/2$ corresponding to a mainly right-handed $\tilde{b}_1$, and the squark naturally decouples from the Z. The concurrence of a low value of the $\tilde{b}_1$ mass and its decoupling from the Z, through the mixing angle, is shown in Fig. 3.6. In addition, we observe that higher order SUSY corrections further decrease the $\tilde{b}_1$ mass, for appropriate values of the other parameters, producing typi-

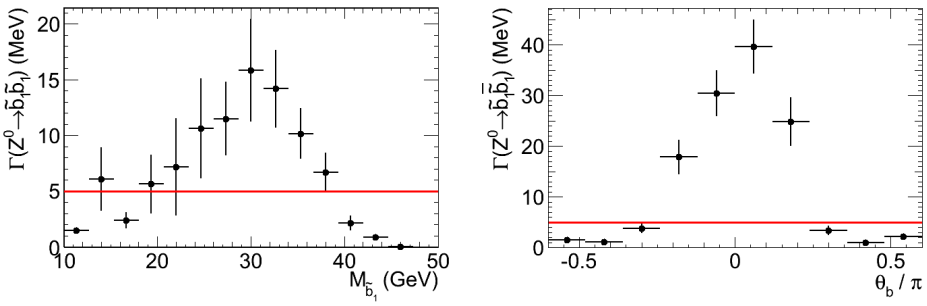

Figure 3.6: Average Z decay width to $\tilde{b}_1\bar{\tilde{b}}_1$ in function of the $\tilde{b}_1$ mass (left panel) and the sbottom mixing angle θ_b (right panel). The horizontal lines correspond to the experimental limit.

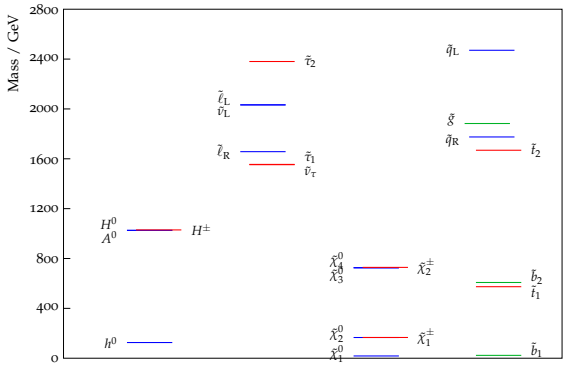

Figure 3.7: Typical mass spectrum corresponding to the light sbottom degenerate with the lightest neutralino (class iii) with $M_{\tilde{\chi}_1^0}$ =18.1 GeV and $M_{\tilde{b}_1}$ = 22.9 GeV

cal spectra as that shown in Fig. 3.7. This "sbottom miracle" makes possible to find pMSSM solutions which reconcile a light neutralino signal at direct detection experiments with the LEP-1 constraints. At LEP-2 the pairs production of these light sbottom pairs has a cross-section of $\simeq$0.2 pb and a selection efficiency of 0.15 – 0.40. The LEP-2 data [24] excludes sbottom pair production with $\tilde{b} \to b\tilde{\chi}^0$ at cross-section values above 0.1 pb in this mass region and therefore rejects points in this scenario unless the ΔM mass splitting between the $\tilde{b}_1$ and the $\tilde{\chi}_1^0$ is smaller, or of the order of, the b quark mass, where the selection efficiency of the LEP-2 analyses drops. In most of cases, the decay $\tilde{b}_1 \to \tilde{\chi}_1^0 b$ is kinematically forbidden. At tree level, the most important open channel is $\tilde{b}_1 \to \tilde{\chi}_1^0\, s$, which is CKM-suppressed and may increase the $\tilde{b}_1$ lifetime up to a value comparable to that of b hadrons.

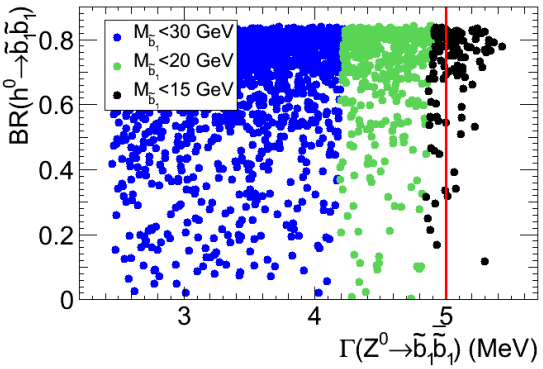

Figure 3.8: h^0 branching fraction to $\tilde{b}_1\bar{\tilde{b}}_1$ as a function of the Z decay width to $\tilde{b}_1\bar{\tilde{b}}_1$ for different values of the lightest sbottom mass.

Furthermore, large QCD corrections can be expected for such a light state, and decay channels with larger decay rate can open up at higher orders, thus decreasing the lifetime.

Considering now this light sbottom and the Higgs boson, we notice that the rate of the decay $h^0 \to \tilde{b}_1\bar{\tilde{b}}_1$ can become important in such scenarios. However, it is possible to find points for which the branching fraction of $h^0 \to \tilde{b}_1\bar{\tilde{b}}_1$ and the Z decay width to $\tilde{b}_1\bar{\tilde{b}}_1$ are simultaneously small. In Fig. 3.8, we show the correlations between the Z decay width and the h^0 branching ratio to two photons. We remark that there is no strong correlations between both decays, and it is possible to have simultaneously a reduced Z decay width to $\tilde{b}_1\bar{\tilde{b}}_1$ and very small h^0 branching fraction to $\tilde{b}_1\bar{\tilde{b}}_1$, even for $\tilde{b}_1$ masses as small as 15 GeV. Moreover, in this scenario, since the neutralino is mainly bino, the h^0 decaying to two light neutralinos is completely suppressed, resulting in an SM-like h^0 decay.

Finally, we check the cosmological constraints by considering the indirect detection constraints by Fermi-LAT [17]. The selected points corresponding to the degenerate $\tilde{b}_1$ scenario have neutralino annihilation cross-sections times relative velocity to $b\bar{b}$ smaller than 5×10^{-27} cm^3/s, which is one order of magnitude below the current Fermi-LAT limits, which makes them compatible also with dark matter indirect detection limits.

In summary, after considering the constraint from the LEP data, the only viable scenario with a neutralino mass below 20 GeV corresponds to the light sbottom NLSP case.

In Fig. 3.9, we present distribution of the points passing the tight relic density bound. Alternatively, in Fig. 3.10, the same distribution is presented in the case where the loose relic density constraint is used.

A comparison of these two figures reveals that the lower bound of the relic

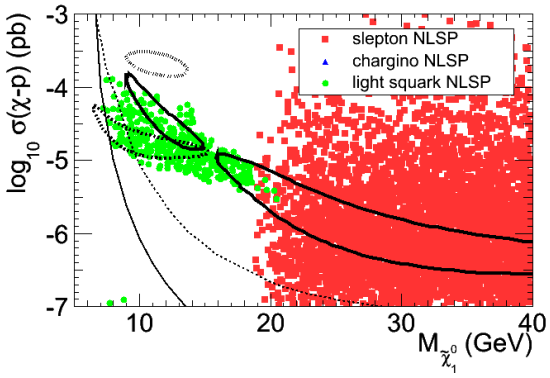

Figure 3.9: Spin independent χ-p scattering cross-section as a function of the $\tilde{\chi}_1^0$ mass. The points presented here pass all the constraints, including the tight relic density bounds. The red squares correspond to a slepton NLSP with a mass slightly above the LEP limits (class i), the blue triangles to scenarios with a chargino NLSP (class ii), and the green points to cases where a scalar quark is degenerate with the light neutralino (class iii).

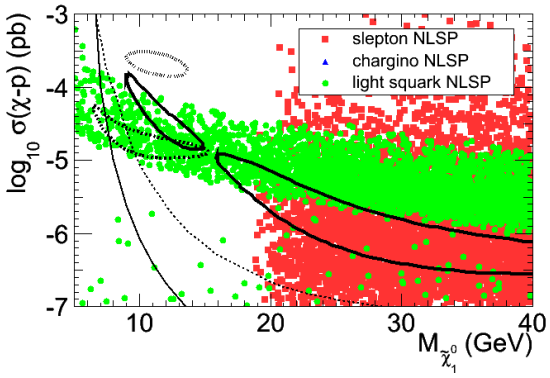

Figure 3.10: Spin independent χ-p scattering cross-section as a function of the $\tilde{\chi}_1^0$ mass. The points presented here pass all the constraints, including the loose relic density bound. The red squares correspond to a slepton NLSP with a mass slightly above the LEP limits (class i), the blue triangles to scenarios with a chargino NLSP (class ii), and the green points to cases where a scalar quark is degenerate with the light neutralino (class iii).

density reduces the overall statistics, but also removes points corresponding to scenarios with a scalar quark degenerate with the light neutralino for neutralino masses above 20 GeV. This can be explained by the fact that points with a very small relic density have a small splitting. However, to get

a relic density in the WMAP interval, the splitting should not be too small relatively to the neutralino mass. Also, the direct search bounds disfavour large splittings. Therefore, combining the relic density and direct search limits, only a small window remains where points can pass all the constraints.

3.1.3 Non-standard scenarios

The calculation of the relic density and the dark matter direct detection constraints rely on many assumptions. In particular, different cosmological scenarios can lead to a relic density which is larger than that computed in the standard cosmological scenario. First, the neutralino could be only one of several dark matter components. Then, if dark energy were the dominant component at the time of the relic freeze-out, it would result in an acceleration of the expansion of the Universe, which would lead to an earlier freeze-out and a much larger relic density [25]. Finally, entropy generation at the time of freeze-out, for example due to the decay of a late inflaton, can also lead to an increase – or a decrease – of the relic density [26]. These effects are however limited by Big-Bang nucleosynthesis constraints, but using AlterBBN [27], that is described in Appendix B, we verified that they can nevertheless lead to an increase of three orders of magnitudes or more of the relic density while still being compatible with BBN constraints.

Similarly to the relic density constraint, the direct detection constraints also rely on several assumptions. In particular, if the neutralino is not the only component of dark matter, or if the local density or velocity of dark matter is widely different from the standard assumptions[1], the constraints in terms of scattering cross-sections can be drastically changed. Therefore, even if the detection of a WIMP particles by a detector would permit to fix its mass, its scattering cross-section with matter would be dependent on large astrophysical uncertainties. The monojet searches at colliders however set constraints on the scattering cross-sections without suffering from astrophysical uncertainties.

With these considerations, it is worth considering the results that we obtain by relaxing the relic density constraint. Fig. 3.11 shows the different classes of points which pass all the constraints, without applying the relic density limits. The three classes described above are well represented. In particular, the scenarios with degenerate squarks and sleptons are now realised over a broader range of scattering cross-sections and light neutralino mass values. In addition, the chargino NLSP scenario is allowed in this case. In particular, the relic density constraint imposes a small splitting between the neutralino and the NLSP. With this constraint removed, the splitting condition is strongly weakened, and it becomes possible to find compressed gaugino scenarios which pass LEP-2 $\chi_1^+\chi_1^-$ and $\chi_2^0\,\chi_1^0$ production constraint.

[1] See for example [28] for a discussion about the local density of dark matter.

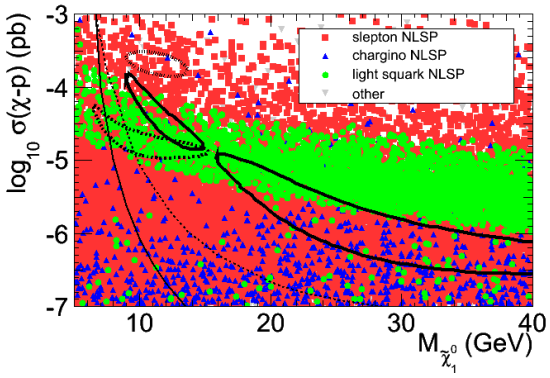

Figure 3.11: Spin independent χ-p scattering cross-section in function of the $\tilde{\chi}_1^0$ mass. The points presented here pass all the constraints, without applying the relic density limits. The red points correspond to a slepton NLSP with a mass slightly above the LEP limits (class i), the blue points to scenarios with a chargino NLSP (class ii), the green points to cases where a scalar quark is degenerate with the light neutralino (class iii), and the gray point to other more canonical scenarios.

Therefore these two classes of spectra can be rehabilitated if the relic density constraint is relaxed.

We also notice that other points which do not belong to any of the three classes can fulfill all the conditions. These scenarios have no other peculiarity than having a light neutralino and a scalar particle with a mass of a few hundreds of GeV, which can increase the scattering cross-sections.

3.2 Sensitivity at LHC

In general terms, MSSM scenarios with a light neutralino offer no specific challenges to the LHC searches. Limits for $\tilde{g}$ and $\tilde{q}$ masses are commonly reported in the $M_{\chi_1^0} = 0$ limit. What makes the most viable scenario identified in this study specific for their search at the LHC is the high level of mass degeneracy between the LSP $\tilde{\chi}_1^0$ and the $\tilde{b}_1$ scalar quark. This implies a very large production cross-section, of order 0.6 μb at 8 TeV accompanied by events with small transverse energy.

We study the distribution of the observables employed in the MET SUSY searches for a few points belonging to the various scenarios identified above. Here a word of caution is in order, since this analysis is carried out using fast simulation for events with a remarkably different kinematics compared to those used for its validation. Results can be considered valid in broader, qualitative terms but not necessary quantitatively. Fig. 3.12 shows the dis-

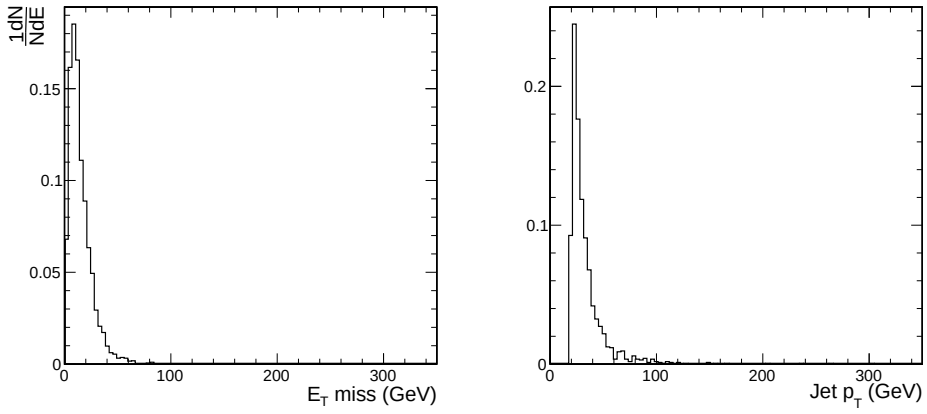

Figure 3.12: Distributions of event missing E_T (left) and jet p_T (right) for $\tilde{b}_1$ production in 8 TeV pp collisions in the almost degenerate light $\tilde{b}_1$ NLSP scenario.

tributions we obtain for the event missing E_T and the jet p_T for one of the selected points in the almost degenerate light $\tilde{b}_1$ NLSP scenario, which are relevant for the trigger and selection cut applied in MET analyses. By applying the jet p_T and event missing E_T cuts adopted in the recent searches for scalar bottom quark pair production with the ATLAS detector [29, 30], from a sample of 10k no events are kept. Similar strong cuts on missing E_T and jet p_T were applied in an earlier CMS search [31]. However, if the cuts on the two variables would be lowered from 130 GeV to 75 and 50 GeV, the selection efficiency would become of the order of 0.003 and 0.012, respectively.

Bibliography

[1] E. Aprile, et al. (XENON 100 Collaboration), Phys. Rev. Lett. **107**, 131302 (2011); E. Aprile *et al.* [XENON100 Collaboration], arXiv:1207.5988 [astro-ph.CO].

[2] Z. Ahmed, et al. (CDMS-II Collaboration), Science **327**, 1619 (2010); Z. Ahmed, et al. (CDMS-II Collaboration), Phys. Rev. Lett. **106**, 131302 (2011); Z. Ahmed, et al. (CDMS Collaboration), arXiv:1203.1309.

[3] R. Bernabei, et al. (DAMA Collaboration), Phys. Lett. **B480**, 23 (2000).

[4] R. Bernabei, P. Belli, F. Cappella, et al., Eur. Phys. J. **C67**, 39 (2010).

[5] C. Aalseth, et al. (CoGeNT Collaboration), Phys. Rev. Lett. **106**, 131301 (2011).

[6] C. Aalseth, P. Barbeau, J. Colaresi, et al., Phys. Rev. Lett. **107**, 141301 (2011).

[7] G. Angloher, M. Bauer, I. Bavykina, et al., Eur. Phys. J. C **72**, 1971 (2012).

[8] C. Savage, G. Gelmini, P. Gondolo, et al., JCAP **0904**, 010 (2009); A. Fitzpatrick, D. Hooper, K. M. Zurek, Phys. Rev. **D81**, 115005 (2010); C. Kelso, D. Hooper, M. R. Buckley, Phys. Rev. D **85**, 043515 (2012); G. B. Gelmini, J. Phys. Conf. Ser. **384**, 012007 (2012).

[9] A. Arbey, M. Battaglia and F. Mahmoudi, arXiv:1205.2557 [hep-ph].

[10] D. Hooper, T. Plehn, Phys. Lett. **B562**, 18 (2003); A. Bottino, N. Fornengo, S. Scopel, Phys. Rev. **D67**, 063519 (2003); A. Bottino, F. Donato, N. Fornengo, et al., Phys. Rev. **D69**, 037302 (2004); S. Profumo, Phys. Rev. **D78**, 023507 (2008); A. Bottino, N. Fornengo, G. Polesello, et al., Phys. Rev. **D77**, 115026 (2008); E. Dudas, S. Lavignac, J. Parmentier, Nucl. Phys. **B808**, 237 (2009); H. K. Dreiner, S. Heinemeyer, O. Kittel, et al., Eur. Phys. J. **C62**, 547 (2009); D. Feldman, Z. Liu,

P. Nath, Phys. Rev. **D81**, 117701 (2010); E. Kuflik, A. Pierce, K. M. Zurek, Phys. Rev. **D81**, 111701 (2010); A. V. Belikov, J. F. Gunion, D. Hooper, et al., Phys. Lett. **B705**, 82 (2011); D. A. Vasquez, G. Belanger, C. Boehm, et al., Phys. Rev. **D82**, 115027 (2010); J. Conley, H. Dreiner, P. Wienemann, Phys. Rev. **D83**, 055018 (2011); S. Choi, S. Scopel, N. Fornengo, et al., Phys. Rev. **D85**, 035009 (2012); D. Albornoz Vasquez, G. Belanger, C. Boehm, Phys. Rev. **D84**, 095015 (2011); N. Bhattacharyya, A. Choudhury, A. Datta, Phys. Rev. D **84**, 095006 (2011); L. Calibbi, T. Ota, Y. Takanishi, JHEP **1107**, 013 (2011); A. Bottino, N. Fornengo, S. Scopel, Phys. Rev. D **85**, 095013 (2012); A. Choudhury, A. Datta, JHEP **1206**, 006 (2012).

[11] V. Barger, P. Langacker, H.-S. Lee, Phys. Lett. **B630**, 85 (2005); J. F. Gunion, D. Hooper, B. McElrath, Phys. Rev. **D73**, 015011 (2006); D. Das, U. Ellwanger, JHEP **1009**, 085 (2010); J. F. Gunion, A. V. Belikov, D. Hooper, arXiv:1009.2555; P. Draper, T. Liu, C. E. Wagner, et al., Phys. Rev. Lett. **106**, 121805 (2011); J.-J. Cao, K.-I. Hikasa, W. Wang, et al., Phys. Lett. **B703**, 292 (2011); M. Carena, N. R. Shah, C. E. Wagner, Phys. Rev. **D85**, 036003 (2012).

[12] G. Aad *et al.* (ATLAS Collaboration), Phys. Lett. B **716**, 1 (2012).

[13] S. Chatrchyan *et al.* (CMS Collaboration), Phys. Lett. B **716**, 30 (2012).

[14] A. Arbey, M. Battaglia, F. Mahmoudi, Eur. Phys. J. **C72**, 1847 (2012).

[15] T. Sjostrand, S. Mrenna, P. Z. Skands, JHEP **05**, 026 (2006).

[16] E. Komatsu, et al. (WMAP Collaboration), Astrophys. J. Suppl. **192**, 18 (2011).

[17] M. Ackermann, et al. (Fermi-LAT collaboration), Phys. Rev. Lett. **107**, 241302 (2011).

[18] D. Y. Bardin, P. Christova, M. Jack, et al., Comput. Phys. Commun. **133**, 229 (2001).

[19] J. Abdallah, et al. (DELPHI), Eur. Phys. J. **C31**, 421 (2003).

[20] S. Chatrchyan, et al. (CMS Collaboration), Phys. Rev. Lett. **108**, 261803 (2012).

[21] J. Goodman, M. Ibe, A. Rajaraman, et al., Phys. Lett. **B695**, 185 (2011).

[22] Y. Bai, P. J. Fox, R. Harnik, JHEP **1012**, 048 (2010).

[23] LEP2 SUSY Working Group (2002), Note LEPSUSYWG/02-04.1.

[24] LEP2 SUSY Working Group (2004), Note LEPSUSYWG/04-02.1.

[25] M. Kamionkowski, M. S. Turner, Phys. Rev. **D42**, 3310 (1990); P. Salati, Phys. Lett. **B571**, 121 (2003); S. Profumo, P. Ullio, JCAP **0311**, 006 (2003); D. J. Chung, L. L. Everett, K. Kong, et al., JHEP **0710**, 016 (2007); A. Arbey, F. Mahmoudi, Phys. Lett. **B669**, 46 (2008).

[26] T. Moroi, L. Randall, Nucl. Phys. **B570**, 455 (2000); G. F. Giudice, E. W. Kolb, A. Riotto, Phys. Rev. **D64**, 023508 (2001); N. Fornengo, A. Riotto, S. Scopel, Phys. Rev. **D67**, 023514 (2003); G. Gelmini, P. Gondolo, A. Soldatenko, et al., Phys. Rev. **D74**, 083514 (2006); A. Arbey, F. Mahmoudi, JHEP **1005**, 051 (2010).

[27] A. Arbey, Comput. Phys. Commun. **183**, 1822 (2012).

[28] C. M. Bidin, G. Carraro, R. Mendez, et al., Astrophys. J. **751**, 30 (2012).

[29] G. Aad, et al. (ATLAS Collaboration), Phys. Rev. Lett. **108**, 181802 (2012).

[30] G. Aad, et al. (ATLAS Collaboration), Phys. Rev. D **85**, 112006 (2012).

[31] CMS Collaboration, CMS-PAS-SUS-11-006.

Perspectives

This report is a summary of selected parts of my work on the MSSM and neutralino dark matter. We have considered the combination of the data from different sectors, such as cosmological and astrophysical dark matter searches, LHC Higgs and SUSY searches, flavour physics, ..., which provides important and interesting contraints on SUSY. We have shown that the 19-parameter pMSSM is still an interesting scenario for physics beyond the SM, is consistent with all the present data from the different sectors, and can even provide light neutralinos consistent with the results of the direct dark matter detection experiments.

Our study of the pMSSM will be further developed, we will continue to investigate the properties of the pMSSM parameter space. New data from LHC will be released during the next months, and we will study their impact in the context of the pMSSM. A necessary ingredient to accomplish this task will be to constantly update and improve our machinery, in order to determine the compatibility between the pMSSM and the experimental results from many different sectors.

With the discovery of the new particle consistent with the SM Higgs boson, valuable information on New Physics has become available. In the next months, my work will be mainly focussed on the consequences of this discovery and of the measurements of its couplings, in addition to the dark matter constraints, in order to try to determine whether this discovery is a path to New Physics or the sign of the vanilla Standard Model.

Scenarios beyond the neutralino dark matter hypothesis are also worth studying. We are currently considering the case of gravitino dark matter in the pMSSM: in this scenario, the LSP, *i.e.* the dark matter particle, is not the neutralino anymore, but the gravitino. The phenomenology at the LHC can be very different in the case of a gravitino LSP, because the NLSP, which is generally not the neutralino and is long-lived, appears at the end of the decay chains. This would result in the production of charged or coloured new particles at the LHC.

Also, the phenomenology of models beyond the MSSM has to be considered. In particular, the NMSSM can be of interest, and extending our analysis machinery in this direction is a complex yet feasible task. A part of my time in the near future will be devoted to this extension.

Depending on the future LHC results, it may be useful to study alternative models beyond the SM, such as extra-dimension scenarios. It can also be interesting to undertake a particle-dependent approach, considering the observations of the yet-to-be-discovered particles to build the different sectors of a realistic new physics model.

Concerning software development, both `AlterBBN` and `SuperIso Relic` will continue being updated and upgraded. In particular, I will continue adding new cosmology models in `AlterBBN` and add a more reliable estimate of the theory error of the abundance of the elements, as suggested by Subir Sarkar. Regarding `SuperIso Relic`, I would like to implement the calculation of direct and indirect dark matter detection observables, including several astrophysical and cosmological models, in order to evaluate the influence of astrophysical assumptions. We also intend to extend SuperIso to other-than-SUSY models, the chosen models depending on the LHC results.

Beside, I have not lost my interest in cosmology. If the Higgs-like nature of the recently discovered boson is confirmed, it will mean the discovery of the first fundamental scalar field. It will therefore be a further – yet weak – justification for the scalar fields of cosmology. In this context, I will investigate a further extension of the dark fluid model, in which a single scalar field explains simultaneously the dark matter and dark energy problems as well as the inflationary period.

At the interface between cosmology and particle physics, I intend to study the possibility to derive constraints on the cosmological models from particle physics models. In particular, if the nature of dark matter in terms of particles could be determined in the near future, and the determination of the underlying new physics model were sufficient to perform an accurate and realistic relic density calculation, any difference between the cosmologically determined dark matter and the computed relic density could be the sign of a modified cosmology at the time of the relic freeze-out. It would then be possible to test the cosmological modifications needed to obtain a correct relic density. `AlterBBN` and `SuperIso Relic` have been designed to provide ways to perform this kind of analysis.

Of course, we are in a very particular period, where discovery of new physics can be announced at any time. For example in astroparticle and cosmology, the Planck Collaboration will present their first public cosmological results in 2013, and new data from the direct and indirect dark matter detection can give hints about the nature of dark matter. From the LHC, answers to many questions are still awaited: is the new boson really the SM Higgs? Could it be a spin-2 imposter? Will the LHC soon find signals for other new particles? All these questions, and the answers that can come from the data, will shape tomorrow's fundamental physics research, and the unexpected is to be expected.

Appendix A

SuperIso Relic

`SuperIso Relic` is an extension of the `SuperIso` program to the calculation of the relic density. The program calculates the relic density as well as the flavour physics observables using a SUSY Les Houches Accord file (SLHA1 [1] or SLHA2 [2]) as input, either generated automatically via a call to SOFTSUSY [3], ISAJET [4], SPheno [5], SuSpect [6] or NMSSMTools [7], or provided by the user. The calculation can be performed automatically for different supersymmetry breaking scenarios in the minimal supersymmetric extension of the Standard Model (MSSM) or in the next-to-minimal supersymmetric extension of the Standard Model (NMSSM).

One of the most important features of `SuperIso Relic` in comparison to the other public relic density calculation codes, DarkSusy [8], IsaRed [9] and Micromegas [10], is that it provides the possibility to alter the underlying cosmological model, by modifying for example the radiation equation-of-state, the expansion rate or the thermal properties of the Universe in the period before Big-Bang nucleosynthesis (BBN), which is experimentally inaccessible and remains theoretically obscure, and is interfaced with `AlterBBN` (see Appendix B) for estimating the BBN constraints on the altered cosmological model. In [11–14], we studied the effects of different parametrizations of modification of the expansion rate or of the entropy content of the Universe before BBN on the relic density calculation and showed that they can strongly modify the calculated relic density and therefore change the relic density constraints on supersymmetric parameter space. `SuperIso Relic` makes it possible to evaluate the uncertainties on the relic density due to the cosmological model, and inversely, to make prediction on the early Universe properties using the particle physics constraints and the BBN constraints.

In the following, first the content of the `SuperIso Relic` package will be presented, as well as the list of the main routines used for the relic density calculation. The procedure to use `SuperIso Relic` will be then explained,

and the inputs and outputs of the program will be introduced. Finally, some examples of results obtained with `SuperIso Relic` will be given. In the Appendices, a description of the formulas and models used for computing the relic density will be detailed.

A.1 Content of the SuperIso Relic package

`SuperIso Relic` is a mixed C / Fortran program devoted to the calculation of the relic density in addition to many flavour observables in Supersymmetry. Sixteen main programs are provided in the package as guidelines, but the users are also invited to write their own main programs. In particular `slha.c` can scan files written following the SUSY Les Houches Accord formats, and calculates the implemented observables. The main programs `cmssm.c`, `amsb.c`, `hcamsb.c`, `gmsb.c`, `mmamsb.c`, and `nuhm.c` have to be linked to at least one of the `SOFTSUSY` [3], the `ISASUGRA/ISAJET` [4], the `SPheno` [5] and/or the `SuSpect` [6] packages, in order to compute supersymmetric mass spectra and couplings within respectively the CMSSM, AMSB, HCAMSB, MMAMSB, GMSB or NUHM scenarios for the MSSM. The programs `cnmssm.c`, `ngmsb.c` and `nnuhm.c` have to be linked to `NMSSMTools` [7] to calculate the spectra within the CNMSSM, NGMSB or NNUHM scenarios for the NMSSM.

The main steps to compute the observables in `SuperIso Relic` are given in the following:

- Generation of a SLHA file with a spectrum generator (or supply of a SLHA file by the user),
- Scan of the SLHA file,
- Calculation of the widths of the Higgs bosons with `FeynHiggs` or `Hdecay`,
- Computation of the squared amplitudes of the annihilation diagrams involved in the relic density calculation,
- Computation of the thermally averaged total annihilation cross section,
- Solving of the Boltzmann equations and computation of the relic density,
- Calculation of the flavour physics observables.

It should be noted that the relic density calculation is performed even if the LSP is a charged particle. A theoretical description of the calculation of the thermally averaged total annihilation cross section can be found in Section A.5 and the detail of the calculation of the relic density in the cosmological standard model is given in Section A.6. We refer to [15] for a complete

description of the calculation of the flavour observables.

The processes involved in the relic density calculation are all the annihilation and co-annihilation processes of the type

$$\tilde{i} + \tilde{j} \to k + l \tag{A.1}$$

where $\tilde{i}, \tilde{j}$ are supersymmetric particles and k, l are Standard Model particles. The number of involved processes is more than 3000 in the MSSM or 5000 in the NMSSM, and the number of diagrams is even larger. To generate all the squared amplitudes, we have written a `Mathematica` [16] script which uses the `LanHEP` [17] Lagrangians in `FeynArts` format, calls `FeynArts` [18] and `FormCalc` [19] and generates the necessary routines for the numerical computation of the amplitudes. These routines are part of `SuperIso Relic` and can be found in `src/relic` and therefore the user does not need to have `Mathematica` or to install other packages. They rely on `FeynHiggs` [20] or `Hdecay` [21] to calculate the widths of the Higgs bosons at two-loop level. `Hdecay 3.53` and `FeynHiggs 2.8.0` are included in the `SuperIso Relic v3.1` package, and they can be found in `src/contrib`. Therefore the user does not need to download these programs separately.

The compilation process of all the needed routines is very long ($\sim$ hour), and their calculation can take time. Fortunately, all the squared amplitude routines are not necessary at the same time, as some processes have only negligible effects. Therefore, all the squared amplitudes are not computed for a SUSY parameter space point, and a selection is performed to save time, as described in Section A.5.

A.1.1 Parameter structures

The package `SuperIso Relic` relies on the definition of a main structure in `src/include.h`, which is defined as follows:

```
typedef struct parameters
/* structure containing all the scanned parameters from the SLHA file */
{
int SM;
int model; /* CMSSM=1, GMSB=2, AMSB=3 */
int generator; /* ISAJET=1, SOFTSUSY=3, SPHENO=4, SUSPECT=5, NMSSMTOOLS=6 */
double Q; /* Qmax ; default = M_EWSB = sqrt(m_stop1*mstop2) */
double m0,m12,tan_beta,sign_mu,A0; /* CMSSM parameters */
double Lambda,Mmess,N5,cgrav,m32; /* AMSB, GMSB parameters */
double mass_Z,mass_W,mass_b,mass_top_pole,mass_tau_pole; /* SM parameters */
double inv_alpha_em,alphas_MZ,Gfermi,GAUGE_Q; /* SM parameters */
```

```
double charg_Umix[3][3],charg_Vmix[3][3],stop_mix[3][3],sbot_mix[3][3],
stau_mix[3][3],neut_mix[6][6],mass_neut[6],alpha; /* mass mixing matrices */
double Min,M1_Min,M2_Min,M3_Min,At_Min,Ab_Min,Atau_Min,M2H1_Min,M2H2_Min,
mu_Min,M2A_Min,tb_Min,mA_Min; /* optional input parameters at scale Min */
double MeL_Min,MmuL_Min,MtauL_Min,MeR_Min,MmuR_Min,MtauR_Min; /* optional
input parameters at scale Min */
double MqL1_Min,MqL2_Min,MqL3_Min,MuR_Min,McR_Min,MtR_Min,MdR_Min,MsR_Min,
MbR_Min; /* optional input parameters at scale Min */
double N51,N52,N53,M2H1_Q,M2H2_Q; /* optional input parameters (N51...3:
GMSB) */
double mass_d,mass_u,mass_s,mass_c,mass_t,mass_e,mass_nue,mass_mu,mass_num,
mass_tau,mass_nut; /* SM masses */
double mass_gluon,mass_photon,mass_Z0; /* SM masses */
double mass_h0,mass_H0,mass_A0,mass_H,mass_dnl,mass_upl,mass_stl,mass_chl,
mass_b1,mass_t1; /* Higgs & superparticle masses */
double mass_el,mass_nuel,mass_mul,mass_numl,mass_tau1,mass_nutl,mass_gluino,
mass_cha1,mass_cha2; /* superparticle masses */
double mass_dnr,mass_upr,mass_str,mass_chr,mass_b2,mass_t2,mass_er,mass_mur,
mass_tau2; /* superparticle masses */
double mass_nuer,mass_numr,mass_nutr,mass_graviton,mass_gravitino;
/* superparticle masses */
double gp,g2,g3,YU_Q,yut[4],YD_Q,yub[4],YE_Q,yutau[4]; /* Yukawa couplings */
double HMIX_Q,mu_Q,tanb_GUT,Higgs_VEV,mA2_Q,MSOFT_Q,M1_Q,M2_Q,M3_Q;
/* parameters at scale Q */
double MeL_Q,MmuL_Q,MtauL_Q,MeR_Q,MmuR_Q,MtauR_Q,MqL1_Q,MqL2_Q,MqL3_Q,
MuR_Q,McR_Q,MtR_Q,MdR_Q,MsR_Q,MbR_Q; /* masses at scale Q */
double AU_Q,A_u,A_c,A_t,AD_Q,A_d,A_s,A_b,AE_Q,A_e,A_mu,A_tau; /* trilinear
couplings */

/* SLHA2 */
int NMSSM,RV,CPV,FV;
double mass_nutau2,mass_e2,mass_nue2,mass_mu2,mass_numu2,mass_d2,mass_u2,
mass_s2,mass_c2;
double CKM_lambda,CKM_A,CKM_rhobar,CKM_etabar;
double PMNS_theta12,PMNS_theta23,PMNS_theta13,PMNS_delta13,PMNS_alpha1,
PMNS_alpha2;
double lambdaNMSSM_Min,kappaNMSSM_Min,AlambdaNMSSM_Min,AkappaNMSSM_Min,
lambdaSNMSSM_Min,
xiFNMSSM_Min,xiSNMSSM_Min,mupNMSSM_Min,mSp2NMSSM_Min,mS2NMSSM_Min,mass_H03,
mass_A02,
NMSSMRUN_Q,lambdaNMSSM,kappaNMSSM,AlambdaNMSSM,AkappaNMSSM,lambdaSNMSSM,
xiFNMSSM,xiSNMSSM,mupNMSSM,mSp2NMSSM,mS2NMSSM; /* NMSSM parameters */
double PMNSU_Q,CKM_Q,IMCKM_Q,MSE2_Q,MSU2_Q,MSD2_Q,MSL2_Q,MSQ2_Q,TU_Q,TD_Q,
TE_Q;
```

```
double CKM[4][4],IMCKM[4][4]; /* CKM matrix */
double H0_mix[4][4],A0_mix[4][4]; /* Higgs mixing matrices */
double sU_mix[7][7],sD_mix[7][7],sE_mix[7][7], sNU_mix[4][4]; /* mixing
matrices */
double sCKM_msq2[4][4],sCKM_msl2[4][4],sCKM_msd2[4][4],sCKM_msu2[4][4],
sCKM_mse2[4][4]; /* super CKM matrices */
double PMNS_U[4][4]; /* PMNS mixing matrices */
double TU[4][4],TD[4][4],TE[4][4]; /* trilinear couplings */

/* non-SLHA*/
double mass_b_1S,mass_b_pole,mtmt;
double Lambda5; /* Lambda QCD */

/* Flavor constants */
double f_B,f_Bs,f_Ds,f_D,fK_fpi;
double m_B,m_Bs,m_pi,m_Ds,m_K,m_Kstar,m_D0,m_D;
double life_pi,life_K,life_B,life_Bs,life_D,life_Ds;

/* Decay widths */
int widthcalc; /* 0=none, 1=hdecay, 2=feynhiggs */
double width_h0,width_H0,width_A0,width_H,width_Z,width_W,width_top,
width_H03,width_A02;
double width_gluino,width_t1,width_t2,width_b1,width_b2,width_ul,width_ur,
width_dl,width_dr;
double width_cl,width_cr,width_sl,width_sr,width_el,width_er,width_ml,width_mr,
width_tau1,width_tau2;
double width_nuel,width_numl,width_nutaul,width_c1,width_c2,width_o1,width_o2,
width_o3,width_o4,width_o5;

/* CKM matrix */
double complex Vud,Vus,Vub,Vcd,Vcs,Vcb,Vtd,Vts,Vtb;

/* 2HDM */
int THDM_model;
double lambda_u[4][4],lambda_d[4][4],lambda_l[4][4];

/* NMSSMTools */
int NMSSMcoll,NMSSMtheory,NMSSMups1S,NMSSMetab1S;
}
parameters;
```

This structure contains all the important parameters and is called by most of the main functions in the program. An additional structure specific to the relic density calculation is also defined:

```
typedef struct relicparam
/* structure containing the cosmological model parameters */
{
int entropy_model;
double dd0,ndd,Tdend;
double sd0,nsd,Tsend;
double Sigmad0,nSigmad,TSigmaend;
double nt0,nnt,Tnend;
double table_eff[276][3];
}
relicparam;
```

This structure is used to define the cosmological model based on which the relic density calculation is performed.

A.1.2 Main routines

We review here the main routines of the code needed for the relic density calculation. For the main procedures related to the flavour observable calculations we refer the reader to [15].

The most relevant C routines are the following:

- `void Init_param(struct parameters* param)`

  This function initializes the `param` structure, setting all the parameters to 0, apart from the SM masses and the value of the strong coupling constant at the Z-boson mass, which receive the values given in the PDG2010 [22].

- `int Les_Houches_Reader(char name[], struct parameters* param)`

  This routine reads the SLHA file named `name`, and put all the read parameters in the structure `param`. It should be noted that a negative value for `param->model` indicates a problem in reading the SLHA file, or a model not yet included in SuperIso (such as R-parity breaking models). In this case, `Les_Houches_Reader` returns 0, otherwise 1.

- `int test_slha(char name[])`

  This routine checks if the SLHA file is valid, and if so returns 1. If not, -1 means that in the SLHA generator the computation did not succeed (*e.g.* because of tachyonic particles), -2 means that the considered model is not currently implemented in `SuperIso`, and -3 indicates

that the provided file is either not in the SLHA format, or some important elements are missing.

- `int softsusy_cmssm(double m0, double m12, double tanb, double A0, double sgnmu, double mtop, double mbot, double alphas_mz, char name[])`
- `int softsusy_nuhm(double m0, double m12, double tanb, double A0, double mu, double mA, double mtop, double mbot, double alphas_mz, char name[])`
- `int softsusy_gmsb(double Lambda, double Mmess, double tanb, int N5, double cGrav, double sgnmu, double mtop, double mbot, double alphas_mz, char name[])`
- `int softsusy_amsb(double m0, double m32, double tanb, double sgnmu, double mtop, double mbot, double alphas_mz, char name[])`

  The above routines call `SOFTSUSY` to compute the mass spectrum corresponding to the input parameters (more details are given in the next sections), and return a SLHA file whose name has to be specified in the string `name`.

- `int isajet_cmssm(double m0, double m12, double tanb, double A0, double sgnmu, double mtop, char name[])`
- `int isajet_gmsb(double Lambda, double Mmess, double tanb, int N5, double cGrav, double sgnmu, double mtop, char name[])`
- `int isajet_nuhm(double m0, double m12, double tanb, double A0, double mu, double mA, double mtop, char name[])`
- `int isajet_amsb(double m0, double m32, double tanb, double sgnmu, double mtop, char name[])`
- `int isajet_mmamsb(double alpha, double m32, double tanb, double sgnmu, double mtop, char name[])`
- `int isajet_hcamsb(double alpha, double m32, double tanb, double sgnmu, double mtop, char name[])`

  The above routines call `ISAJET` to compute the mass spectrum corresponding to the input parameters (more details are given in the next sections), and return a SLHA file whose name has to be specified in the string `name`.

- `int spheno_cmssm(double m0, double m12, double tanb, double A0, double sgnmu, double mtop, double mbot, double alphas_mz, char name[])`
- `int spheno_gmsb(double Lambda, double Mmess, double tanb, int N5, double sgnmu, double mtop, double mbot, double alphas_mz, char name[])`
- `int spheno_amsb(double m0, double m32, double tanb, double sgnmu, double mtop, double mbot, double alphas_mz, char name[])`

  The above routines call `SPheno` to compute the mass spectrum corresponding to the input parameters (more details are given in the next sections), and return a SLHA file whose name has to be specified in the string `name`.

- `int suspect_cmssm(double m0, double m12, double tanb, double A0, double sgnmu, double mtop, double mbot, double alphas_mz, char name[])`
- `int suspect_gmsb(double Lambda, double Mmess, double tanb, int N5, double sgnmu, double mtop, double mbot, double alphas_mz, char name[])`
- `int suspect_amsb(double m0, double m32, double tanb, double sgnmu, double mtop, double mbot, double alphas_mz, char name[])`

  The above routines call `SuSpect` to compute the mass spectrum corresponding to the input parameters (more details are given in the next sections), and return a SLHA file whose name has to be specified in the string `name`.

- `int nmssmtools_cnmssm(double m0, double m12, double tanb, double A0, double lambda, double AK, double sgnmu, double mtop, double mbot, double alphas_mz, char name[])`
- `int nmssmtools_nnuhm(double m0, double m12, double tanb, double A0, double MHDGUT, double MHUGUT, double lambda, double AK, double sgnmu, double mtop, double mbot, double alphas_mz, char name[])`
- `int nmssmtools_ngmsb(double Lambda, double Mmess, double tanb, int N5, double lambda, double AL, double Del_h, double sgnmu, double mtop, double mbot, double alphas_mz, char name[])`

  The above routines call `NMSSMTools` to compute the mass spectrum corresponding to the input parameters (more details are given in the next sections), and return a SLHA file whose name has to be specified in the string `name`.

- `void ModelIni(struct parameters* param, double relicmass, double maxenergy)`

  This routine is an interface between the C routines and the Fortran routines and it defines all the Fortran variables using the C variables.

- `double findrelicmass(struct parameters* param, int *scalar)`

  This function determines the LSP mass, and checks if the LSP is scalar (`*scalar=1`) or fermionic (`*scalar=0`).

- `int Weff(double* res, double sqrtS, struct parameters* param, double relicmass)`

  This function calls the Fortran routines and returns the effective annihilation rate $W_{\rm eff}$ at a given center of mass energy `sqrtS`, following the procedure described in Section A.5.

- `int Init_relic(double Wefftab[NMAX][2], int *nlines_Weff, struct parameters* param)`

  This routine computes for different values of $\sqrt{s}$ the effective annihilation rates $W_{\rm eff}$ needed for the calculation of $\langle\sigma v\rangle$ using the `Weff` function, and collects them in table `Wefftab`.

- `double sigmav(double T, double relicmass, double Wefftab[NMAX][2], int nlines, struct parameters* param)`

  This function computes the averaged annihilation cross section $\langle\sigma v\rangle$ using the effective annihilation rates $W_{\rm eff}$ collected in table `Wefftab`.

- `double heff(double T, struct relicparam* paramrelic)`
  `double sgstar(double T, struct relicparam* paramrelic)`
  `double geff(double T, struct relicparam* paramrelic)`

  These three functions compute respectively $h_{\rm eff}$, $\sqrt{g_*}$ and $g_{\rm eff}$ at the temperature `T`.

- `double Yeq(double T,struct parameters* param, struct relicparam* paramrelic)`
  `double dYeq_dT(double T,struct parameters* param, struct relicparam*`

`paramrelic)`

The first function computes Y_{eq} at a temperature `T`, and the second one its derivative.

- `double Tfo(double Wefftab[NMAX][2], int nlines_Weff, double relicmass, struct parameters* param, double d, struct relicparam* paramrelic)`

  This function computes the freeze-out temperature following Eq. (A.24), using the `Wefftab` generated previously.

- `double relic_density(double Wefftab[NMAX][2], int nlines_Weff, struct parameters* param, struct relicparam* paramrelic)`
  `double relic_calculator(char name[])`

  This main procedure computes the relic density using the `Wefftab` generated previously. `relic_calculator` is a container function which scans the SLHA file and computes the relic density.

- `void Init_cosmomodel(struct relicparam* paramrelic)`
  `void Init_modeleff(int model_eff, struct relicparam* paramrelic)`
  `void Init_dark_density(double dd0, double ndd, double T_end, struct relicparam* paramrelic)`
  `void Init_dark_entropy(double sd0, double nsd, double T_end, struct relicparam* paramrelic)`
  `void Init_dark_entropySigmaD(double Sigmad0, double nSigmad, double T_end, struct relicparam* paramrelic)`

  These procedures define the cosmological model based on which the relic density is computed. `Init_cosmomodel` has to be called first to initialize the `paramrelic` structure. To alter the QCD equation-of-state as in Section A.7, `Init_modeleff` must be called while specifying the model: `model_eff`$= 1 \cdots 5$ corresponds respectively to the models A, B, B2, B3 and C developed in [23], and `model_eff`$= 0$ to the older model formerly used in `Micromegas` and `DarkSusy`, in which the hadrons are considered as ideal gas. If not specified, the model is set by default to B (`model_eff`$= 2$). `Init_dark_density` adds a dark energy density as in Eq. (A.34), with `dd0`$=\kappa_\rho$ and `ndd`$=n_\rho$, `Init_dark_entropy` adds a dark entropy density as in Eq. (A.35), with `sd0`$=\kappa_s$ and `nsd`$=n_s$, and `Init_dark_entropySigmaD` adds a dark entropy production as in Eq. (A.36), with `Sigmad0`$=\kappa_\Sigma$, `nSigmad`$=n_\Sigma$

and `T_end`=T_r. If these routines are not called, no additional density will be added, and the calculation will be performed in the standard cosmological model.

- `double dark_density(double T, struct relicparam* paramrelic)`
  `double dark_entropy(double T, struct relicparam* paramrelic)`
  `double dark_entropy_derivative(double T, struct relicparam* paramrelic)`
  `double dark_entropy_Sigmad(double T, struct relicparam* relicparam)`

  These functions compute energy and entropy densities needed for the alternative cosmological models described in Section A.8.

- `int FeynHiggs(char name[], struct parameters* param)`
  `int Hdecay(char name[], struct parameters* param)`

  These routines call `FeynHiggs` or `Hdecay` to compute the widths and masses of the Higgs bosons corresponding to the SLHA file `name` at the two-loop level, and puts these variables in the `param` structure.

The complete list of C procedures implemented in `SuperIso Relic` is available in `src/include.h`.

The Fortran routines can be found in `src/relic`. They have been generated automatically by a `Mathematica`/`FormCalc` script and they perform the computation of all squared amplitudes. Because of the large number of these routines they will not be described further here. For the `FormCalc` specific routines, we refer the reader to the `FormCalc` manual [19].

A.2 Compilation and installation instructions

The `SuperIso Relic` package can be downloaded from:

`http://superiso.in2p3.fr/relic`

It can be compiled in two different ways:

- the shared library compilation, which compiles the squared amplitude procedures on-the-fly, if they are needed. The initial compilation is fast, but the execution is slightly slower.
- the static library compilation. Here all the squared amplitude routines need to be compiled before running, and therefore the initial compilation process can take about an hour, and the generated executables

are large. This compilation enables slightly faster execution than the shared library compilation, and is therefore intended for the scans over a large number of SUSY points.

The shared compilation is recommended.

The following main directory is created after unpacking:

`superiso_vX.X`

This directory contains the `src/` directory, in which all the source files can be found. The main directory contains also a `Makefile`, a `README`, sixteen sample main programs (such as `cmssm.c`, `nnuhm.c`, or `test_modeleff.c`) and one example of input file in the SUSY Les Houches Accord format (`example.lha`).

The paths to the different spectrum generators should be defined in the `Makefile`, if needed by the user. To set the compilation options automatically, simply type:

`./configure`

To use a different C/Fortran compiler, type for example:

`./configure --with-cc=gcc --with-fc=gfortran`

`SuperIso Relic` is written for a C compiler respecting the C99 standard and a Fortran compiler. In particular, it has been tested successfully with the GNU C and GNU Fortran Compilers and the Intel C and Intel Fortran Compilers on Linux and Mac 32-bits or 64-bits machines. Additional information can be found in the `README` file.
To compile the library, type

`make shared` or `make static`

followed by

`make`

This creates `libisospin.a` in `src/` and `librelic.a` in `src/relic`, and compiles `FeynHiggs` and `Hdecay`. After this step, if the paths to the spectrum generators are modified, type:

`make resetpaths`.

To compile one of the sixteen programs provided in the main directory, type

`make name` or `make name.c`

where `name` can be `cmssm`, `gmsbm`, ... This generates an executable program with the `.x` extension. Note that `slha.x`, `test_modeleff.x`, `test_standmod.x`, `test_reheating.x`, `test_widthcalc.x` and `sm.x` do not need any spectrum generator.

`slha.x` calculates the implemented observables, using the parameters contained in the SLHA file whose name has to be passed as input parameter.

`amsb.x`, `cmssm.x`, `gmsb.x`, `hcamsb.x`, `mmamsb.x` and `nuhm.x` compute the observables, starting first by calculating the mass spectrum and couplings thanks to `ISAJET`, `SOFTSUSY`, `SPheno` and/or `SuSpect` within respectively the AMSB, CMSSM, GMSB, HCAMSB, MMAMSB or NUHM parameter spaces.

`cnmssm.x`, `ngmsb.x`, and `nnuhm.x` compute the observables, starting first by calculating the mass spectrum and couplings thanks to `NMSSMTools` within respectively the CNMSSM, NGMSB or NNUHM parameter spaces.

`test_modeleff.x`, `test_standmod.x`, `test_reheating.x` and `test_widthcalc.x` calculate the relic density, using the parameters contained in the SLHA file whose name has to be passed as input parameter, in the cosmological models described in the Appendices.

A.3 Input and output description

The input and output of the SuperIso Relic-specific main programs are described in the following. For the description of the other main programs, please refer to the SuperIso manual [15].

A.3.1 SLHA input file

The program `slha.x` calculates the observables while reading the needed parameters in a given SLHA file. For example, the command

`./slha.x example.lha`

returns

Observable	Value
BR(b->s gamma)	3.017e-04
delta0(B->K* gamma)	7.943e-02
BR(Bs->mu mu)	3.475e-09
BR(Bs->mu mu)_untag	3.810e-09
BR(Bd->mu mu)	1.109e-10
BR(B->K* mu mu)_low	2.303e-07
AFB(B->K* mu mu)_low	-5.633e-02
FL(B->K* mu mu)_low	7.287e-01
AT1(B->K* mu mu)_low	9.992e-01
AT2(B->K* mu mu)_low	-3.566e-02
AT3(B->K* mu mu)_low	5.913e-01
AT4(B->K* mu mu)_low	8.485e-01
AT5(B->K* mu mu)_low	3.676e-01
AI(B->K* mu mu)_low	-1.678e-02
BR(B->K* mu mu)_high	1.291e-07
AFB(B->K* mu mu)_high	4.414e-01
FL(B->K* mu mu)_high	3.610e-01
HT1(B->K* mu mu)_high	1.000e+00
HT2(B->K* mu mu)_high	-9.897e-01
HT3(B->K* mu mu)_high	-9.898e-01
AI(B->K* mu mu)_high	-8.804e-04
q0^2(AFB(B->K* mu mu))	4.197e+00
q0^2(AI(B->K* mu mu))	1.875e+00
BR(B->Xs mu mu)_low	1.780e-06
BR(B->Xs mu mu)_high	2.203e-07
q0^2(AFB(B->Xs mu mu)	3.338e+00
BR(B->Xs tau tau)_high	1.616e-07
BR(B->tau nu)	7.979e-05
R(B->tau nu)	9.966e-01
BR(B->D tau nu)	6.743e-03
BR(B->D tau nu)/BR(B->D e nu)	2.972e-01
BR(Ds->tau nu)	5.096e-02
BR(Ds->mu nu)	5.230e-03
BR(D->mu nu)	3.850e-04
BR(K->mu nu)/BR(pi->mu nu)	6.342e-01
Rmu23(K->mu nu)	1.000e+00

```
a_muon                          2.029e-10

excluded_Higgs_mass             0
excluded_SUSY_mass              0
charged_LSP                     0

Relic density Oh2               1.195e+01
```

If the SLHA file provided to `slha.x` is invalid, a message will be displayed:

- `Invalid point` means that the SLHA generator had not succeeded in generating the mass spectrum (*e.g.* due to the presence of tachyonic particles).
- `Model not yet implemented` means that the SLHA file is intended for a model not implemented in SuperIso, such as R-parity violating models.
- `Invalid SLHA file` means that the SLHA file is broken and misses important parameters.

More details on the definitions and calculations of the flavour observables are given in [15].

A.3.2 Alternative QCD equations of state

The program `test_modeleff.x` calculates the relic density while reading the needed parameters in the SLHA file, for the different QCD equations of state (*i.e.* alternative models of $g_{\rm eff}$ and $h_{\rm eff}$) described in Section A.7. For example, the command

```
./test_modeleff.x example.lha
```

returns

```
Dependence of the relic density on the calculation of heff and geff
For model_eff=1 (model A): omega=1.195e+01
For model_eff=2 (model B (default)): omega=1.195e+01
For model_eff=3 (model B2): omega=1.202e+01
For model_eff=4 (model B3): omega=1.188e+01
For model_eff=5 (model C): omega=1.196e+01
For model_eff=0 (old model): omega=1.171e+01
```

A.3.3 Effective energy and entropy densities

The program `test_standmodel.x` reads the needed parameters in the SLHA file, and calculates the relic density while adding to the standard cosmological model an effective energy density such that

$$\rho_D = \kappa_\rho \rho_{rad}(T_{BBN})\big(T/T_{BBN}\big)^{n_\rho} , \tag{A.2}$$

and/or an effective entropy density

$$s_D = \kappa_s s_{rad}(T_{BBN})\big(T/T_{BBN}\big)^{n_s} , \tag{A.3}$$

which modify the Early Universe properties without having observational consequences if chosen adequately [12]. A description of the model and of the related equations can be found in Section A.8. The necessary arguments to this program are[1]:

- SLHA file name,
- κ_ρ: ratio of dark energy density over radiation energy density at BBN time (preferentially < 1),
- n_ρ: dark energy density decrease exponent (preferentially > 4),
- κ_s: ratio of dark entropy density over radiation entropy density at BBN time (preferentially < 1),
- n_s: dark entropy density decrease exponent (preferentially > 3).

Two optional parameters can be given:

- T_ρ: temperature in GeV below which the dark energy density is set to 0,
- T_s: temperature in GeV below which the dark entropy density is set to 0.

Note that $n_\rho = 4$ corresponds to a radiation-like energy density, $n_\rho = 6$ to a quintessence-like energy density and $n_\rho = 8$ to a decaying scalar field energy density. Also, $n_s = 3$ corresponds to a radiation-like entropy density and $n_s = 4$ can appear in reheating models.
For example, the command

```
./test_standmod.x example.lha 1e-3 6 1e-3 4
```

returns

```
For the cosmological standard model:
omega=1.195e+01
For the specified model with dark density/entropy/non thermal relics:
omega=5.758e+02
Model compatible with BBN constraints
```

The BBN constraints are tested using `AlterBBN` (see Appendix B).

[1]The preferential values given inside the brackets correspond to cosmological models without observational consequences, *i.e.* as valid as the cosmological standard model.

A.3.4 Entropy generation and reheating

The program `test_reheating.x` reads the needed parameters in the SLHA file, and calculates the relic density while adding to the standard cosmological model an effective energy density such that

$$\rho_D = \kappa_\rho \rho_{rad}(T_{BBN})\big(T/T_{BBN}\big)^{n_\rho} , \tag{A.4}$$

and/or an effective entropy production

$$\Sigma_D = \kappa_\Sigma \Sigma_{rad}(T_{BBN})\big(T/T_{BBN}\big)^{n_\Sigma} , \tag{A.5}$$

which modify the Early Universe properties without having observational consequences if chosen adequately [12]. A description of the model and of the related equations can be found in Section A.8. The necessary arguments to this program are:

- SLHA file name,
- κ_Σ: ratio of dark energy density over radiation energy density at BBN time (preferentially < 1),
- n_Σ: dark energy density decrease exponent (preferentially > 4),
- κ_Σ: ratio of dark entropy production over radiation entropy evolution at BBN time (preferentially < 1),
- n_Σ: dark entropy production exponent (preferentially < 0).
- T_r: reheating temperature in GeV (preferentially $> 10^{-3}$ GeV), above which the dark energy density and entropy production are set to 0.

Note that $n_\rho = 4$ corresponds to a radiation-like energy density, $n_\rho = 6$ to a quintessence-like energy density and $n_\rho = 8$ to a decaying scalar field energy density. Also, $n_\Sigma \sim -1$ corresponds to standard reheating models.
For example, the command

```
./test_reheating.x example.lha 0 0 0.1 -1 1e-3
```

returns

```
For the cosmological standard model:
omega=1.195e+01
For the specified model with dark density/entropy/non thermal relics:
omega=1.085e+01
Model compatible with BBN constraints
```

The BBN constraints are tested using `AlterBBN` (see Appendix B).

A.3.5 Width calculators

The program `test_widthcalc.x` calculates the relic density while reading the needed parameters in the SLHA file, using `Hdecay` at two-loop and at tree level, and `FeynHiggs` at two-loop and at tree level. For example, the command

```
./test_widthcalc.x example.lha
```

returns

```
Dependence of the relic density on the width calculator
Widths in the SLHA file: omega=1.195e+01
With Hdecay: omega=1.195e+01
With FeynHiggs: omega=1.195e+01
With FeynHiggs Tree: omega=1.190e+01
```

Using the aforementioned main programs as examples, the user is encouraged to write his/her own programs in order to, for example, perform scans in a given supersymmetric scenario, or test different cosmological models.

A.4 Results

`SuperIso Relic` computes the relic density, and the results have been compared extensively to those of `DarkSusy` and `Micromegas`. A very good agreement has been found even at the level of the calculation of the effective annihilation rate W_{eff} (see Section A.5), as can be seen in Fig. A.1. In general, the results of `DarkSusy`, `Micromegas`, and `SuperIso Relic` differ only by a few percents, but in some rare cases where a Higgs resonance occurs approximately at twice the mass of the LSP, the differences can be large. To avoid this problem, a very precise calculation of the masses and widths of the Higgs bosons is required, and we decided to use the two-loop calculations of `FeynHiggs` and `Hdecay` to obtain a better evaluation of the relic density in this kind of scenarios.

`SuperIso Relic` can also be used in order to constrain SUSY parameter spaces, as it provides many different observables from flavour physics as well as the relic density. It allows in particular to test easily the influence of the cosmological model by modifying for example the QCD equation-of-state (Section A.7) or the expansion rate (Section A.8), as can be seen in Fig. A.2.

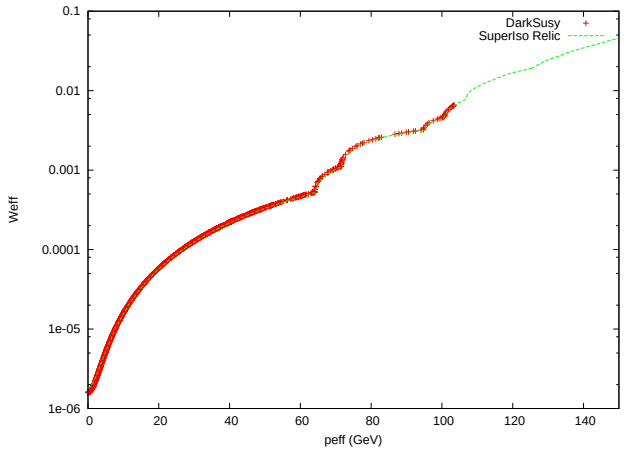

Figure A.1: W_{eff} in function of p_{eff}, computed with SuperIso Relic (dashed green line), and with DarkSusy (red crosses). This comparison shows an excellent agreement.

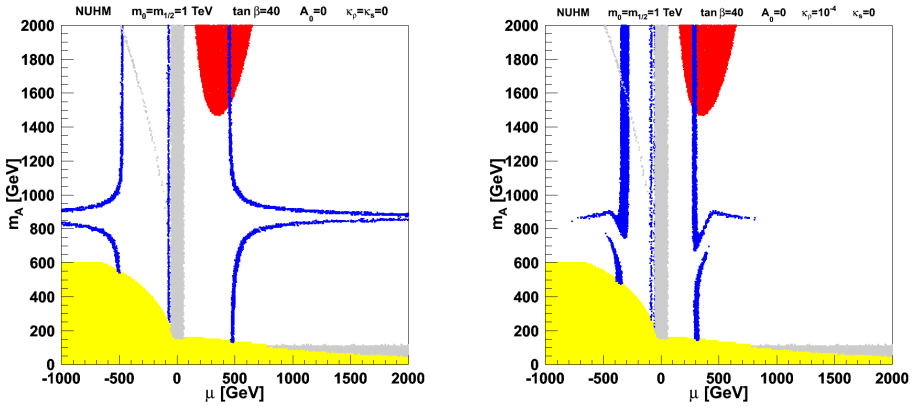

Figure A.2: Constraints on the NUHM parameter plane (μ,m_A), in the standard cosmological model (left), and in presence of a tiny energy overdensity with $\kappa_\rho = 10^{-4}$ and $n_\rho = 6$ (right). The red points are excluded by the isospin asymmetry of $B \to K^*\gamma$, the gray area is excluded by direct collider limits, the yellow zone involves tachyonic particles, and the blue strips are favored by the WMAP constraints [24].

A.5 Thermally averaged annihilation cross section

The computation of the thermally averaged annihilation cross section $\langle \sigma v \rangle$ is the most time consuming part of the relic density computation, as it requires the computation of the many annihilation and co-annihilation amplitudes. One can define the annihilation rate of supersymmetric particles i and j into SM particles k and l [25, 26]:

$$W_{ij\to kl} = \frac{p_{kl}}{16\pi^2 g_i g_j S_{kl}\sqrt{s}} \sum_{\text{internal d.o.f.}} \int |\mathcal{M}(ij \to kl)|^2 \, d\Omega \,, \tag{A.6}$$

where $\mathcal{M}$ is the transition amplitude, s is the center-of-mass energy, g_i is the number of degrees of freedom of the particle i, p_{kl} is the final center-of-mass momentum such as

$$p_{kl} = \frac{\left[s-(m_k+m_l)^2\right]^{1/2}\left[s-(m_k-m_l)^2\right]^{1/2}}{2\sqrt{s}} \,, \tag{A.7}$$

S_{kl} is a symmetry factor equal to 2 for identical final particles and to 1 otherwise, and the integration is over the outgoing directions of one of the final particles. Moreover, an average over initial internal degrees of freedom is performed.

We also define an effective annihilation rate W_{eff} by

$$g_{LSP}^2 p_{\text{eff}} W_{\text{eff}} \equiv \sum_{ij} g_i g_j p_{ij} W_{ij} \tag{A.8}$$

with

$$p_{\text{eff}}(\sqrt{s}) = \frac{1}{2}\sqrt{(\sqrt{s})^2 - 4m_{LSP}^2} \,. \tag{A.9}$$

In `SuperIso Relic` we compute

$$\frac{dW_{\text{eff}}}{d\cos\theta} = \sum_{ijkl} \frac{p_{ij}p_{kl}}{8\pi g_{LSP}^2 p_{\text{eff}} S_{kl}\sqrt{s}} \sum_{\text{helicities}} \left| \sum_{\text{diagrams}} \mathcal{M}(ij \to kl) \right|^2 \,, \tag{A.10}$$

where θ is the angle between particles i and k. We integrate over $\cos\theta$ numerically by means of the Gauss-Legendre quadrature of order 5.

Since $W_{\text{eff}}(\sqrt{s})$ does not depend on the temperature T, it can be tabulated once for each model point. It is however important to make sure that the maximum $\sqrt{s}$ in the table is large enough to include all important resonances, thresholds and coannihilation thresholds.

To improve the calculation speed, we use two different thresholds:

- a cut such that the coannihilation of SUSY particles i and j is only taken into account if

$$m_i + m_j < \sqrt{s}_{\text{cut coann}} \,, \tag{A.11}$$

where we have taken

$$\sqrt{s}_{\text{cut coann}} = 3\, m_{LSP} \,, \tag{A.12}$$

- a maximum energy up to which $W_{\text{eff}}(\sqrt{s})$ is calculated, such that

$$\sqrt{s}_{max} = 2m_{LSP} - T_{fo} \log(B_\epsilon) \,, \tag{A.13}$$

where $T_{fo} = 25$ GeV is a typical upper limit freeze-out temperature, and B_ϵ is the Boltzmann suppression factor limit that we fixed at 10^{-6} [27].

The thermal average of the effective cross section is then

$$\langle \sigma_{\text{eff}} v \rangle = \frac{\displaystyle\int_0^\infty dp_{\text{eff}} p_{\text{eff}}^2 W_{\text{eff}}(\sqrt{s}) K_1\left(\frac{\sqrt{s}}{T}\right)}{m_{LSP}^4 T \left[\displaystyle\sum_i \frac{g_i}{g_{LSP}} \frac{m_i^2}{m_1^2} K_2\left(\frac{m_i}{T}\right)\right]^2} \,, \tag{A.14}$$

where K_1 and K_2 are the modified Bessel functions of the second kind of order 1 and 2 respectively. The average is performed numerically using a Gaussian integration, and the ∞ limit can be safely replaced by $p_{\text{eff}}(\sqrt{s}_{max})$ using the properties of K_1.

A.6 Cosmological Standard Model

The cosmological standard model is based on a Friedmann-Lemaître Universe filled with radiation, baryonic matter and cold dark matter, approximately flat and incorporating a cosmological constant accelerating its expansion. Before recombination, the Universe expansion was dominated by a radiation density, and therefore the expansion rate H of the Universe is determined by the Friedmann equation

$$H^2 = \frac{8\pi G}{3} \rho_{rad} \,, \tag{A.15}$$

where

$$\rho_{rad}(T) = g_{\text{eff}}(T) \frac{\pi^2}{30} T^4 \tag{A.16}$$

is the radiation density and $g_{\rm eff}$ is the effective number of degrees of freedom of radiation. The computation of the relic density is based on the solution of the Boltzmann evolution equation [25, 26]

$$dn/dt = -3Hn - \langle\sigma_{\rm eff}v\rangle(n^2 - n_{\rm eq}^2) \,, \tag{A.17}$$

where n is the number density of all supersymmetric particles, $n_{\rm eq}$ their equilibrium density, and $\langle\sigma_{\rm eff}v\rangle$ is the thermal average of the annihilation rate of the supersymmetric particles to the Standard Model particles. By solving this equation, the density number of supersymmetric particles in the present Universe and consequently the relic density can be determined.
The ratio of the number density to the radiation entropy density, $Y(T) = n(T)/s(T)$ can be defined, where

$$s(T) = h_{\rm eff}(T)\frac{2\pi^2}{45}T^3 \,. \tag{A.18}$$

$h_{\rm eff}$ is the effective number of entropic degrees of freedom of radiation. Combining Eqs. (A.15) and (A.17) and defining $x = m_{\rm LSP}/T$, the ratio of the LSP mass over temperature, yield

$$\frac{dY}{dx} = -\sqrt{\frac{\pi}{45G}}\frac{g_*^{1/2}m_{\rm LSP}}{x^2}\langle\sigma_{\rm eff}v\rangle(Y^2 - Y_{\rm eq}^2) \,, \tag{A.19}$$

with

$$g_*^{1/2} = \frac{h_{\rm eff}}{\sqrt{g_{\rm eff}}}\left(1 + \frac{T}{3h_{\rm eff}}\frac{dh_{\rm eff}}{dT}\right) \,, \tag{A.20}$$

where

$$Y_{eq} = \frac{45}{4\pi^4T^2h_{\rm eff}}\frac{1}{(1+\tilde{s}_D)}\sum_i g_i m_i^2 K_2\left(\frac{m_i}{T}\right) \,, \tag{A.21}$$

i runs over all supersymmetric particles of mass m_i and with g_i degrees of freedom.
The freeze-out temperature T_f is the temperature at which the LSP leaves the initial thermal equilibrium when $Y(T_f) = (1+\delta)Y_{\rm eq}(T_f)$, with $\delta \simeq 1.5$. The relic density is obtained by integrating Eq. (A.19) from $x = 0$ to $m_{\rm LSP}/T_0$, where $T_0 = 2.726$ K is the temperature of the Universe today [25, 26]:

$$\Omega_{\rm LSP}h^2 = \frac{m_{\rm LSP}s(T_0)Y(T_0)h^2}{\rho_c^0} \approx 2.755\times10^8\frac{m_{\rm LSP}}{1\ {\rm GeV}}Y(T_0) \,, \tag{A.22}$$

where ρ_c^0 is the critical density of the Universe, such as

$$H_0^2 = \frac{8\pi G}{3}\rho_c^0 \,, \tag{A.23}$$

H_0 being the Hubble constant.

In practice, to improve the speed of the code, the freeze-out temperature T_f is determined by solving the implicit equation:

$$\frac{dY_{\rm eq}}{dx} = -\sqrt{\frac{\pi}{45G}}\frac{g_*^{1/2} m_{\rm LSP}}{x_f^2}\langle\sigma_{\rm eff} v\rangle \delta(2+\delta) Y_{\rm eq}^2 \,. \tag{A.24}$$

and the evolution equation (A.17) is only solved from $T = T_f$ to T_0, with the initial condition $Y(T_f) = (1+\delta)Y_{\rm eq}$. This method is known to provide results with less than a few percent error for the calculation of the relic density.

A.7 QCD equation of state

To evaluate the relic density, it is necessary to know the number of effective degrees of freedom $g_{\rm eff}$ and $h_{\rm eff}$ which give access to the energy and entropy densities of radiation. To compute them, one generally assumes that above the QCD phase transition critical temperature $T_c \sim 200$ MeV, the primordial plasma is weakly interacting because of asymptotic freedom, and can therefore be treated as an ideal gas.

However, non-perturbative studies have shown that the QCD plasma departs strongly from the ideal gas behavior at high temperatures, and more realistic models have been studied in [23]. In these models, below T_c the hadronic degrees of freedom are modeled by an interacting gas of hadrons, while above T_c the quarks and gluons are taken to interact and are replaced by hadronic models. In `SuperIso Relic`, the models depicted in [23] are available, and can be selected in the routine `Init_modeleff (int model_eff, struct relicparam* paramrelic)` by setting the value of `model_eff` as given below (see subsection A.1.2). The different models are:

- Model A (`model_eff`=1): ignores hadrons completely.
- Model B (`model_eff`=2): considers $T_c = 154$ MeV, and models hadrons as a gas of free mesons and hadrons, with a sharp switch to the hadronic gas at $T_{hg} = T_c$.
- Model B2 (`model_eff`=3): variation of model B constructed by scaling the pressure and energy density lattice data by 0.9.
- Model B3 (`model_eff`=4): variation of model B constructed by scaling the pressure and energy density lattice data by 1.1.

- Model C (`model_eff`=5): assumes $T_c = 185.5$ MeV, and models hadrons as a gas of free mesons and hadrons, with a sharp switch to the hadronic gas at $T_{hg} = 200$ MeV.
- Old Model (`model_eff`=0): models hadrons as an ideal gas.

An example main program is provided as `test_modeleff.c`. For more information about these models, the reader is referred to [23].

A.8 Modified Cosmological Model

The density number of supersymmetric particles is determined by the Boltzmann equation:

$$\frac{dn}{dt} = -3Hn - \langle\sigma v\rangle(n^2 - n_{eq}^2) + N_D \ , \tag{A.25}$$

where n is the number density of supersymmetric particles, $\langle\sigma v\rangle$ is the thermally averaged annihilation cross-section, H is the Hubble parameter, n_{eq} is the relic particle equilibrium number density. The term N_D has been added to provide a parametrization of the non-thermal production of SUSY particles. The expansion rate H is determined by the Friedmann equation:

$$H^2 = \frac{8\pi G}{3}(\rho_{rad} + \rho_D) \ , \tag{A.26}$$

where ρ_{rad} is the radiation energy density, which is considered as dominant before BBN in the standard cosmological model. Following [11, 12], ρ_D is introduced as an effective dark density which parametrizes the expansion rate modification. The entropy evolution reads:

$$\frac{ds}{dt} = -3Hs + \Sigma_D \ , \tag{A.27}$$

where s is the total entropy density. Σ_D parametrizes here effective entropy fluctuations due to unknown properties of the Early Universe. The radiation energy and entropy densities can be written as usual:

$$\rho_{rad} = g_{\rm eff}(T)\frac{\pi^2}{30}T^4 \ , \qquad s_{rad} = h_{\rm eff}(T)\frac{2\pi^2}{45}T^3 \ . \tag{A.28}$$

Separating the radiation entropy density from the total entropy density, *i.e.* setting $s \equiv s_{rad} + s_D$ where s_D is an effective entropy density, the following relation between s_D and Σ_D can be derived:

$$\Sigma_D = \sqrt{\frac{4\pi^3 G}{5}}\sqrt{1+\tilde{\rho}_D}T^2\left[\sqrt{g_{\rm eff}}s_D - \frac{1}{3}\frac{h_{\rm eff}}{g_*^{1/2}}T\frac{ds_D}{dT}\right] \ . \tag{A.29}$$

Following the standard relic density calculation method [25,26], we introduce $Y \equiv n/s$, and Eq. (A.25) becomes

$$\frac{dY}{dx} = -\frac{m_{LSP}}{x^2}\sqrt{\frac{\pi}{45G}}g_*^{1/2}\left(\frac{1+\tilde{s}_D}{\sqrt{1+\tilde{\rho}_D}}\right)\left[\langle\sigma v\rangle(Y^2 - Y_{eq}^2) + \frac{Y\Sigma_D - N_D}{\left(h_{\rm eff}(T)\frac{2\pi^2}{45}T^3\right)^2(1+\tilde{s}_D)^2}\right] , \tag{A.30}$$

where $x = m_{LSP}/T$, m_{LSP} being the mass of the relic particle, and

$$\tilde{s}_D = \frac{s_D}{h_{\rm eff}(T)\frac{2\pi^2}{45}T^3} , \qquad \tilde{\rho}_D \equiv \frac{\rho_D}{g_{\rm eff}\frac{\pi^2}{30}T^4} , \tag{A.31}$$

and

$$Y_{eq} = \frac{45}{4\pi^4 T^2 h_{\rm eff}}\frac{1}{(1+\tilde{s}_D)}\sum_i g_i m_i^2 K_2\left(\frac{m_i}{T}\right) , \tag{A.32}$$

where i runs over all supersymmetric particles of mass m_i and with g_i degrees of freedom. Following the methods described in Section A.6, the relic density can then be calculated:

$$\Omega h^2 = 2.755 \times 10^8 Y_0 m_{LSP}/\text{GeV} . \tag{A.33}$$

where Y_0 is the present value of Y. In the limit where $\rho_D = s_D = \Sigma_D = N_D = 0$, usual relations are retrieved. We should note here that s_D and Σ_D are not independent variables.

In `SuperIso Relic`, we adopt the parametrizations described in [11, 12] for ρ_D and s_D:

$$\rho_D = \kappa_\rho \rho_{rad}(T_{BBN})\big(T/T_{BBN}\big)^{n_\rho} \tag{A.34}$$

and

$$s_D = \kappa_s s_{rad}(T_{BBN})\big(T/T_{BBN}\big)^{n_s} , \tag{A.35}$$

where T_{BBN} stands for the BBN temperature. κ_ρ and κ_s are respectively the ratio of effective dark energy/entropy density over radiation energy/entropy density, and n_ρ and n_s are parameters describing the behavior of the densities. We refer the reader to [11,12] for detailed descriptions and discussions of these parametrizations.

Another parametrization of entropy inspired by reheating scenarios is present in `SuperIso Relic`. In this reheating-like parametrization the entropy production Σ_D evolves like [14]

$$\Sigma_D = \kappa_\Sigma \Sigma_{rad}(T_{BBN})\left(\frac{T}{T_{BBN}}\right)^{n_\Sigma} . \tag{A.36}$$

κ_Σ is the ratio of effective dark entropy production over radiation entropy production, and n_Σ is a parameter describing the behavior of this entropy

production ($n_\Sigma \sim -1$ in most reheating scenarios). The radiation entropy production reads:

$$\Sigma_{rad}(T_{BBN}) = \left(\frac{4\pi^3 G}{5} g_{\text{eff}}(T_{BBN})\right)^{1/2} T_{BBN}^2 s_{rad}(T_{BBN}) \,. \tag{A.37}$$

The dark entropy density can then be calculated by:

$$s_D(T) = 3\sqrt{\frac{5}{4\pi^3 G}} h_{\text{eff}} T^3 \int_0^T dT' \frac{g_*^{1/2} \Sigma_D(T')}{\sqrt{1 + \frac{\rho_D}{\rho_{rad}}} h_{\text{eff}}^2(T') T'^6} \,. \tag{A.38}$$

An extra-parameter has to be introduced to remain consistent with cosmological observations: the reheating temperature T_r below which entropy production stops. This parametrization is further described in [14].

Bibliography

[1] P. Skands *et al.*, "SUSY Les Houches accord: Interfacing SUSY spectrum calculators, decay packages, and event generators", JHEP **0407**, 036 (2004).

[2] B. Allanach *et al.*, "SUSY Les Houches Accord 2", Comput. Phys. Commun. **180**, 8 (2009).

[3] B.C. Allanach, "SOFTSUSY: A C++ program for calculating supersymmetric spectra", Comput. Phys. Commun. **143**, 305 (2002).

[4] H. Baer *et al.*, "ISAJET 7.69: A Monte Carlo event generator for pp, $\bar{p}p$, and e^+e^- reactions", hep-ph/0312045.

[5] W. Porod, "SPheno, a program for calculating supersymmetric spectra, SUSY particle decays and SUSY particle production at e^+e^- colliders", Comput. Phys. Commun. 153, 275 (2003).

[6] A. Djouadi, J.L. Kneur and G. Moultaka, "SuSpect: A Fortran code for the supersymmetric and Higgs particle spectrum in the MSSM", Comput. Phys. Commun. 176, 426 (2007).

[7] U. Ellwanger and C. Hugonie, "NMSPEC: A Fortran code for the sparticle and Higgs masses in the NMSSM with GUT scale boundary conditions", Comput. Phys. Commun. 177, 399 (2007); "NMHDECAY 2.0: An Updated program for sparticle masses, Higgs masses, couplings and decay widths in the NMSSM", Comput. Phys. Commun. 175, 290 (2006).

[8] P. Gondolo *et al.*, "DarkSUSY: Computing supersymmetric dark matter properties numerically", JCAP **0407**, 008 (2004).

[9] H. Baer, C. Balazs and A. Belyaev, "Neutralino relic density in minimal supergravity with coannihilations", JHEP **0203**, 042 (2002).

[10] G. Bélanger, F. Boudjema, A. Pukhov and A. Semenov, "micrOMEGAs: Version 1.3", Comput. Phys. Commun. **174**, 577 (2006).

[11] A. Arbey and F. Mahmoudi, "SUSY constraints from relic density: High sensitivity to pre-BBN expansion rate", Phys. Lett. B**669**, 46 (2008).

[12] A. Arbey and F. Mahmoudi, "SUSY Constraints, Relic Density, and Very Early Universe", JHEP**1005** (2010), 051.

[13] A. Arbey and F. Mahmoudi, "LHC and ILC Data and the Early Universe Properties", Nuovo Cim. C**33**, 151 (2010).

[14] A. Arbey, A. Deandrea and A. Tarhini, "Anomaly mediated SUSY breaking scenarios in the light of cosmology and in the dark (matter)", JHEP **1105**, 078 (2011).

[15] F. Mahmoudi, "SuperIso: A Program for calculating the isospin asymmetry of $B \to K^* \gamma$ in the MSSM", Comput. Phys. Commun. **178**, 745 (2008);
F. Mahmoudi, "SuperIso v2.3: A Program for calculating flavour physics observables in Supersymmetry", Comput. Phys. Commun. **180**, 1579 (2009); F. Mahmoudi, "SuperIso v3.0, flavor physics observables calculations: Extension to NMSSM", Comput. Phys. Commun. **180**, 1718 (2009), `http://superiso.in2p3.fr` .

[16] S. Wolfram, "The Mathematica Book", ISBN 1579550223.

[17] A. Semenov, "LanHEP: A Package for the automatic generation of Feynman rules in field theory. Version 3.0", Comput. Phys. Commun. **180**, 431 (2009).

[18] T. Hahn, "Generating Feynman Diagrams and Amplitudes with FeynArts 3", Comput. Phys. Commun. **140**, 418 (2001);
T. Hahn and C. Schappacher, "The Implementation of the Minimal Supersymmetric Standard Model in FeynArts and FormCalc", Comput. Phys. Commun. **143**, 54 (2002).

[19] T. Hahn and M. Perez-Victoria, "Automatized One-Loop Calculations in 4 and D dimensions", Comput. Phys. Commun. **118**, 153 (1999) [hep-ph/9807565];
T. Hahn and M. Rauch, "News from FormCalc and LoopTools", hep-ph/0601248.

[20] S. Heinemeyer, W. Hollik and G. Weiglein, "FeynHiggs: A Program for the calculation of the masses of the neutral CP even Higgs bosons in the MSSM", Comput. Phys. Commun. **124**, 76 (2000).

[21] A. Djouadi, J. Kalinowski and M. Spira, "HDECAY: A program for Higgs boson decays in the standard model and its supersymmetric extension", Comput. Phys. Commun. **108**, 56 (1998).

[22] K. Nakamura *et al.* [Particle Data Group], "Review of particle physics", J. Phys. G**37**, 075021 (2010).

[23] M. Hindmarsh and O. Philipsen, "WIMP dark matter and the QCD equation of state", Phys. Rev. D**71**, 087302 (2005).

[24] J. Dunkley *et al.*, "Five-Year Wilkinson Microwave Anisotropy Probe (WMAP) Observations: Likelihoods and Parameters from the WMAP data", Astrophys. J. Suppl. **180**, 306 (2009).

[25] P. Gondolo and G. Gelmini, "Cosmic abundances of stable particles: Improved analysis", Nucl. Phys. B**360**, 145 (1991).

[26] J. Edsjö and P. Gondolo, "Neutralino relic density including coannihilations", Phys. Rev. D**56**, 1879 (1997).

[27] G. Bélanger, F. Boudjema, A. Pukhov and A. Semenov, "MicrOMEGAs: A Program for calculating the relic density in the MSSM", Comput. Phys. Commun. **149**, 103 (2002).

Appendix B

AlterBBN

Big Bang Nucleosynthesis (BBN) is an important part of the Cosmological Standard Model, as it gave birth to the first nuclei. Based on BBN models it is possible to calculate the abundances of the light elements in the Universe [1], which can then be compared to the measured abundances. This allows to probe the Universe properties at the time of nucleosynthesis, which is the most ancient period observationally accessible. In standard cosmology, only one free parameter, the baryon-to-photon ratio at BBN time is needed to determine the abundances of the elements, and this parameter can be deduced from the observation of the Cosmic Microwave Background [2]. To calculate the abundances of the elements in the standard model of cosmology, several "semi-public" or private codes, such as NUC123 [3, 4] or PArthENoPE [5], already exist.

I have written a public code, `AlterBBN`, which enables the calculation of the abundances of the elements in the standard cosmological model, as well as in alternative cosmological models such as quintessence or reheating scenarios. Indeed, many different phenomena in the Early Universe could have modified the Universe properties at the time of BBN, and in such cases the calculations could lead to abundances of the elements different from the predictions in the standard cosmological model. One of the main features of `AlterBBN` is that it provides calculations in such cosmological models, which can enable the user to test alternative scenarios and to constrain their parameters.

B.1 BBN physics

In the following section, we use the natural unit system $c = \hbar = k = 1$.

B.1.1 BBN in the Cosmological Standard Model

All the nuclear reactions implemented in `AlterBBN` have evolution equations of the form:

$$n_i\,{}^{A_i}Z_i \,+\, n_j\,{}^{A_j}Z_j \longleftrightarrow n_k\,{}^{A_k}Z_k \,+\, n_l\,{}^{A_l}Z_l\ . \tag{B.1}$$

Therefore, the abundance change for nuclide i is given by [4]:

$$\frac{dY_i}{dt} = \sum_{j,k,l} n_i \left(-\frac{Y_i^{n_i} Y_j^{n_j}}{n_i!\, n_j!}\Gamma_{ij}^k + \frac{Y_l^{n_l} Y_k^{n_k}}{n_l!\, n_k!}\Gamma_{lk}^j \right)\ , \tag{B.2}$$

where the nuclide abundance is $Y_i = X_i/A_i$, X_i being the mass fraction in nuclide i and A_i its atomic number. n_i is the number of nuclides i involved in the reaction, Γ_{ij}^k is the forward reaction rate and Γ_{lk}^j the reverse rate. The expansion rate of the Universe is given by the Friedmann equation:

$$H^2 = \left(\frac{\dot{a}}{a}\right) = \frac{8\pi G}{3}\rho_{tot}\ , \tag{B.3}$$

and the equation of energy conservation can be written as:

$$\frac{d}{dt}(\rho_{tot}a^3) + P_{tot}\frac{d}{dt}(a^3) - a^3\ \left.\frac{d\rho_{tot}}{dt}\right|_{T=cst} = 0\ , \tag{B.4}$$

where

$$\rho_{tot} = \rho_\gamma + \rho_\nu + \rho_b + (\rho_{e^-} + \rho_{e^+})\ , \tag{B.5}$$

and

$$P_{tot} = P_\gamma + (P_{e^-} + P_{e^+}) + P_b\ . \tag{B.6}$$

We have

$$P_\gamma = \frac{1}{3}\rho_\gamma\ , \qquad \rho_\gamma = \frac{\pi}{15}T^4\ . \tag{B.7}$$

In `AlterBBN`, we consider that the neutrinos are non-degenerate, *i.e.* the neutrino chemical potential ϕ_ν is negligible. In this context, the neutrino energy density writes:

$$\rho_\nu = N_\nu \frac{7}{8}\,\frac{\pi}{15}T_\nu^4 = N_\nu \frac{7\pi}{120}\left(\frac{4}{11}\right)^{4/3} T^4\ , \tag{B.8}$$

where $N_\nu = 3$ is the number of neutrino families. The sum of the electron and positron densities is

$$\rho_{e^-} + \rho_{e^+} = \frac{2}{\pi^2}m_e^4 \sum_{n=1}^{\infty}(-1)^{n+1}\cosh(n\phi_e)M(nz)\ , \tag{B.9}$$

and the sum of their pressures is

$$P_{e^-} + P_{e^+} = \frac{2}{\pi^2}m_e^4 \sum_{n=1}^{\infty}\frac{(-1)^{n+1}}{nz}\cosh(n\phi_e)L(nz)\ , \tag{B.10}$$

where $z = m_e/T$,

$$L(z) = \frac{K_2(z)}{z} , \qquad M(z) = \frac{1}{z}\left[\frac{3}{4}K_3(z) + \frac{1}{4}K_1(z)\right] , \tag{B.11}$$

the K_i being the modified Bessel functions. The charge conservation gives

$$n_{e^-} - n_{e^+} = \mathcal{N}_A h T^3 S , \tag{B.12}$$

where $\mathcal{N}_A$ is the Avogadro number,

$$S = \sum_i Z_i Y_i , \tag{B.13}$$

and the difference between the electron and positron densities is

$$n_{e^-} - n_{e^+} = \frac{2}{\pi^2} m_e^3 \sum_{n=1}^{\infty} (-1)^{n+1} \sinh(n\phi_e) L(nz) , \tag{B.14}$$

from which ϕ_e can be determined using:

$$\frac{d\phi_e}{dt} = \frac{\partial \phi_e}{\partial T}\frac{dT}{dt} + \frac{\partial \phi_e}{\partial a}\frac{da}{dt} + \frac{\partial \phi_e}{\partial S}\frac{dS}{dt} . \tag{B.15}$$

The baryon energy density reads

$$\rho_b = hT^3 \left[1 + \sum_i \left(\frac{\Delta M_i}{M_u} + \zeta T\right) Y_i\right] , \tag{B.16}$$

where ΔM_i is the mass excess of nuclide i, and the pressure is

$$P_b = hT^3 \left(\frac{2}{3}\zeta T \sum_i Y_i\right) , \tag{B.17}$$

with $\zeta = 1.388 \times 10^{-4}$. $h \sim \rho_b/T^3 \sim 1/a^3/T^3$ can be determined by the equation:

$$\frac{dh}{dt} = -3h\left(\frac{1}{a}\frac{da}{dt} + \frac{1}{T}\frac{dT}{dt}\right) . \tag{B.18}$$

To solve the system of differential equations which gives the abundances of the elements, we assume the following initial conditions:

$$h(T_i) = M_u \frac{n_\gamma(T_i)}{T_i^3}\eta, \tag{B.19}$$

where M_u is the unit atomic mass, n_γ is the number density of photons and η the baryon-to-photon ratio. Also,

$$\phi_e(T_i) \approx \frac{\pi^2}{2}\mathcal{N}_A \frac{h(T_i)Y_p}{z_i^3} \frac{1}{\sum_{n=1}^{\infty}(-1)^{n+1} n L(nz_i)} , \tag{B.20}$$

and the initial abundances of protons and neutrons are

$$Y_p(T_i) = \frac{1}{1+e^{-q/T_i}} \ , \qquad Y_n(T_i) = \frac{1}{1+e^{q/T_i}} \ , \tag{B.21}$$

where $q = m_n - m_p$. The other quantities needed at this point are the initial baryon energy density

$$\rho_b(T_i) \approx h(T_i) T_i^3 \ , \tag{B.22}$$

and the time

$$t_i = (12\pi G\sigma)^{1/2} T_i^{-2} \ , \tag{B.23}$$

where σ is the Stefan-Boltzmann constant.

To solve this system of equations, a linearization of the nuclear abundance differential equations is performed, followed by a Runge-Kutta integration. Uncertainties can then be evaluated by computing the abundances of the elements using lower or higher limits of the nuclear reaction rates.

B.1.2 Modified Cosmological Scenarios

The Early Universe is a relatively unknown period, and therefore the properties of the Universe at that period are not well-known either. We consider in the following several alternative descriptions of the Early Universe properties, already described in Section 1 and Appendix A.

Modified expansion rate

Many phenomena at the time of BBN could have effects on the expansion rate of the Universe. In such cases, the Friedmann equation is affected, and we parametrize the modification of the expansion by adding an effective dark energy density ρ_D to the total energy of the Universe. The Friedmann equation then reads:

$$H^2 = \left(\frac{\dot{a}}{a}\right) = \frac{8\pi G}{3}(\rho_{tot} + \rho_D) \ . \tag{B.24}$$

We adopt the parametrizations described in [6, 7] for ρ_D:

$$\rho_D = \kappa_\rho \rho_{tot}(T_0) \left(\frac{T}{T_0}\right)^{n_\rho} \ , \tag{B.25}$$

where $T_0 = 1$ MeV. κ_ρ is therefore the ratio of effective dark energy density over total energy density, and n_ρ is a parameter describing the behavior of this density. We refer the reader to [6, 7] for detailed descriptions and discussions of this parametrization.

Modified entropy content

The entropy content can also receive various contributions in the BBN period. We parametrize the contributions by considering an effective dark entropy density s_D. The energy conservation equation reads in this case:

$$\frac{d}{dt}(\rho_{tot}a^3) + P_{tot}\frac{d}{dt}(a^3) - a^3\left.\frac{d\rho_{tot}}{dt}\right|_{T=cst} - T\frac{d}{dt}(s_D a^3) = 0\ . \tag{B.26}$$

We adopt two different parametrization for s_D. The first one has been introduced in [7]:

$$s_D = \kappa_s s_{rad}(T_0)\left(\frac{T}{T_0}\right)^{n_s}\ , \tag{B.27}$$

where $T_0 = 1$ MeV and

$$s_{rad}(T) = h_{\rm eff}(T)\frac{2\pi^2}{45}T^3\ , \tag{B.28}$$

$h_{\rm eff}$ being the effective number of entropic degrees of freedom of radiation, κ_s the ratio of effective dark entropy density over radiation entropy density, and n_s a parameter describing the behavior of this density. We refer the reader to [7] for detailed descriptions and discussions of this parametrization.

The second parametrization is inspired by reheating scenarios in which the entropy production Σ_D evolves like [8]

$$\Sigma_D(T) = \kappa_\Sigma \Sigma_{rad}(T_0)\left(\frac{T}{T_0}\right)^{n_\Sigma} \tag{B.29}$$

where $T_0 = 1$ MeV. κ_Σ is the ratio of effective dark entropy production over radiation entropy production, and n_Σ is a parameter describing the behavior of this entropy production ($n_\Sigma \sim -1$ in most reheating scenarios). The radiation entropy production reads:

$$\Sigma_{rad}(T_0) = \left(\frac{4\pi^3 G}{5}g_{\rm eff}(T_0)\right)^{1/2} T_0^2 s_{rad}(T_0)\ , \tag{B.30}$$

$g_{\rm eff}$ being the effective number of degrees of freedom of radiation, and where the entropy production stops at $T = T_r$. The function $\Sigma_D(T)$ is related to the entropy density by:

$$s_D(T) = 3\sqrt{\frac{5}{4\pi^3 G}}h_{\rm eff}T^3\int_0^T dT' \frac{g_*^{1/2}\Sigma_D(T')}{\sqrt{1+\dfrac{\rho_D}{\rho_{rad}}}h_{\rm eff}^2(T')T'^6}\ , \tag{B.31}$$

where

$$g_*^{1/2} = \frac{h_{\rm eff}}{\sqrt{g_{\rm eff}}}\left(1 + \frac{T}{3h_{\rm eff}}\frac{dh_{\rm eff}}{dT}\right)\ . \tag{B.32}$$

This parametrization is further described in [8].

B.2 Content of the AlterBBN package

`AlterBBN` is based on the library `libbbn.a`, which contains all the procedure necessary to the abundance computation, and is provided with five different programs.

B.2.1 Parameter structure

The main structure of the package `AlterBBN` is defined in `src/include.h` and is provided below:

```
typedef struct relicparam
{
int entropy_model;
double dd0,ndd,Tdend;
double sd0,nsd,Tsend;
double Sigmad0,nSigmad,TSigmaend;
double nt0,nnt,Tnend;
double mgravitino;
double table_eff[276][3];
double eta0;
double nbnu;
double life_neutron;
}
relicparam;
```

This structure contains all the parameters which are necessary to the computation of the abundances of the elements in the standard cosmological model as well as in alternative models.

B.2.2 Main routines

The main routines of the `libbbn.a` library, which are needed for the abundance calculation, are detailed in the following:

- `void Init_cosmomodel(struct relicparam* paramrelic)`

  This function initializes the `paramrelic` structure, setting all the parameters to 0, apart from the number of neutrinos which is set to 3, the neutron lifetime to 885.7s, and the baryon-to-photon ratio to $\eta = 6.19 \times 10^{-10}$ [2].

- `void Init_cosmomodel_param(double eta, double nbnu, double life_neutron, struct relicparam* paramrelic)`

This routine specifies values of the `paramrelic` structure, enabling the user to modify the baryon-to-photon ratio `eta`, the number of neutrinos `nbnu` and the neutron lifetime `life_neutron`.

- `void Init_dark_density(double dd0, double ndd, double T_end, struct relicparam* paramrelic)`

  This routine changes values in the `paramrelic` structure, initializing the effective dark density parameters described in Section B.1.2, with κ_ρ=`dd0`, n_ρ=`ndd`, and where `T_end` is a temperature cut at which the dark density is set to 0.

- `void Init_dark_entropy(double sd0, double nsd, double T_end, struct relicparam* paramrelic)`

  This routine changes values in the `paramrelic` structure, initializing the effective dark entropy density parameters described in Section B.1.2, with κ_s=`sd0`, n_s=`nsd`, and where `T_end` is a temperature cut at which the dark entropy density is set to 0.

- `void Init_dark_entropySigmaD(double Sigmad0, double nSigmad, double T_end, struct relicparam* paramrelic)`

  This routine specifies values of the `paramrelic` structure, initializing the effective dark entropy production parameters described in Section B.1.2, with κ_Σ=`Sigmad0`, n_Σ=`nSigmad`, and where `T_end` is a temperature cut at which the dark entropy production is set to 0.

- `void rate_weak(int err, double f[])`

  This procedure computes the decay rates of the weak interaction reactions, and stores them in `f`. The `err` parameter is a switch to choose if the central (`err=0`), high (`err=1`) or low (`err=2`) values of the nuclear rates is used.

- `void rate_pn(int err, struct relicparam* paramrelic, double f[], double r[], double T9)`

  This procedure computes the decay rate and reverse rate of $p \leftrightarrow n$ reactions, and stores them in `f` and `r` respectively, at a temperature `T9` (in unit of 10^9 K). The `err` parameter is a switch to choose if the

central (`err=0`), high (`err=1`) or low (`err=2`) values of the nuclear rates is used.

- `void rate_all(int err, double f[], double T9)`

  This procedure computes all the other reactions (summarized in Section B.6) at temperature `T9` and stores them in `f`. The `err` parameter is a switch to choose if the central (`err=0`), high (`err=1`) or low (`err=2`) values of the nuclear rates is used.

- `int nucl(int err, struct relicparam* paramrelic, double *eta, double *H2_H, double *He3_H2, double *Yp, double *Li7_H, double *Li6_Li7, double *Be7_H)`

  This function is the main routine of the program, as it calculates using the `paramrelic` structure the baryon-to-photon ratio `eta`, the ratio of the element abundances `H2_H`, `He3_H2`, `Li7_H`, `Li6_Li7`, `Be7_H`, and the helium abundance `Y_p`. The `err` parameter is a switch to choose if the central (`err=0`), high (`err=1`) or low (`err=2`) values of the nuclear rates is used. It can be used to evaluate the uncertainties. The function returns 0 if the calculation failed, or 1 otherwise.

- `int bbn_excluded(int err, struct relicparam* paramrelic)`

  This function is a "container" function which calls the routine `nucl` and returns 0 if the abundances satisfy the constraints of Section B.7, 1 otherwise, and -1 if the calculation failed. The `err` parameter is a switch to choose if the central (`err=0`), high (`err=1`) or low (`err=2`) values of the nuclear rates is used.

B.3 Compilation and installation instructions

`AlterBBN` is written for a C compiler respecting the C99 standard, and it has been tested successfully with the GNU C and the Intel C Compilers on Linux and Mac. The package can be downloaded from:

`http://superiso.in2p3.fr/relic/alterbbn`

After unpacking, the following main directory is created:

`alterbbn_vX.X`

This directory contains the `src/` directory, in which all the source files can be found. The main directory contains also a `Makefile`, a `README`, six sample main programs (`stand_cosmo.c`, `alter_eta.c`, `alter_neutrinos.c`, `alter_etannutau.c`, `alter_standmod.c` and `alter_reheating.c`). The compilation options should be defined in the `Makefile`, and in particular the C compiler name and its specific flags, if needed.
Additional information can be found in the `README` file.
To compile the library, type

```
make
```

This creates `libbbn.a` in `src/`. Then, to compile one of the six programs provided in the main directory, type

`make name` or `make name.c`

where `name` can be `stand_cosmo`, `alter_eta`, `alter_neutrinos`, `alter_etannutau`, `alter_standmod` or `alter_reheating`. This generates an executable program with the `.x` extension:

`stand_cosmo.x` calculates the abundance of the elements in the standard cosmological model, assuming the baryon-to-photon ratio measured by WMAP.

`alter_eta.x` computes the abundance of the elements in the standard cosmological model, with the baryon-to-photon ratio given by the user.

`alter_neutrinos.x` calculates the abundance of the elements in the standard cosmological model, and give the user the possibility to alter the number of neutrinos.

`alter_etannutau.x` computes the abundance of the elements in the standard cosmological model, with the baryon-to-photon ratio, number of neutrinos and neutron lifetime given by the user.

`alter_standmod.x` and `alter_reheating` computes the abundance of the elements in cosmological scenarios with modified expansion rates and entropy contents.

B.4 Input and output description

In the following, we describe the input and output of the main programs.

B.4.1 Standard cosmology

The program `stand_cosmo.x` computes the abundance of the elements in the standard cosmological model assuming the baryon-to-photon ratio $\eta = 6.19 \times 10^{-10}$ measured by WMAP [2]. No parameter is needed by this program. Running the program with:

```
./stand_cosmo.x
```

returns

```
      Yp          H2/H            He3/H2          Li7/H           Li6/Li7         Be7/H
 low: 2.475e-01  2.581e-05        4.193e-01       5.020e-10       3.391e-06       4.172e-10
cent: 2.476e-01  2.515e-05        4.037e-01       4.694e-10       2.343e-05       4.433e-10
high: 2.476e-01  2.458e-05        1.770e-01       1.587e-10       2.236e-04       1.494e-10
Compatible with BBN constraints
```

On the lines `low`, `cent` and `high` are given the abundances of the elements computed using the lower, central and higher values of the nuclear rates respectively. This gives an evaluation of the errors due to the uncertainties in the nuclear rates. The information `Compatible with BBN constraints` corresponds to the fact that the abundances computed with the central values of the nuclear rates are compatible with the constraints of Section B.7.

B.4.2 Standard cosmology with η modification

The program `alter_eta.x` computes the abundance of the elements in the standard cosmological model, and needs the baryon-to-photon ratio η as input. Running the program with:

```
./alter_eta.x 3e-10
```

returns

```
      Yp          H2/H            He3/H2          Li7/H           Li6/Li7         Be7/H
 low: 2.400e-01  8.006e-05        2.210e-01       3.176e-10       1.656e-05       4.760e-11
cent: 2.400e-01  7.833e-05        2.085e-01       1.146e-10       2.829e-04       5.710e-11
high: 2.401e-01  7.648e-05        1.087e-01       4.714e-11       2.216e-03       2.461e-11
Excluded by BBN constraints
```

On the lines `low`, `cent` and `high` are given the abundances of the elements computed using the lower, central and higher values of the nuclear rates respectively. This gives an evaluation of the errors due to the uncertainties in the nuclear rates. The information `Excluded by BBN constraints` corresponds to the fact that the abundances computed with the central values of the nuclear rates are not compatible with the constraints of Section B.7.

B.4.3 Standard cosmology with modified neutrino number

The program `alter_neutrinos.x` computes the abundance of the elements in the standard cosmological model with a modified neutrino number. It

needs as input the number of neutrino families N_ν.
Running the program with:
`./alter_neutrinos.x 4.5`
returns

```
      Yp          H2/H            He3/H2          Li7/H           Li6/Li7         Be7/H
 low: 2.657e-01   3.094e-05       3.744e-01       4.606e-10       4.900e-06       3.480e-10
cent: 2.658e-01   3.017e-05       3.596e-01       4.105e-10       3.525e-05       3.774e-10
high: 2.658e-01   2.949e-05       1.607e-01       1.420e-10       3.295e-04       1.301e-10
Excluded by BBN constraints
```

On the lines `low`, `cent` and `high` are given the abundances of the elements computed using the lower, central and higher values of the nuclear rates respectively. This gives an evaluation of the errors due to the uncertainties in the nuclear rates. The information `Excluded by BBN constraints` corresponds to the fact that the abundances computed with the central values of the nuclear rates are not compatible with the constraints of Section B.7.

B.4.4 Standard cosmology with modified η, neutrino number and neutron lifetime

The program `alter_etannutau.x` computes the abundance of the elements in the standard cosmological model with a modified baryon-to-photon ratio, neutrino number and neutron lifetime. It needs as input η, the number of neutrino families N_ν and the neutron lifetime in second.
Running the program with:
`./alter_etannutau.x 3e-10 4.5 890`
returns

```
      Yp          H2/H            He3/H2          Li7/H           Li6/Li7         Be7/H
 low: 2.590e-01   9.639e-05       1.997e-01       4.054e-10       1.741e-05       3.394e-11
cent: 2.591e-01   9.436e-05       1.874e-01       1.172e-10       3.685e-04       4.145e-11
high: 2.591e-01   9.214e-05       1.020e-01       4.888e-11       2.839e-03       1.896e-11
Excluded by BBN constraints
```

On the lines `low`, `cent` and `high` are given the abundances of the elements computed using the lower, central and higher values of the nuclear rates respectively. This gives an evaluation of the errors due to the uncertainties in the nuclear rates. The information `Excluded by BBN constraints` corresponds to the fact that the abundances computed with the central values of the nuclear rates are not compatible with the constraints of Section B.7.

B.4.5 Effective energy and entropy densities

The program `alter_standmod.x` computes the abundance of the elements while adding to the standard cosmological model an effective energy density

such that

$$\rho_D = \kappa_\rho \rho_{rad}(T_{BBN})\big(T/T_{BBN}\big)^{n_\rho} \ , \tag{B.33}$$

and/or an effective entropy density

$$s_D = \kappa_s s_{rad}(T_{BBN})\big(T/T_{BBN}\big)^{n_s} \ , \tag{B.34}$$

which modify the Early Universe properties without having observational consequences if chosen adequately [6, 7]. A description of the model and of the related equations can be found in Sections B.1.2 and B.1.2. The necessary arguments to this program are:

- κ_ρ: ratio of dark energy density over radiation energy density at BBN time,
- n_ρ: dark energy density decrease exponent,
- κ_s: ratio of dark entropy density over radiation entropy density at BBN time,
- n_s: dark entropy density decrease exponent.

Optional arguments can also be given:

- T_ρ: temperature in GeV below which the dark energy density is set to 0,
- T_s: temperature in GeV below which the dark entropy density is set to 0.

For example, the command `./alter_standmod.x 0.1 6 1.e-3 5` returns

```
      Yp          H2/H          He3/H2          Li7/H          Li6/Li7         Be7/H
 low: 2.341e-01  4.601e-05      2.991e-01       2.875e-10      9.974e-06       1.456e-10
cent: 2.341e-01  4.492e-05      2.858e-01       2.010e-10      9.010e-05       1.651e-10
high: 2.342e-01  4.390e-05      1.345e-01       7.484e-11      7.827e-04       6.137e-11
Compatible with BBN constraints
```

On the lines `low`, `cent` and `high` are given the abundances of the elements computed using the lower, central and higher values of the nuclear rates respectively. This gives an evaluation of the errors due to the uncertainties in the nuclear rates. The information `Compatible with BBN constraints` corresponds to the fact that the abundances computed with the central values of the nuclear rates are compatible with the constraints of Section B.7.

B.4.6 Effective reheating model

The program `alter_standmod.x` computes the abundance of the elements while adding to the standard cosmological model an effective energy density such that

$$\rho_D = \kappa_\rho \rho_{rad}(T_{BBN})\big(T/T_{BBN}\big)^{n_\rho} , \tag{B.35}$$

and/or an effective entropy production

$$\Sigma_D = \kappa_\Sigma \Sigma_{rad}(T_{BBN})\big(T/T_{BBN}\big)^{n_\Sigma} , \tag{B.36}$$

which modify the Early Universe properties without having observational consequences if chosen adequately [8]. A description of the model and of the related equations can be found in Sections B.1.2 and B.1.2. Note that Σ_D is related to s_D by Eq. (B.31). The necessary arguments to this program are:

- κ_ρ: ratio of dark energy density over radiation energy density at BBN time,
- n_ρ: dark energy density decrease exponent,
- κ_Σ: ratio of dark entropy production over radiation entropy production at BBN time,
- n_Σ: dark entropy production exponent,
- T_r: temperature in GeV below which the dark energy density and the entropy production are set to 0.

For example, the command `./alter_reheating.x 0.1 6 0.1 -1 1e-3` returns

```
      Yp          H2/H            He3/H2          Li7/H           Li6/Li7         Be7/H
 low: 2.589e-01   2.654e-05       4.123e-01       5.175e-10       3.595e-06       4.249e-10
cent: 2.590e-01   2.587e-05       3.968e-01       4.813e-10       2.496e-05       4.530e-10
high: 2.590e-01   2.528e-05       1.745e-01       1.632e-10       2.374e-04       1.532e-10
Excluded by BBN constraints
```

On the lines `low`, `cent` and `high` are given the abundances of the elements computed using the lower, central and higher values of the nuclear rates respectively. This gives an evaluation of the errors due to the uncertainties in the nuclear rates. The information `Excluded by BBN constraints` corresponds to the fact that the abundances computed with the central values of the nuclear rates are not compatible with the constraints of Section B.7.

In order to perform scans in different cosmological models, the user is invited to write his/her own programs using the above main programs as guidelines.

B.5 Results

`AlterBBN` has been thoroughly tested, and provides results in agreement with those of NUC123 [3, 4].

Considering the different cosmological models implemented, it is possible to perform scans on the cosmological parameters of these models to determine constraints. For example, in Fig. B.1, the current limits on the modified expansion properties from the Y_p and $^2H/H$ BBN constraints are presented. The area between the back lines on the left plot and the area on the top of the black lines on the right plot lead to unfavored element abundances. The constraints of Section B.7 are used in this figure.

Also, `AlterBBN` has been interfaced and provided in the SuperIso Relic package [9] (described in Appendix A, so that the implemented cosmological models can be tested at the same time by BBN constraints as well as by particle physics constraints.

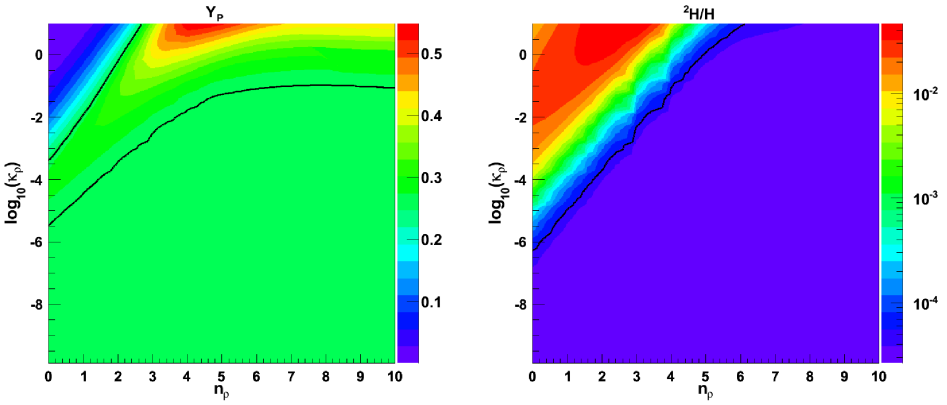

Figure B.1: Constraints from Y_p (left) and $^2H/H$ (right) on the effective dark energy density parameters (n_ρ, κ_ρ). The parameter regions excluded by BBN are located between the black lines for Y_p, and in the upper left corner for $^2H/H$. The colours correspond to different values of Y_p and $^2H/H$.

B.6 Nuclear reaction network

`AlterBBN` currently includes a network of 88 nuclear reactions, which are gathered in the following table.

nb	ref	reaction
0	[10]	$n \leftrightarrow p$
1	[11]	${}^3H \rightarrow e^- + \nu + {}^3He$
2	[12]	${}^8Li \rightarrow e^- + \nu + 2\,{}^4He$
3	[13]	${}^{12}B \rightarrow e^- + \nu + {}^{12}C$
4	[14]	${}^{14}C \rightarrow e^- + \nu + {}^{14}N$
5	[12]	${}^8B \rightarrow e^+ + \nu + 2\,{}^4He$
6	[13]	${}^{11}C \rightarrow e^+ + \nu + {}^{11}B$
7	[13]	${}^{12}N \rightarrow e^+ + \nu + {}^{12}C$
8	[14]	${}^{13}N \rightarrow e^+ + \nu + {}^{13}C$
9	[14]	${}^{14}O \rightarrow e^+ + \nu + {}^{14}N$
10	[14]	${}^{15}O \rightarrow e^+ + \nu + {}^{15}N$
11	[15]	$H + n \rightarrow \gamma + {}^2H$
12	[3]	${}^2H + n \rightarrow \gamma + {}^3H$
13	[3]	${}^3He + n \rightarrow \gamma + {}^4He$
14	[16]	${}^6Li + n \rightarrow \gamma + {}^7Li$
15	[15]	${}^3He + n \rightarrow p + {}^3H$
16	[15]	${}^7Be + n \rightarrow p + {}^7Li$
17	[17]	${}^6Li + n \rightarrow \alpha + {}^3H$
18	[3]	${}^7Be + n \rightarrow \alpha + {}^4He$
19	[15]	${}^2H + p \rightarrow \gamma + {}^3He$
20	[10]	${}^3H + p \rightarrow \gamma + {}^4He$
21	[18]	${}^6Li + p \rightarrow \gamma + {}^7Be$
22	[15]	${}^6Li + p \rightarrow \alpha + {}^3He$
23	[15]	${}^7Li + p \rightarrow \alpha + {}^4He$
24	[18]	${}^2H + \alpha \rightarrow \gamma + {}^6Li$
25	[15]	${}^3H + \alpha \rightarrow \gamma + {}^7Li$
26	[15]	${}^3He + \alpha \rightarrow \gamma + {}^7Be$
27	[5]	${}^2H + D \rightarrow p + {}^3He$
28	[5]	${}^2H + D \rightarrow n + {}^3H$
29	[15]	${}^3H + D \rightarrow n + {}^4He$
30	[15]	${}^3He + D \rightarrow p + {}^4He$
31	[18]	${}^3He + {}^3He \rightarrow 2\,p + {}^4He$
32	[15]	${}^7Li + D \rightarrow n + \alpha + {}^4He$
33	[17]	${}^7Be + D \rightarrow p + \alpha + {}^4He$
34	[3]	${}^7Li + n \rightarrow \gamma + {}^8Li$
35	[3]	${}^{10}B + n \rightarrow \gamma + {}^{11}B$
36	[16]	${}^{11}B + n \rightarrow \gamma + {}^{12}B$
37	[17]	${}^{11}C + n \rightarrow p + {}^{11}B$
38	[18]	${}^{10}B + n \rightarrow \alpha + {}^7Li$
39	[18]	${}^7Be + p \rightarrow \gamma + {}^8B$
40	[17]	${}^9Be + p \rightarrow \gamma + {}^{10}B$
41	[18]	${}^{10}B + p \rightarrow \gamma + {}^{11}C$
42	[18]	${}^{11}B + p \rightarrow \gamma + {}^{12}C$
43	[17]	${}^{11}C + p \rightarrow \gamma + {}^{12}N$
44	[3]	${}^{12}B + p \rightarrow n + {}^{12}C$
45	[18]	${}^9Be + p \rightarrow \alpha + {}^6Li$
46	[18]	${}^{10}B + p \rightarrow \alpha + {}^7Be$
47	[3]	${}^{12}B + p \rightarrow \alpha + {}^9Be$
48	[17]	${}^6Li + \alpha \rightarrow \gamma + {}^{10}B$
49	[18]	${}^7Li + \alpha \rightarrow \gamma + {}^{11}B$
50	[18]	${}^7Be + \alpha \rightarrow \gamma + {}^{11}C$
51	[3]	${}^8B + \alpha \rightarrow p + {}^{11}C$
52	[16]	${}^8Li + \alpha \rightarrow n + {}^{11}B$
53	[17]	${}^9Be + \alpha \rightarrow n + {}^{12}C$
54	[4]	${}^9Be + D \rightarrow n + {}^{10}B$
55	[4]	${}^{10}B + D \rightarrow p + {}^{11}B$
56	[4]	${}^{11}B + D \rightarrow n + {}^{12}C$
57	[17]	${}^4He + \alpha + n \rightarrow \gamma + {}^9Be$
58	[17]	${}^4He + 2\,\alpha \rightarrow \gamma + {}^{12}C$
59	[4]	${}^8Li + p \rightarrow n + \alpha + {}^4He$
60	[4]	${}^8B + n \rightarrow p + \alpha + {}^4He$
61	[17]	${}^9Be + p \rightarrow d + \alpha + {}^4He$
62	[17]	${}^{11}B + p \rightarrow 2\,\alpha + Be4$
63	[3]	${}^{11}C + n \rightarrow 2\,\alpha + {}^4He$
64	[3]	${}^{12}C + n \rightarrow \gamma + {}^{13}C$
65	[3]	${}^{13}C + n \rightarrow \gamma + {}^{14}C$
66	[3]	${}^{14}N + n \rightarrow \gamma + {}^{15}N$
67	[18]	${}^{13}N + n \rightarrow p + {}^{13}C$
68	[17]	${}^{14}N + n \rightarrow p + {}^{14}C$
69	[18]	${}^{15}O + n \rightarrow p + {}^{15}N$
70	[17]	${}^{15}O + n \rightarrow \alpha + {}^{12}C$
71	[18]	${}^{12}C + p \rightarrow \gamma + {}^{13}N$
72	[18]	${}^{13}C + p \rightarrow \gamma + {}^{14}N$
73	[17]	${}^{14}C + p \rightarrow \gamma + {}^{15}N$
74	[17]	${}^{13}N + p \rightarrow \gamma + O14$
75	[17]	${}^{14}N + p \rightarrow \gamma + {}^{15}O$
76	[17]	${}^{15}N + p \rightarrow \gamma + {}^{16}O$
77	[18]	${}^{15}N + p \rightarrow \alpha + {}^{12}C$
78	[17]	${}^{12}C + \alpha \rightarrow \gamma + {}^{16}O$
79	[3]	${}^{10}B + \alpha \rightarrow p + {}^{13}C$
80	[17]	${}^{11}B + \alpha \rightarrow p + {}^{14}C$
81	[17]	${}^{11}C + \alpha \rightarrow p + {}^{14}N$
82	[17]	${}^{12}N + \alpha \rightarrow p + {}^{15}O$
83	[17]	${}^{13}N + \alpha \rightarrow p + {}^{16}O$
84	[17]	${}^{10}B + \alpha \rightarrow n + {}^{13}N$
85	[17]	${}^{11}B + \alpha \rightarrow n + {}^{14}N$
86	[3]	${}^{12}B + \alpha \rightarrow n + {}^{15}N$
87	[18]	${}^{13}C + \alpha \rightarrow n + {}^{16}O$

Table B.1: Network of nuclear reactions implemented in `AlterBBN`.

B.7 BBN constraints

The following conservative constraints [19] are used in the function `bbn_excluded`:

$$0.240 < Y_p < 0.258\ , \qquad 1.2 \times 10^{-5} < {}^2H/H < 5.3 \times 10^{-5}\ , \qquad \text{(B.37)}$$
$$0.57 < {}^3H/{}^2H < 1.52\ , \qquad {}^7Li/H > 0.85 \times 10^{-10}\ , \qquad {}^6Li/{}^7Li < 0.66\ ,$$

for the helium abundance Y_p and the primordial ${}^2H/H$, ${}^3H/{}^2H$, ${}^7Li/H$ and ${}^6Li/{}^7Li$ ratios.
It is possible for the user to change these constraints in routine `bbn_excluded` which can be found in `src/bbn.c`.

Bibliography

[1] G. Steigman, Ann. Rev. Nucl. Part. Sci. **57**, 463 (2007).

[2] E. Komatsu *et al.* [WMAP Collaboration], Astrophys. J. Suppl. **192**, 18 (2011).

[3] R.V. Wagoner, Astrophys. J. Suppl. **18**, 247 (1969).

[4] L. Kawano, FERMILAB-PUB-92-004-A (1992).

[5] O. Pisanti *et al.*, Comput. Phys. Commun. **178**, 956 (2008).

[6] A. Arbey and F. Mahmoudi, Phys. Lett. B**669**, 46 (2008).

[7] A. Arbey and F. Mahmoudi, JHEP **1005**, 051 (2010).

[8] A. Arbey, A. Deandrea and A. Tarhini, JHEP **1105**, 078 (2011).

[9] A. Arbey and F. Mahmoudi, Comput. Phys. Commun. **181**, 1277 (2010); A. Arbey and F. Mahmoudi, Comput. Phys. Commun. **182**, 1582 (2011); `http://superiso.in2p3.fr/relic`.

[10] M.S. Smith, L.H. Kawano and R.A. Malaney, Astrophys. J. Suppl. **85**, 219 (1993).

[11] D.R. Tilly, H.R. Weller and H.H. Hasan, Nucl. Phys. A**474**, 1 (1987).

[12] F. Ajzenberg-Selove, Nucl. Phys. A**490**, 1 (1988).

[13] F. Ajzenberg-Selove, Nucl. Phys. A**506**, 1 (1990).

[14] F. Ajzenberg-Selove, Nucl. Phys. A**449**, 1 (1986).

[15] P.D. Serpico *et al.*, JCAP **0412**, 010 (2004).

[16] R.A. Malaney and G. Mathews, Phys. Rept. **229**, 149 (1993).

[17] G.R. Caughlan and W.A. Fowler, Atomic data and nuclear data tables **40**, 291 (1988).

[18] C. Angulo *et al.*, Nucl. Phys. A**656**, 3 (1999).

[19] K. Jedamzik, Phys. Rev. D **74**, 103509 (2006).

Résumé

La nature de la matière noire est l'une des plus importantes énigmes de la physique des hautes énergies, aussi bien du point de vue de la cosmologie que de la physique des particules. Dans ce rapport, je présente mes travaux de recherche sur la question de la matière noire dans le cadre de l'extension supersymétrique minimale du Modèle Standard (MSSM). En particulier, je m'intéresse à des scénarios dans lesquelles le neutralino est la particule supersymétrique la plus légère, et les confronte à des données expérimentales issues de différents secteurs, tels que les mesures cosmologiques de la densité de matière noire, la détection directe de matière noire, les données expérimentales du LEP et de Tevatron, les contraintes de physique des saveurs, les résultats expérimentaux des recherches de Higgs et de Supersymétrie au LHC. Je montre que le MSSM propose des solutions compatibles avec toutes les contraintes considérées.

Mots-clés : Supersymétrie, Cosmologie, Matière Noire

Abstract

The nature of dark matter is one of the most important questions of high energy physics, in the context of cosmology as well as particle physics. In this report, I present my work on the nature of dark matter in the context of the Minimal Supersymmetric extension of the Standard Model (MSSM). In particular, I consider scenarios in which the neutralino is the lightest supersymmetric particle, and confront them to experimental data from different sectors, such as cosmological measurements of dark matter density, dark matter direct detection, experimental data from LEP and Tevatron, constraints from flavour physics, experimental results from Higgs and Supersymmetry searches at the LHC. I show that the MSSM provides solutions compatible with all the considered constraints.

Keywords : Supersymmetry, Cosmology, Dark Matter